Universität Hamburg
DER FORSCHUNG | DER LEHRE | DER BILDUNG

Analysis of meiosis-specific gene expression regulation and establishment of a cytological framework of female meiosis by live-cell imaging in *Arabidopsis thaliana*

Dissertation with the aim of achieving a doctoral degree
at the Faculty of Mathematics, Informatics and Natural Sciences
Department of Developmental Biology
Universität Hamburg

Submitted by

Bingyan Hu

2025 in Hamburg, Germany

Supervisor: **Prof. Dr. Arp Schnittger**

1st Examnier: **Prof. Dr. Arp Schnittger**

2nd Examiner: **Dr. Magdalena Weingartner**

Date of oral defense: 02.10.2025

Table of Contents

List of Abbreviations

ASY1	ASYNAPTIC 1
REM	REPRODUCTIVE MERISTEM
wildtype	WT
CDKs	Cyclin-Dependent Kinases
KRP	KIP27-RELATED PROTEIN
RTR-complex	RECQ4A-TOPOIIIα-RMI1
KNO1	KNOTEN1
AEs	axial elements
RMF1/2	REDUCED MALE FERTILITY1/2
NL	nuclear lamina
NE	nuclear envelope
DSBs	DNA double-strand breaks
SPO11	SPORULATION 11
SPO11-1	SPORULATION 11-1
SPO11-2	SPORULATION 11-2
SC	synaptonemal complex
PCH2	PACHYTENE CHECKPOINT 2
ZYP1A	ZYGOTENE PACHYTENE 1A
ZYP1B	ZYGOTENE PACHYTENE 1B
DMC1	DISRUPTION of MEIOTIC CONTROL 1
RAD51	RADIATION SENSITIVE 51
CO	crossover
HEI10	ENHANCER OF CELL INVASION NO.10
MSH4	MUTS HOMOLOG 4
MSH5	MUTS HOMOLOG 5
MLH1	MUTL-HOMOLOGUE 1
MLH3	MUTL-HOMOLOGUE 3
NEB	nuclear envelope break down
SAC	spindle assembly checkpoint
PMC	pollen mother cell
MMC	megaspore mother cell
TF	transcription factors
EMGs	early meiotic genes
IME1	INDUCER OF MEIOSIS 1
MEIOSIN	meiosis initiator
STRA8	retinoic acid 8
RNAPII	RNA polymerase II
SPL	sporocyteless
NZZ	NOZZLE
MMD1	Male meiocyte death 1
AM1	Ameiotic1
JAS	JASON
TDM1	THREE DIVISION MUTANT 1
MEL2	MEIOSIS ARRESTED AT LEPTOTENE2
IME	intron-mediated enhancement
TSS	transcriptional start sites
CTD	carboxy-terminal domain
GTFs	general transcription factors
PIC	preinitiation complex
EJC	exon junction complex
SKIP	Ski-interacting Protein

SC35	Splicing Component 35 kDa
STRA8	Stimulated by Retinoic Acid8
5’ UTR	5’ untranslated region
3’ UTR	3’ untranslated region
UBQ10	UBIQUITIN 10
mRNA	Messenger Ribonucleic Acid
pre-mRNA	precursor mRNA
RACE	Rapid Amplification of cDNA Ends
gDNA	genomic DNA
amiRNA	Artificial MicroRNA
LE	lateral elements
CE	central element
SCEP1	Synaptonemal Complex Central Element Protein 1
SCEP2	Complex Central Element Protein 2
RBR1	Retinoblastoma (Rb) homolog RETINOBLASTOMA-RELATED1
WUS	WUSCHEL
KRP	KIP-RELATED PROTEIN
BrdU	bromodeoxyuridine
LINC	linker of the nucleoskeleton and cytoskeleton
SUN	Sad1/UNC-84
KINGBIRD	Kleisin IN Green microtubules in ReD
SCF	Skp-Cul1-F-box-protein
RPMs	Rapid Prophase Movements
PCR	polymerase chain reaction
MS	Murashige and Skoog
AIC	Akaike Information Criterion
SLiCE	seamless ligation cloning extract
ROIs	regions of interest

List of Publications and Presentations

Publications with my contributions

- C Yang, **B Hu**, SM Portheine, P Chuenban, A Schnittger. (2020) State changes of the HORMA protein ASY1 are mediated by an interplay between its closure motif and PCH2. Nucleic Acids Research 48 (20), 11521-11535

- C Yang, K Sofroni, Y Hamamura, **B Hu**, HT Elbasi, M Balboni, L Chu, D Stang, M Heese, A Schnittger. (2022) ZYP1-mediated recruitment of PCH2 to the synaptonemal complex remodels the chromosome axis leading to crossover restriction. Nucleic Acids Research 50 (22), 12924-12937

- G Pochon, IM Henry, C Yang, N Lory, N Fernández-Jiménez, F Böwer, **B Hu**, L Carstens, HT Tsai, M Pradillo, L Comai, A Schnittger. (2023) The Arabidopsis Hop1 homolog ASY1 mediates cross-over assurance and interference. PNAS nexus 2 (3), pgac302

Publications in preparation

- **B Hu**, S Ono, M Chen, Y Wang, S Seemann, M Hesse, A Schnittger. Analysis of meiosis-specific gene expression regulation in *Arabidopsis Thaliana*. (Chapter I, written in the form of a manuscript)

- **B Hu**, MA Prusicki, K Srahlmann, Y Wang, L Krause, A Schnittger. A cytological framework of female meiosis in Arabidopsis. (Chapter II, written in the form of a manuscript)

Poster presentations

- Gordon Research Conference on Meiosis. 5-10 June 2022. New Hampshire, USA. **A cytological framework of female meiosis in Arabidopsis by live cell imaging**

- EMBO workshop – Current methods in cell biology. 4-13 Sep 2022. Heidelberg, Germany. **A cytological framework of female meiosis in Arabidopsis by live cell imaging – win a best POSTER PRIZE.**

- The 33rd International Conference on Arabidopsis Research (ICAR2023). 5-9 June 2023. Chiba, Japan. **A cytological framework of female meiosis in Arabidopsis by live cell imaging**

- Plant Meiosis Meeting. 4-6 Sep 2024.Poznan, Poland. **A cytological framework of female meiosis in Arabidopsis by live cell imaging**

Abstract

Meiosis is a tightly regulated process crucial for sexual reproduction, requiring precise control at every step from meiotic entry to the formation of haploid cells. Although meiosis is fundamental to plant reproduction, its regulatory mechanisms remain poorly understood.

In the first part of this dissertation, the regulation of meiosis-specific genes has been analyzed. Different regions of the *ASY1* gene were investigated for their contribution to its expression in meiocytes, identifying intron 3-5 as an essential element for meiocyte-specific expression, with additional introns and untranslated regions enhancing expression strength. Given that many meiotic genes are intron-rich, this work indicates that the intron-driven transcriptional regulation may represent a broader principle in meiosis. A yeast one-hybrid screen further identified REM transcription factors as potential regulators, and multiplex knockdown of REM35, REM34, REM36, and REM37 in meiosis led to fertility defects, revealing their essential role in ASY1 expression during female meiosis. As a proof of concept, the mitotic gene *KNO1,* which interacts with the RTR-complex, was ectopically expressed in meiocytes using the ASY1 promoter-intron system. This led to GFP-KNO1 accumulation in meiocytes, reduced fertility, and chromosome entanglement, resembling the phenotypes of RTR-complex mutants, demonstrating the potential of using intron-mediated gene regulation for control of meiotic gene expression in both basic and applied science.

Similar to many other organisms, studying female meiosis in *Arabidopsis thaliana* is very challenging. Female meiocytes are deeply embedded in maternal tissues and thus are not readily accessible. Moreover, there are much fewer female than male meiocytes, making it difficult to first find these cells in whole-mount preparations and second to obtain statistically robust sample sizes. Thus, much less is known about female meiosis in plants. To close this gap, in the second part of this dissertation, the previously established live cell imaging system for male meiocytes has been adapted and optimized for the analysis of female meiosis. Using several central meiotic regulator reporter lines, the duration of distinct stages of prophase I has been analyzed, and the chromosome dynamics have been documented. The nuclear envelope and cell wall formation between meiosis I and meiosis II have also

been monitored. This gave rise to a temporally resolved cytological framework of female meiosis in the wildtype that serves as a guiding system for future studies. Furthermore, this live cell imaging system has been applied to study a family of CDK inhibitors (KIP27-RELATED PROTEIN, KRP), in which a designated female meiocyte undergoes several mitotic divisions before entering meiosis. One important outcome of this work is to map the point of commitment to female meiosis and the determination of the cellular setting when a meiocyte is destined to enter meiosis.

Zusammenfassung

Die Meiose ist ein streng regulierter Prozess, der für die sexuelle Fortpflanzung von entscheidender Bedeutung ist und in jedem Schritt vom Beginn der Meiose bis zur Bildung haploider Zellen eine präzise Kontrolle erfordert. Obwohl die Meiose für die pflanzliche Reproduktion von grundlegender Bedeutung ist, sind ihre Regulationsmechanismen noch wenig verstanden.

Im ersten Teil dieser Arbeit wurde die Regulation meiosespezifischer Gene analysiert. Es wurde untersucht, wie verschiedene Regionen des ASY1-Gens zu dessen Expression in Meiozyten beitragen. Dabei wurden die Introns 3-5 als essentielles Element für die meiozytenspezifische Expression identifiziert, wobei zusätzliche Introns und untranslatierte Regionen die Expression zusätzlich erhöhten. Da viele meiotische Gene intronreich sind, deutet diese Arbeit darauf hin, dass die intronvermittelte transkriptionelle Regulation ein allgemeines Prinzip der Meiose darstellt. Ein Hefe-One-Hybrid-Screening identifizierte zudem REM-Transkriptionsfaktoren als potenzielle Regulatoren. Der multiple Knockdown von REM35, REM34, REM36 und REM37 in der Meiose führte zu Fertilitätsdefekten und verdeutlichte deren wichtige Rolle bei der Expression von ASY1 während der weiblichen Meiose. Als Proof-of-concept wurde das mitotische Gen KNO1, das mit dem RTR-Komplex interagiert, mithilfe des ASY1-Promoter-Intron-Systems in Meiozyten ektopisch exprimiert. Dies führte zu einer Anreicherung von GFP-KNO1 in Meiozyten, verringerter Fertilität und Chromosomenverwicklungen, die den Phänotypen von Mutanten des RTR-Komplexes ähnelten, und zeigt das Potenzial der intronvermittelten Genregulation zur Steuerung der meiotischen Genexpression in der Grundlagenforschung und angewandten Wissenschaft.

Wie bei vielen anderen Organismen ist die Erforschung der weiblichen Meiose in *Arabidopsis thaliana* eine große Herausforderung. Weibliche Meiozyten sind tief im maternalen Gewebe eingebettet und daher schwer zugänglich. Zudem gibt es deutlich weniger weibliche als männliche Meiozyten, was es schwierig macht, diese Zellen in Präparaten zu beobachten und statistisch belastbare Probengrößen zu erhalten. Daher ist über die weibliche Meiose bei Pflanzen deutlich weniger bekannt. Um diese Wissenslücke zu schließen, wurde im zweiten Teil dieser Arbeit das bereits etablierte Live-Cell-Imaging-System für männliche Meiozyten an die Analyse der weiblichen

Meiose angepasst und optimiert. Mithilfe mehrerer Reporterlinien zentraler meiotischer Regulatoren wurden die Dauer einzelner Phasen der Prophase I analysiert, die Chromosomendynamik dokumentiert, sowie die Kernhüllen- und Zellwandbildung zwischen Meiose I und Meiose II beobachtet. Dadurch konnte ein zeitlich aufgelöstes zytologisches Modell der weiblichen Meiose im Wildtyp erstellt werden, das als Leitsystem für zukünftige Studien dient. Anschließend wurde dieses Live-Cell-Imaging-System genutzt, um eine Familie von CDK-Inhibitoren (KIP27-RELATED PROTEIN, KRP) zu untersuchen, bei denen die designierte, weibliche Meiozyte mehrere mitotische Teilungen durchläuft, bevor sie in die Meiose eintritt. Ein wichtiges Ergebnis dieser Arbeit ist die zeitliche Einordnung des Übergangs zur weiblichen Meiose und die Bestimmung des zellulären Zustands, in dem eine Meiozyte in die Meiose eintritt.

General Introduction

Overview of meiosis

Meiosis is a fundamental process for sexual reproduction in eukaryotes, regulating genetic diversity through chromosome recombination and ensuring genetic stability across generations by reduction division, which is restored during fertilization.

The process of meiosis is highly conserved among eukaryotes (Gao, Qin, and Schimenti 2024). Meiosis consists of two main division events: meiosis I and meiosis II. Each of them can be divided into four substages: prophase, metaphase, anaphase, and telophase in a standard model. Among these eight stages in meiosis, prophase I is the longest and most complex stage, which contains three crucial events that differentiate from mitosis, such as homologous pairing, synapsis, and recombination (Grey and de Massy 2021). Prophase I of meiosis is further divided into five substages based on chromosome behavior and morphology during the meiotic progression. They are leptotene, zygotene, pachytene, diplotene, and diakinesis (Dawe 1998; Zickler and Kleckner 1999; Armstrong and Jones 2003). In *Arabidopsis thaliana*, these processes are regulated by numerous genes to ensure proper chromosome behavior and meiotic progression.

Leptotene, derived from the Greek words meaning ‘thin threads’. It suggests that each chromosome forms a thin thread-like structure, as indicated by its name. Chromosomes undergo significant structural reorganization during the leptotene stage. Condensin complexes initiate chromosome condensation, causing diffuse chromatin to begin condensing into thin thread structures by reorganizing chromatin loops along the forming chromosome axis(Liu and Qu 2008). Cohesion complexes (REC8 as one of the subunits) load to establish sister chromatid cohesion along the chromosome axis, then the axial elements (AEs) assemble along the cohesion-bound axes, where ASY1, as one of the AEs, transitions from diffuse foci to linear signals (Armstrong et al. 2002; Cai et al. 2003; Sanchez-Moran et al. 2007; Pochon et al. 2023). During leptotene, RMF1/2 is expressed to form the SCF^{RMF} E3 ligase complex mediating the degradation of nuclear lamina (NL), releasing the telomeres to the nuclear envelope (NE), promoting chromosome bouquet formation and homologous pairing (Yuan et al. 2025). Another key feature of leptotene is the initiation of programmed DNA double-

strand breaks (DSBs). Two SPO11 homologs SPO11-1 and SPO11-2 cooperate to catalyze the formation of DSBs that initiate homologous recombination (Stacey et al. 2006; Shingu et al. 2010; Keeney, Giroux, and Kleckner 1997).

Zygotene is characterized by the initiation and progression of homologous chromosome synapsis. The synaptonemal complex (SC) is initiated from multiple synapsis sites. The assembly of SC is a dynamic process, where transverse filament proteins ZYP1A and ZYP1B polymerize between homologs, forming a zipper-like structure, and two newly identified central elements SCEP1 and SCEP2 (Vrielynck et al. 2023) that connect chromosomes. At the same time, ASY1 is progressively removed from synapsed axes via PCH2-mediated remodeling (Higgins et al. 2005; Lambing et al. 2015; C. Yang et al. 2020, 2022). The formation of SC is completed with fully synapsed chromosomes by the onset of pachytene. During zygotene, the recombinase DMC1, together with RAD51, accumulates at DSB sites on chromatin loops that extend from the chromosome axes, where it facilitates homologous search and strand invasion (Kurzbauer et al. 2012).

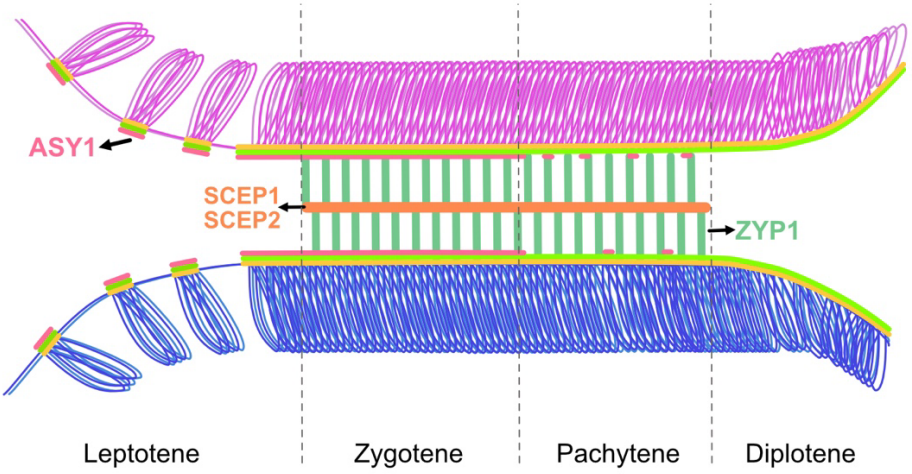

Figure 1. Schematic diagram of the synaptonemal complex (SC) in Arabidopsis. The SC is composed of three parts: the lateral element, the transferase element, and the central element. ASY1 (in pink) is one of the components of lateral element; ZYP1(in dark green) is the identified component of the transverse elements; SCEP1 and SCEP2 are components of the central elements.

In pachytene, homologous chromosomes are fully synapsed by a continuous SC along each bivalent, appearing as thick, tightly paired threads under the microscope. Besides that, the active formation and maturation of crossover (CO) events is another signature for pachytene. The E3 ligase HEI10 is first distributed

evenly along the SC and then coarsens into discrete foci that indicate the CO-designated sites, of which number and intensity correlate with the final positions of COs (Morgan et al. 2021). In the meantime, class I crossover factors MSH4 and MSH5 form a heterodimer to stabilize early intermediates and promote interference-sensitive CO formation during the process of HEI10 coarsening (Higgins et al. 2004). Afterwards, MLH1 and MLH3 co-localized at the late recombination nodules (LNs) to resolve the double Holliday junctions (dHJs) into COs (Jackson et al. 2006; Durand et al. 2025). RAD51 and DMC1 collaboratively facilitate the final steps of homologous recombination, with DMC1 favoring interhomolog repair and RAD51 helping strand invasion and stabilization of recombination intermediates (Kurzbauer et al. 2012; Chen et al. 2021; Da Ines et al. 2022).

Diplotene marks the stage where homologous chromosomes begin to separate but remain connected at chiasmata, so each bivalent looks like two double threads. The SC disassembles progressively along chromosome arms while the rapid chromosome movement slows down during diplotene (Pradillo et al. 2007; Cromer et al. 2024).

Diakinesis represents intensive chromosome remodeling. During diakinesis, chromosomes shorten and thicken into distinct bivalents, exhibiting the maximum condensation. The arm cohesion complexes, such as REC8, are released, preparing for the division during meiosis I, while the centromeric cohesion remains intact to maintain sister chromatid association until anaphase II (X. Yang et al. 2009; Cromer et al. 2013; Zamariola et al. 2014). By the end of diakinesis, the nuclear envelope breaks down (NEB), marking the beginning of the first meiotic nuclear division.

After the NEB, bivalents align at the center of the cell during metaphase I, and their correct attachment to spindle microtubules is verified by the spindle assembly checkpoint (SAC) (Watanabe 2012; Gorbsky 2015; Makrantoni and Marston 2018). After passing through the SAC, homologous chromosomes are pulled towards the two opposite poles of the cell, representing anaphase I. Then, the nuclear envelope reforms around the two sets of condensed chromosomes at each pole during telophase I.

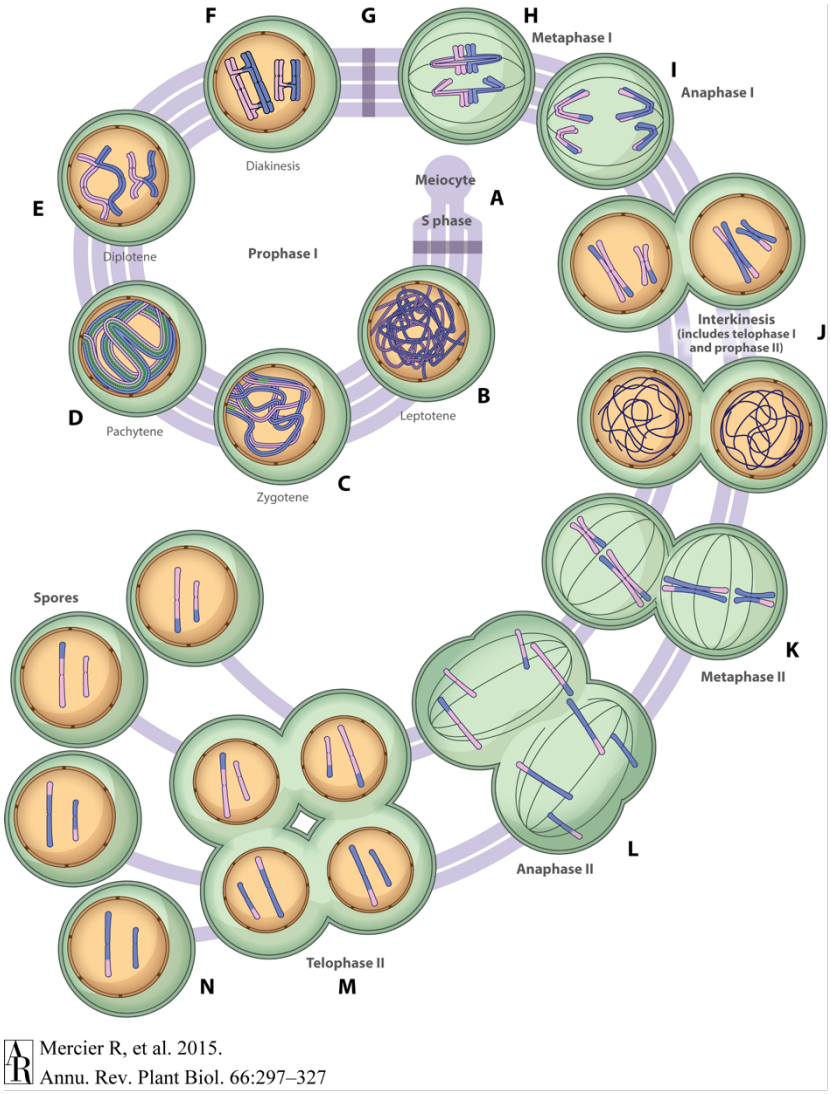

Figure 2. Overview of meiosis progression in the anthers of *Arabidopsis Thaliana*. Picture taken from (Mercier R, et al. 2015). **(A)** Meiosis commitment happens, and the cell enters S-phase. (B) Leptotene, chromosomes condense along axial elements, with Spo11-mediated DSBs forming to initiate homologous recombination. (C) Zygotene, homologous chromosomes synapse via SC assembly, facilitated by DSB repair intermediates and strand invasion. (D) Pachytene, SC assembly complete, CO formation, meiotic checkpoint. (E) Diplotene, SC disassembly, homologous chromosomes remain connected at chiasmata. (F) Diakinesis, chromosomes condense into short, thick structures and thicken into distinct bivalents. (G) Prophase exit and NEB. (H) Metaphase I, the bivalents align at the metaphase plate. (I) Anaphase I, chromosomes migrate to the two poles. (J) Interkinesis includes telophase I and prophase II, during which chromosomes undergo decondensation. (K) Metaphase II, two sets of sister chromatids align at the metaphase plate with the help of two spindles. (L) Anaphase II, sister chromatids separation. (M) Telophase II, formation of four nuclei. (N) Cytokinesis, formation of four haploid spores.

Meiosis II resembles mitosis division both in mechanical processes and duration. Sister chromatids align at the metaphase plate and are pulled apart during

anaphase II following centromeric cohesion cleavage. Final cytokinesis produces four haploid cells in diploid organisms, such as *Arabidopsis thaliana*.

Transcriptional regulation in meiosis

Meiosis is a highly regulated process essential for sexual reproduction. From the cell entry into meiosis to the accurate pairing, recombination, and segregation into four genetically distinct haploid cells, each step must be precisely controlled. Therefore, understanding how meiotic genes are precisely regulated at the right time and in the right place is crucial for understanding the process of meiosis. Although the process of meiosis is highly conserved among eukaryotes, regulatory factors and specific molecular players can vary between lineages.

Any diploid yeast cell can enter meiosis in response to nutrient starvation. The transcription factor (TF), IME1 in yeast, serves as the primary master regulator to activate the transcription of a bunch of early meiotic genes (EMGs), initiating the transcriptional switch from mitosis to meiosis (Colomina et al. 1999; Kociemba et al. 2024). In IME1 deletion strains, cells are arrested before the pre-meiotic S phase, unable to activate EMGs or initiate meiosis, even under starvation (Lee and Honigberg 1996; Colomina et al. 1999). In contrast, expressing IME1 ectopically in haploid yeast cells, where meiosis is blocked, still leads to meiotic entry in haploids under starvation (Mitchell and Bowdish 1992; Colomina et al. 1999). This confirms that IME1 integrates environmental and developmental signals to directly control the transcriptional switch from mitosis to meiosis.

In mammals, there are two meiosis-specific TFs: meiosis initiator (MEIOSIN) and stimulated by retinoic acid 8 (STRA8), forming a heterodimeric complex that functions as the primary transcription factor complex, enhancing DNA binding and transcriptional activation of hundreds of meiosis genes during early meiotic entry (Anderson et al. 2008; Kojima, de Rooij, and Page 2019; Ishiguro et al. 2020; Oatley and Griswold 2020; Desimio et al. 2021). Unlike IME1, the MEIOSIN-STRA8 complex mainly upregulates the transcription of early meiotic genes that are already expressed at low levels in pre-meiotic cells, leading to a 4 to 23-fold increase in their expression (Kojima, de Rooij, and Page 2019; Pfaltzgraff et al. 2024). The complex recruits RNA polymerase II (RNAPII) to target promoters, facilitating transcriptional initiation or

releasing paused polymerase into productive elongation, finally increasing the target gene expression level beyond the functional thresholds required for the meiotic process (Kojima, de Rooij, and Page 2019; Pfaltzgraff et al. 2024; Shimada and Ishiguro 2024). Disruption of either MEIOSIN or STRA8 leads to infertility due to failed meiotic initiation and progression in both sexes (Anderson et al. 2008; Ishiguro and Shimada 2022; Zhang et al. 2023). Taken together, the MEIOSIN-STRA8 complex functions as a master regulator, regulating the mitosis-to-meiosis transition in both male and female germ cells, offering key insights into the molecular control of gametogenesis in mammals.

However, no single master transcription factor regulator, such as IME1 or MEIOSIN-STRA8, has yet been identified in plants to control meiotic entry or the meiotic process. Different from yeast or mammals, the plant meiotic regulators commonly discussed, some are TFs, while some are not. In *Arabidopsis thaliana*, sporocyteless (SPL, also known as NOZZLE, NZZ) is a TF that functions as a repressor to inhibit genes that maintain the mitotic state, allowing their differentiation into sporocytes to initiate meiotic entry (W. C. Yang et al. 1999). The *spl* mutants show the arrest of sporocyte development in both anthers and ovules, resulting in sterility (W. C. Yang et al. 1999). Male meiocyte death 1 (MMD1, also known as DUET) is another confirmed meiosis-specific TF in *Arabidopsis thaliana* male meiosis, which is only expressed in diplotene, and binds H3K4me2-marked chromatin, directly activating meiotic genes such as *JAS* for microtubule organization, *TDM1* for meiotic exit (Andreuzza et al. 2015). Disruption of MMD1 causes premature meiotic death and chromosome missegregation (Dukowic-Schulze and Chen 2014). In maize, the Ameiotic1 (AM1, called SWI1/DYAD in Arabidopsis) is not a TF but a coiled-coil protein that controls the mitosis-to-meiosis switch by facilitating histone modifications and directing the assembly of chromosome axis elements and cohesion complexes (Mercier et al. 2003; Nan et al. 2011; C. Yang et al. 2019; Y. Wang et al. 2021). In rice, instead of TFs, the RNA-binding protein called MEIOSIS ARRESTED AT LEPTOTENE2 (MEL2) regulates the timing of meiotic initiation. It controls the transition via post-transcriptional regulation mediated by cytoplasmic RNA granules to enforce synchronized meiotic entry (Nonomura et al. 2011; Mimura et al. 2024). MEL2 defects disrupt RNA-mediated regulation of meiotic timing, leading to asynchronous meiosis, leptotene arrest, and sterility (Mimura, Ono, and Nonomura 2021).

Overall, the regulators reported in plants display distinct functions in regulating specific genes or events via different molecular mechanisms and evolutionary contexts. The regulation strategies in meiosis vary among different plant species, although the outcome is all for the proper meiotic initiation and progression. This divergence indicates lineage-specific regulation in meiosis. More studies will be needed to gain a better understanding of meiosis regulation.

Intron-mediated enhancement

Introns were long considered non-functional intervening sequences between coding regions that had to be removed during RNA processing. However, this view changed when they were first found to enhance gene expression by increasing mRNA accumulation in cultured maize cells (Callis, Fromm, and Walbot 1987). Since then, introns have been recognized as important regulatory elements in gene expression. In addition to acting as classical enhancers, introns enhance gene expression by a different process called intron-mediated enhancement (IME), which has been widely reported among eukaryotes, including mice (Palmiter et al. 1991), humans (Jonsson et al. 1992; Kowal et al. 2025), *Caenorhabditis elegans* (Okkema et al. 1993; Ho, So, and Chow 2001), silkworms (Jiang et al. 2015), yeast (Furger et al. 2002; Moabbi et al. 2012), maize (Mascarenhas et al. 1990; Luehrsen and Walbot 1991), rice (Xu, Yu, and Hall 1994; Ueki et al. 1999), and Arabidopsis (A. B. Rose and Last 1997; Casas-Mollano, Lao, and Kavanagh 2006).

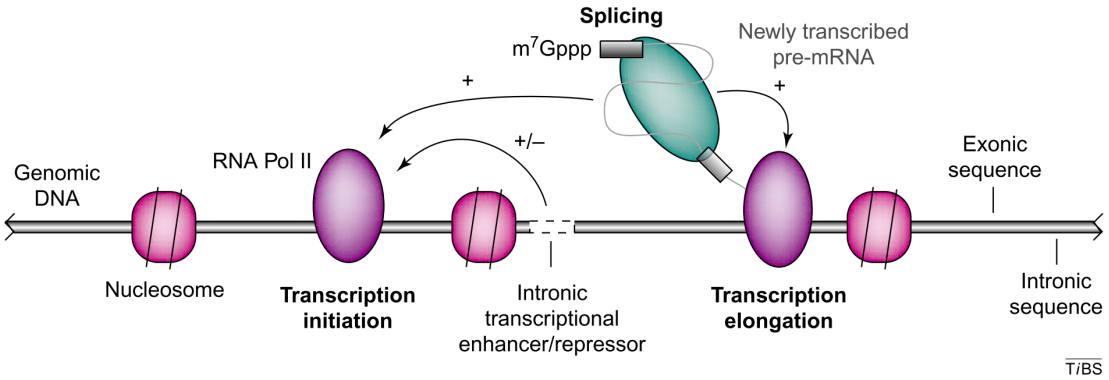

Figure 3. Introns can affect the transcription through multiple mechanisms. Picture taken from (Hervé Le Hir, Nott, and Moore 2003). Intron sequences may contain transcriptional enhancers, repressors, or nucleosome-positioning sequences that can affect the initiation of transcription.

Additionally, the recruitment of spliceosome components to a nascent intron can further promote transcription by enhancing both initiation and elongation of transcription.

Although IME has been known for more than three decades across various species, the molecular mechanism underlying this phenomenon remains largely unknown. This is because IME is a complex phenomenon, where introns can influence the expression of target genes through several mechanisms, acting at transcriptional, post-transcriptional, and translational levels (Kowal et al. 2025). However, the predominant effect typically involves transcriptional regulation, which results in increased mRNA accumulation. Transcriptional regulation mediated by introns can generally be classified into two types: (1) splicing-dependent and (2) splicing-independent regulation. One common feature is that introns in both IME mechanisms must be located within the transcribed region of the gene. Those located upstream of the transcriptional start sites (TSS) will lose their enhancement.

Splicing-dependent transcriptional regulation requires introns located within the transcribed region of the gene that undergo splicing. In most cases, introns near the TSS have the strongest enhancement and gradually weaken as the distance increases from the TSS, indicating that the position of introns within the gene plays a crucial role in determining the ability to enhance transcription (Callis, Fromm, and Walbot 1987; Alan B. Rose 2004; Bieberstein et al. 2012; Gallegos and Rose 2017). The first step in transcription is initiation, which is also most significantly affected by introns. Splicing factors are recruited to the 5′ splice site of the intron via the carboxy-terminal domain (CTD) of RNAP II. The CTD acts as a platform to connect splicing to transcription (Millhouse and Manley 2005; Nojima et al. 2018). Among these, splicing factor like U1-snRNP interacts not only with RNAP II but also with general transcription factors (GTFs) such as TFIIH, TFIID, and TFIIB, thereby facilitating the assembly of the preinitiation complex (PIC) to promote initiation and reinitiation (Tian 2001; Kwek et al. 2002; Damgaard et al. 2008; Jobert et al. 2009). Another splicing factor, HNRNPU, promotes transcriptional initiation in a similar manner by recruiting TFIIF to the PIC (Fiszbein, Krick, and Burge 2019). In addition to directly helping PIC formation, chromosome modification by H3K9 acetylation and H3K4 trimethylation can be increased by promoter-proximal introns near the TSS to stabilize transcription initiation further (Bieberstein et al. 2012). Beyond initiation, introns also contribute to elongation by interacting with elongation factors directly through splicing factors such as SKIP and SC35, and by promoting H3K36 trimethylation to affect chromatin structure to

elongate the transcription (Brès et al. 2005; Lin et al. 2008; de Almeida et al. 2011). In a few cases, terminator-proximal introns in mammalian cell lines can enhance transcription termination by promoting the recruitment of 3′ end processing factors and reducing H3K36 trimethylation at the end of the gene, thereby facilitating poly(A) site usage and proper termination (Lutz et al. 1996; McCracken, Lambermon, and Blencowe 2002; Kim et al. 2011).

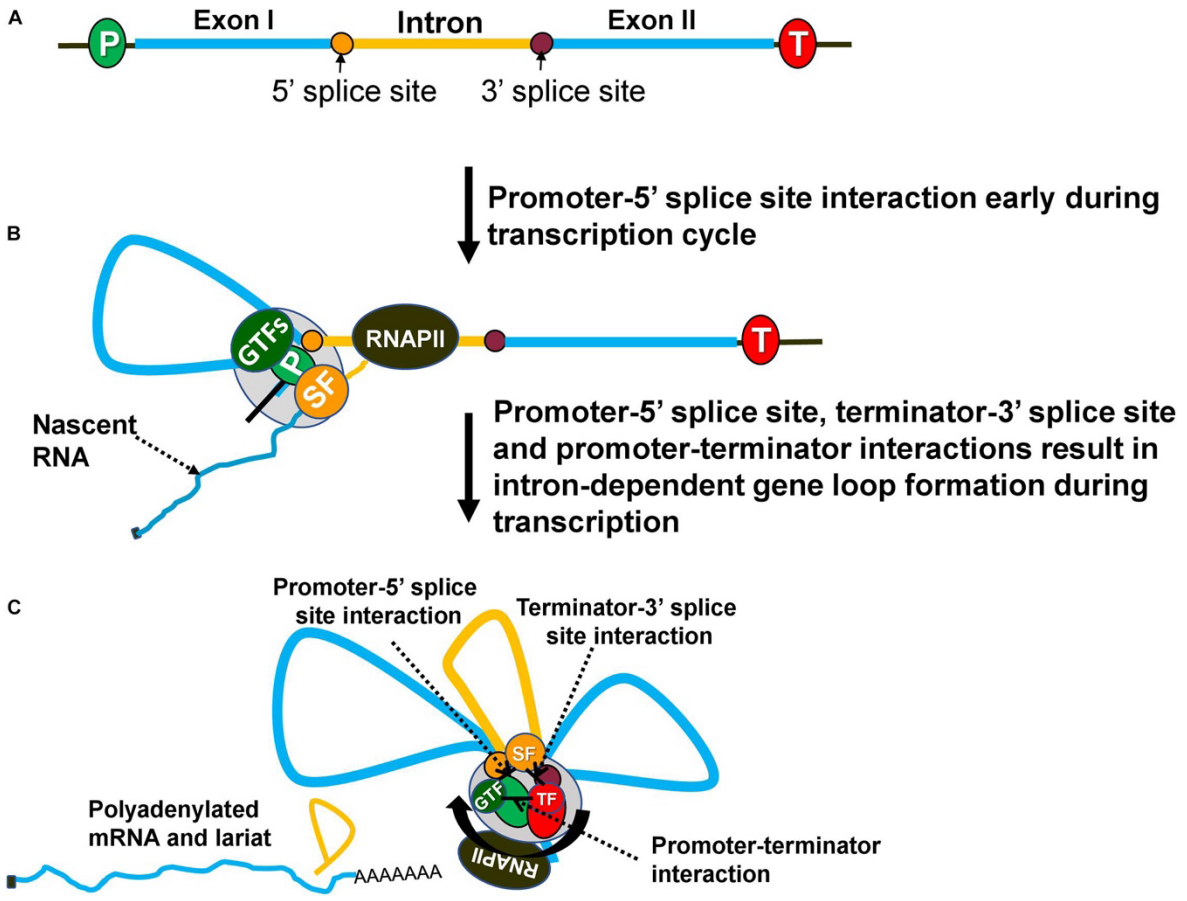

Figure 4. Intron-dependent gene loop formation to enhance gene expression by facilitating transcriptional initiation, reinitiation and promoter directionality. Picture taken from (Dwyer et al. 2021). **(A)** The gene structure with promoter (green), exon (blue), intron (yellow) and terminator (red). **(B)** During the early transcription cycle, RNA polymerase II (RNAPII) recruits splicing factors (SFs) to remove introns, leading to the 5' splice site physically interacting with general transcription factors (GTFs) at the promoter, generating a chromatin loop. **(C)** After the intron is transcribed, splicing components associated with the 3' splice site engage with termination factors (TFs) located near the end of the gene, creating another loop. Ultimately, these spatial interactions result in a tripartite loop structure, bringing the promoter and terminator into close proximity to facilitate transcriptional reinitiation.

Apart from being involved in the splicing machinery, introns in budding yeast can promote the formation of a looped gene architecture, where the promoter contacts the 5′ splice site and the terminator interacts with the 3′ splice site (Moabbi et al. 2012; Tan-Wong et al. 2012). However, the mechanism by which introns facilitate loop formation is not clear. It has been proposed that the promoter-5′ splice site interaction helps stabilize the preinitiation complex. At the same time, promoter–terminator proximity promotes transcriptional reinitiation by recycling RNA polymerase, to contribute to IME of transcription (Al Husini, Kudla, and Ansari 2013; Damgaard et al. 2008). In looping-defective yeast mutants, the IME effect was lost even though the splicing was normal (Dwyer et al. 2021). This indicates that intron-mediated enhancement of transcription depends on the formation of a splicing-dependent looped gene architecture rather than splicing itself.

IME could also be achieved by another poorly understood splicing-independent mechanism involving intronic motifs (e.g., TTNGATYTG in Arabidopsis) to enhance mRNA accumulation but independent of transcription factors (Gallegos and Rose 2019). This motif only increases expression when located less than 1 kb downstream of the transcription start sites in a location-dependent manner, not when it is located upstream or far downstream of the TSS, implying that it does not bind to TF-binding enhancers in a location-independent fashion. The motif enhances mRNA accumulation in a dose-dependent manner, with each copy contributing 1.5-fold more mRNA, suggesting a cumulative, modular effect. The motif still enhances mRNA accumulation even if placed in the exons or 5′ UTR of an intronless construct, which indicates splicing is not required for enhancement. The activity is from the DNA sequence itself, not the splicing process (Gallegos and Rose 2019). However, the motif must be transcribed, as placing it outside the transcribed region will lose its effect. There are some hypotheses about the possible mechanisms, but the exact molecular mechanism remains unclear (Gallegos and Rose 2019).

The IME of translation depends on post-transcriptional mechanisms, facilitated by the exon junction complex (EJC), which assembles on spliced mRNA during the splicing process to stabilize transcripts against degradation and promote nuclear export (H. Le Hir et al. 2001; Wiegand, Lu, and Cullen 2003). This assembly recruits ribosomal subunits to enhance translation initiation and increase protein yield (H. Le Hir et al. 2001).

In summary, IME enhances gene expression through multiple interconnected mechanisms that affect transcription by boosting initiation and elongation, post-transcription by enhancing mRNA stability and accumulation, and translation by improving translation initiation and efficiency.

Sexual dimorphism in meiosis

Although the process of meiosis is highly conserved among eukaryotes, meiosis exhibits pronounced sex-specific differences in meiosis timing, duration, cellular organization, and molecular mechanisms in the same species.

In mammals, oocytes initiate meiosis synchronously together during fetal ovarian development but get arrested twice during meiosis for decades (Handel and Eppig 1998). The first arrest occurs at the diplotene of prophase I, which lasts a maximum of five decades, then resumes cyclically after puberty. Then the oocytes get arrested again at metaphase II until fertilization occurs (Solc, Schultz, and Motlik 2010). In contrast, spermatocytes start meiosis at puberty and regularly undergo continuous meiosis without interruption (Handel and Eppig 1998; Solc, Schultz, and Motlik 2010; Hua and Liu 2021). Not only do meiosis timing and duration differ, but the cellular organization also differs between female and male meiosis in mammals. During oogenesis, the metaphase spindle migrates to the oocyte periphery, resulting in asymmetric divisions with one single large ovum and three small polar bodies (Fabritius, Ellefson, and McNally 2011; H. Wang et al. 2020; Londoño-Vásquez et al. 2022). While in spermatogenesis, the spermatocytes go through symmetric divisions, resulting in four small viable sperm cells (Chu and Shakes 2013). Another key difference is that the chromosome axes in female meiocytes are significantly longer than in male meiocytes, which correlates with higher recombination rates in oocytes compared to spermatocytes in mice (Cahoon and Libuda 2019). Similar to mice, the genome-wide female crossover rate in humans is about 1.6-fold higher than that of males (Bhérer, Campbell, and Auton 2017). Meiosis exhibits sexual dimorphism across various levels in mammals, reflecting the evolutionary adaptations to different reproductive functional roles of oogenesis and spermatogenesis.

Similar to mammals, plant meiosis exhibits significant sexual dimorphism since plants generate the reproductive lineage late in development from the somatic cells of

their floral organs. This process differs from that in animals, where the germline is established early in embryogenesis. In plants, microsporogenesis takes place in the pollen sacs of anthers, while megasporogenesis occurs in ovules. Like in mammals, male meiosis in plants produces four functional haploid microspores, which develop into pollen grains. While in female meiosis four megaspores are produced after the second meiotic division, but only one survives and then develops into the female gametophyte. Plant meiosis exhibits significant differences in chromosome architecture between sexes as well as plant species. In *Arabidopsis thaliana*, the SC length in the megaspore mother cell (MMC) is shorter than in the pollen mother cell (PMC), which is the opposite of the pattern observed in mice (Drouaud et al. 2007; Giraut et al. 2011). The chromosome recombination frequency in males is approximately 1.7 times higher than in females (Giraut et al. 2011). Besides the CO frequency, the distribution pattern of COs shows high CO rates in the telomeric region for males but low rates for females, even though there are more DSBs in these areas (Giraut et al. 2011; Cahoon and Libuda 2019). However, in *Brassica napus* and *Zea mays*, there is no difference in CO distribution and frequency between female and male meiosis (Kelly et al. 1997; Kianian et al. 2018).

In summary, sexual dimorphism is a widespread phenomenon among sexually reproducing organisms, but it varies across different species.

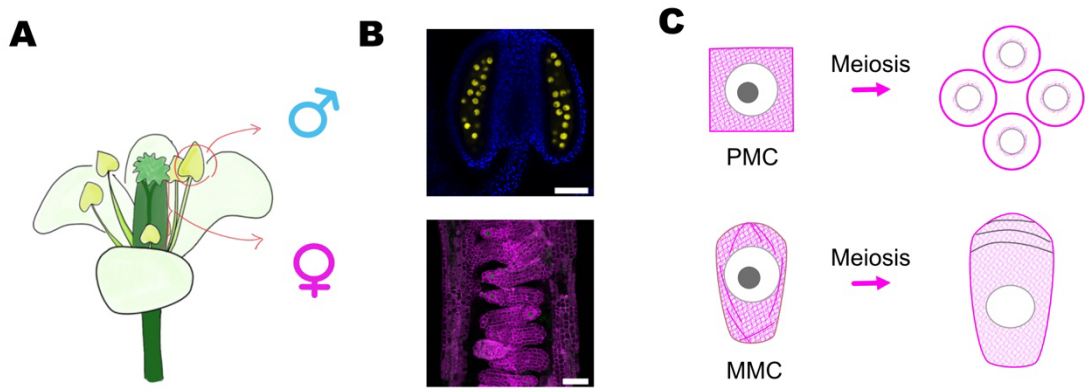

Figure 5. Sexual dimorphism in Arabidopsis. (A) A flower bud of *Arabidopsis Thaliana*. Anthers (yellow, red circle) and pistil (green, red brace) are the developmental organs. (B) Microscopy pictures of a chromosome reporter (yellow) in an anther (blue, auto fluorescent) and a combination of chromosome reporter (green) with tubulin marker (magenta) in the pistil. Scale bar: 20 µm. (C) A pollen mother cell (PMC) and a megaspore mother cell (MMC) go through meiosis division, resulting in four microspores and one functional megaspore (with the other three degenerating).

References

Al Husini, Nadra, Paul Kudla, and Athar Ansari. 2013. “A Role for CF1A 3’ End Processing Complex in Promoter-Associated Transcription.” *PLoS Genetics* 9 (8). Public Library of Science (PLoS): e1003722. doi:10.1371/journal.pgen.1003722.

Almeida, Sérgio Fernandes de, Ana Rita Grosso, Frederic Koch, Romain Fenouil, Sílvia Carvalho, Jorge Andrade, Helena Levezinho, et al. 2011. “Splicing Enhances Recruitment of Methyltransferase HYPB/Setd2 and Methylation of Histone H3 Lys36.” *Nature Structural & Molecular Biology* 18 (9). Springer Science and Business Media LLC: 977–83. doi:10.1038/nsmb.2123.

Anderson, Ericka L., Andrew E. Baltus, Hermien L. Roepers-Gajadien, Terry J. Hassold, Dirk G. de Rooij, Ans M. M. van Pelt, and David C. Page. 2008. “Stra8 and Its Inducer, Retinoic Acid, Regulate Meiotic Initiation in Both Spermatogenesis and Oogenesis in Mice.” *Proceedings of the National Academy of Sciences of the United States of America* 105 (39). Proceedings of the National Academy of Sciences: 14976–80. doi:10.1073/pnas.0807297105.

Andreuzza, Sébastien, Bindu Nishal, Aparna Singh, and Imran Siddiqi. 2015. “The Chromatin Protein DUET/MMD1 Controls Expression of the Meiotic Gene TDM1 during Male Meiosis in Arabidopsis.” *PLoS Genetics* 11 (9). Public Library of Science (PLoS): e1005396. doi:10.1371/journal.pgen.1005396.

Armstrong, Susan J., Anthony P. Caryl, Gareth H. Jones, and F. Christopher H. Franklin. 2002. “Asy1, a Protein Required for Meiotic Chromosome Synapsis, Localizes to Axis-Associated Chromatin in Arabidopsis and Brassica.” *Journal of Cell Science* 115 (Pt 18): 3645–55. doi:10.1242/jcs.00048.

Armstrong, Susan J., and Gareth H. Jones. 2003. “Meiotic Cytology and Chromosome Behaviour in Wild-Type Arabidopsis Thaliana.” *Journal of Experimental Botany* 54 (380). Oxford University Press (OUP): 1–10. doi:10.1093/jxb/erg034.

Bhérer, Claude, Christopher L. Campbell, and Adam Auton. 2017. “Refined Genetic Maps Reveal Sexual Dimorphism in Human Meiotic Recombination at Multiple Scales.” *Nature Communications* 8 (1). Springer Science and Business Media LLC: 14994. doi:10.1038/ncomms14994.

Bieberstein, Nicole I., Fernando Carrillo Oesterreich, Korinna Straube, and Karla M. Neugebauer. 2012. “First Exon Length Controls Active Chromatin Signatures and Transcription.” *Cell Reports* 2 (1). Elsevier BV: 62–68. doi:10.1016/j.celrep.2012.05.019.

Brès, Vanessa, Nathan Gomes, Loni Pickle, and Katherine A. Jones. 2005. “A Human Splicing Factor, SKIP, Associates with P-TEFb and Enhances Transcription Elongation by HIV-1 Tat.” *Genes & Development* 19 (10). Cold Spring Harbor Laboratory: 1211–26. doi:10.1101/gad.1291705.

Cahoon, Cori K., and Diana E. Libuda. 2019. “Leagues of Their Own: Sexually Dimorphic Features of Meiotic Prophase I.” *Chromosoma* 128 (3). Springer Science and Business Media LLC: 199–214. doi:10.1007/s00412-019-00692-x.

Cai, Xue, Fugui Dong, Richard E. Edelmann, and Christopher A. Makaroff. 2003. “The Arabidopsis SYN1 Cohesin Protein Is Required for Sister Chromatid Arm Cohesion and Homologous Chromosome Pairing.” *Journal of Cell Science* 116 (Pt 14). The Company of Biologists: 2999–3007. doi:10.1242/jcs.00601.

Callis, J., M. Fromm, and V. Walbot. 1987. “Introns Increase Gene Expression in Cultured Maize Cells.” *Genes & Development* 1 (10). Cold Spring Harbor Laboratory: 1183–1200. doi:10.1101/gad.1.10.1183.

Casas-Mollano, Juan A., Nga T. Lao, and Tony A. Kavanagh. 2006. “Intron-Regulated Expression of SUVH3, an Arabidopsis Su(Var)3-9 Homologue.” *Journal of Experimental Botany* 57 (12). Oxford University Press (OUP): 3301–11. doi:10.1093/jxb/erl093.

Chen, Hanchen, Chengpeng He, Chongyang Wang, Xuanpeng Wang, Fengyin Ruan, Junjie Yan, Ping Yin, Yingxiang Wang, and Shunping Yan. 2021. “RAD51 Supports DMC1 by Inhibiting the SMC5/6 Complex during Meiosis.” *The Plant Cell* 33 (8). Oxford University Press (OUP): 2869–82. doi:10.1093/plcell/koab136.

Chu, Diana S., and Diane C. Shakes. 2013. “Spermatogenesis.” *Advances in Experimental Medicine and Biology* 757: 171–203. doi:10.1007/978-1-4614-4015-4_7.

Colomina, N., E. Garí, C. Gallego, E. Herrero, and M. Aldea. 1999. “G1 Cyclins Block the Ime1 Pathway to Make Mitosis and Meiosis Incompatible in Budding Yeast.” *The EMBO Journal* 18 (2). Wiley: 320–29. doi:10.1093/emboj/18.2.320.

Cromer, Laurence, Sylvie Jolivet, Christine Horlow, Liudmila Chelysheva, Jefri Heyman, Geert De Jaeger, Csaba Koncz, Lieven De Veylder, and Raphael Mercier. 2013. “Centromeric Cohesion Is Protected Twice at Meiosis, by SHUGOSHINs at Anaphase I and by PATRONUS at Interkinesis.” *Current Biology: CB* 23 (21). Elsevier BV: 2090–99. doi:10.1016/j.cub.2013.08.036.

Cromer, Laurence, Mariana Tiscareno-Andrade, Sandrine Lefranc, Aurélie Chambon, Aurélie Hurel, Manon Brogniez, Julie Guérin, et al. 2024. “Rapid Meiotic Prophase Chromosome Movements in Arabidopsis Thaliana Are Linked to Essential Reorganization at the Nuclear Envelope.” *Nature Communications* 15 (1). Springer Science and Business Media LLC: 5964. doi:10.1038/s41467-024-50169-4.

Da Ines, Olivier, Jeanne Bazile, Maria E. Gallego, and Charles I. White. 2022. “DMC1 Attenuates RAD51-Mediated Recombination in Arabidopsis.” *PLoS Genetics* 18 (8). Public Library of Science (PLoS): e1010322. doi:10.1371/journal.pgen.1010322.

Damgaard, Christian Kroun, Søren Kahns, Søren Lykke-Andersen, Anders Lade Nielsen, Torben Heick Jensen, and Jørgen Kjems. 2008. “A 5’ Splice Site Enhances the Recruitment of Basal Transcription Initiation Factors in Vivo.” *Molecular Cell* 29 (2). Elsevier BV: 271–78. doi:10.1016/j.molcel.2007.11.035.

Dawe, R. Kelly. 1998. “Meiotic Chromosome Organization and Segregation in Plants.” *Annual Review of Plant Physiology and Plant Molecular Biology* 49 (1). Annual Reviews: 371–95. doi:10.1146/annurev.arplant.49.1.371.

Desimio, Maria Giovanna, Eleonora Cesari, Maria Sorrenti, Massimo De Felici, and Donatella Farini. 2021. “Stimulated by Retinoic Acid Gene 8 (STRA8) Interacts with the Germ Cell Specific BHLH Factor SOHLH1 and Represses c-KIT Expression in Vitro.” *Journal of Cellular and Molecular Medicine* 25 (1). Wiley: 383–96. doi:10.1111/jcmm.16087.

Drouaud, Jan, Raphaël Mercier, Liudmila Chelysheva, Aurélie Bérard, Matthieu Falque, Olivier Martin, Vanessa Zanni, Dominique Brunel, and Christine Mézard. 2007. “Sex-Specific Crossover Distributions and Variations in Interference Level along Arabidopsis Thaliana Chromosome 4.” *PLoS Genetics* 3 (6). Public Library of Science (PLoS): e106. doi:10.1371/journal.pgen.0030106.

Dukowic-Schulze, Stefanie, and Changbin Chen. 2014. “The Meiotic Transcriptome Architecture of Plants.” *Frontiers in Plant Science* 5 (June). Frontiers Media SA: 220. doi:10.3389/fpls.2014.00220.

Durand, Stéphanie, Qichao Lian, Victor Solier, Joiselle Blanche Fernandes, and Raphael Mercier. 2025. “MutLγ Enforces Meiotic Crossovers in Arabidopsis Thaliana.” *Nucleic Acids Research* 53 (5). doi:10.1093/nar/gkaf157.

Dwyer, Katherine, Neha Agarwal, Lori Pile, and Athar Ansari. 2021. “Gene Architecture Facilitates Intron-Mediated Enhancement of Transcription.” *Frontiers in Molecular Biosciences* 8 (April). Frontiers Media SA: 669004. doi:10.3389/fmolb.2021.669004.

Fabritius, Amy S., Marina L. Ellefson, and Francis J. McNally. 2011. “Nuclear and Spindle Positioning during Oocyte Meiosis.” *Current Opinion in Cell Biology* 23 (1). Elsevier BV: 78–84. doi:10.1016/j.ceb.2010.07.008.

Fiszbein, Ana, Keegan S. Krick, and Christopher B. Burge. 2019. “Exon-Mediated Activation of Transcription Starts.” *BioRxiv*. bioRxiv. doi:10.1101/565184.

Furger, Andre, Justin M. O’Sullivan, Alexandra Binnie, Barbara A. Lee, and Nick J. Proudfoot. 2002. “Promoter Proximal Splice Sites Enhance Transcription.” *Genes & Development* 16 (21). Cold Spring Harbor Laboratory: 2792–99. doi:10.1101/gad.983602.

Gallegos, Jenna E., and Alan B. Rose. 2017. “Intron DNA Sequences Can Be More Important than the Proximal Promoter in Determining the Site of Transcript Initiation.” *The Plant Cell* 29 (4): 843–53. doi:10.1105/tpc.17.00020.

Gallegos, Jenna E., and Alan B. Rose. 2019. “An Intron-Derived Motif Strongly Increases Gene Expression from Transcribed Sequences through a Splicing Independent Mechanism in Arabidopsis Thaliana.” *Scientific Reports* 9 (1). Springer Science and Business Media LLC: 13777. doi:10.1038/s41598-019-50389-5.

Gao, Jingyi, Yiwen Qin, and John C. Schimenti. 2024. “Gene Regulation during Meiosis.” *Trends in Genetics: TIG* 40 (4): 326–36. doi:10.1016/j.tig.2023.12.006.

Giraut, Laurène, Matthieu Falque, Jan Drouaud, Lucie Pereira, Olivier C. Martin, and Christine Mézard. 2011. “Genome-Wide Crossover Distribution in Arabidopsis Thaliana Meiosis Reveals Sex-Specific Patterns along Chromosomes.” *PLoS Genetics* 7 (11). Public Library of Science (PLoS): e1002354. doi:10.1371/journal.pgen.1002354.

Gorbsky, Gary J. 2015. “The Spindle Checkpoint and Chromosome Segregation in Meiosis.” *The FEBS Journal* 282 (13). Wiley: 2471–87. doi:10.1111/febs.13166.

Grey, Corinne, and Bernard de Massy. 2021. “Chromosome Organization in Early Meiotic Prophase.” *Frontiers in Cell and Developmental Biology* 9 (June). Frontiers Media SA: 688878. doi:10.3389/fcell.2021.688878.

Handel, M. A., and J. J. Eppig. 1998. “Sexual Dimorphism in the Regulation of Mammalian Meiosis.” *Current Topics in Developmental Biology* 37: 333–58. doi:10.1016/s0070-2153(08)60179-9.

Higgins, James D., Susan J. Armstrong, F. Christopher H. Franklin, and Gareth H. Jones. 2004. “The Arabidopsis MutS Homolog AtMSH4 Functions at an Early Step in Recombination: Evidence for Two Classes of Recombination in Arabidopsis.” *Genes & Development* 18 (20). Cold Spring Harbor Laboratory: 2557–70. doi:10.1101/gad.317504.

Higgins, James D., Eugenio Sanchez-Moran, Susan J. Armstrong, Gareth H. Jones, and F. Chris H. Franklin. 2005. “The Arabidopsis Synaptonemal Complex Protein ZYP1 Is Required for Chromosome Synapsis and Normal Fidelity of Crossing Over.” *Genes & Development* 19 (20). Cold Spring Harbor Laboratory: 2488–2500. doi:10.1101/gad.354705.

Ho, S. H., G. M. So, and K. L. Chow. 2001. “Postembryonic Expression of Caenorhabditis Elegans Mab-21 and Its Requirement in Sensory Ray Differentiation.” *Developmental Dynamics: An Official Publication of the American Association of Anatomists* 221 (4). Wiley: 422–30. doi:10.1002/dvdy.1161.

Hua, Rong, and Mingxi Liu. 2021. “Sexual Dimorphism in Mouse Meiosis.” *Frontiers in Cell and Developmental Biology* 9 (May). Frontiers Media SA: 670599. doi:10.3389/fcell.2021.670599.

Ishiguro, Kei-Ichiro, Kumi Matsuura, Naoki Tani, Naoki Takeda, Shingo Usuki, Mariko Yamane, Michihiko Sugimoto, et al. 2020. “MEIOSIN Directs the Switch from Mitosis to Meiosis in Mammalian Germ Cells.” *Developmental Cell* 52 (4). Elsevier BV: 429-445.e10. doi:10.1016/j.devcel.2020.01.010.

Ishiguro, Kei-Ichiro, and Ryuki Shimada. 2022. “MEIOSIN Directs Initiation of Meiosis and Subsequent Meiotic Prophase Program during Spermatogenesis.” *Genes & Genetic Systems* 97 (1). Genetics Society of Japan: 27–39. doi:10.1266/ggs.21-00054.

Jackson, Neil, Eugenio Sanchez-Moran, Ewen Buckling, Susan J. Armstrong, Gareth H. Jones, and Frederick Christopher Hugh Franklin. 2006. “Reduced Meiotic Crossovers and Delayed Prophase I Progression in AtMLH3-Deficient Arabidopsis.” *The EMBO Journal* 25 (6). Wiley: 1315–23. doi:10.1038/sj.emboj.7600992.

Jiang, Liang, Chunlin Huang, Qiang Sun, Huizhen Guo, Tingcai Cheng, Zhengwen Peng, Yinghui Dang, Weiqiang Liu, Guowen Xu, and Qingyou Xia. 2015. “The 5’-UTR Intron of the Midgut-Specific BmAPN4 Gene Affects the Level and Location of Expression in Transgenic Silkworms.” *Insect Biochemistry and Molecular Biology* 63 (August). Elsevier BV: 1–6. doi:10.1016/j.ibmb.2015.05.005.

Jobert, Laure, Natalia Pinzón, Elodie Van Herreweghe, Beáta E. Jády, Apostolia Guialis, Tamás Kiss, and László Tora. 2009. “Human U1 SnRNA Forms a New Chromatin-Associated SnRNP with TAF15.” *EMBO Reports* 10 (5). EMBO: 494–500. doi:10.1038/embor.2009.24.

Jonsson, J. J., M. D. Foresman, N. Wilson, and R. S. McIvor. 1992. “Intron Requirement for Expression of the Human Purine Nucleoside Phosphorylase Gene.” *Nucleic Acids Research* 20 (12). Oxford University Press (OUP): 3191–98. doi:10.1093/nar/20.12.3191.

Keeney, S., C. N. Giroux, and N. Kleckner. 1997. “Meiosis-Specific DNA Double-Strand Breaks Are Catalyzed by Spo11, a Member of a Widely Conserved Protein Family.” *Cell* 88 (3). Elsevier BV: 375–84. doi:10.1016/s0092-8674(00)81876-0.

Kelly, A. L., A. G. Sharpe, J. H. Nixon, D. J. Lydiate, and E. J. Evans. 1997. “Indistinguishable Patterns of Recombination Resulting from Male and Female Meioses in Brassica Napus (Oilseed Rape).” *Genome* 40 (1). Canadian Science Publishing: 49–56. doi:10.1139/g97-007.

Kianian, Penny M. A., Minghui Wang, Kristin Simons, Farhad Ghavami, Yan He, Stefanie Dukowic-Schulze, Anitha Sundararajan, et al. 2018. “High-Resolution Crossover Mapping Reveals Similarities and Differences of Male and Female Recombination in Maize.” *Nature Communications* 9 (1): 2370. doi:10.1038/s41467-018-04562-5.

Kim, Soojin, Hyunmin Kim, Nova Fong, Benjamin Erickson, and David L. Bentley. 2011. “Pre-MRNA Splicing Is a Determinant of Histone H3K36 Methylation.”

Proceedings of the National Academy of Sciences of the United States of America 108 (33). Proceedings of the National Academy of Sciences: 13564–69. doi:10.1073/pnas.1109475108.

Kociemba, Johanna, Andreas Christ Sølvsten Jørgensen, Nika Tadić, Anthony Harris, Theodora Sideri, Wei Yee Chan, Fairouz Ibrahim, et al. 2024. “Multi-Signal Regulation of the GSK-3β Homolog Rim11 Controls Meiosis Entry in Budding Yeast.” *The EMBO Journal* 43 (15). Springer Science and Business Media LLC: 3256–86. doi:10.1038/s44318-024-00149-7.

Kojima, Mina L., Dirk G. de Rooij, and David C. Page. 2019. “Amplification of a Broad Transcriptional Program by a Common Factor Triggers the Meiotic Cell Cycle in Mice.” *ELife* 8 (February). eLife Sciences Publications, Ltd. doi:10.7554/eLife.43738.

Kowal, Emma J. K., Yuta Sakai, Michael P. McGurk, Zoe J. Pasetsky, and Christopher B. Burge. 2025. “Sequence-Dependent and -Independent Effects of Intron-Mediated Enhancement Learned from Thousands of Random Introns.” *Nucleic Acids Research* 53 (4). doi:10.1093/nar/gkaf097.

Kurzbauer, Marie-Therese, Clemens Uanschou, Doris Chen, and Peter Schlögelhofer. 2012. “The Recombinases DMC1 and RAD51 Are Functionally and Spatially Separated during Meiosis in Arabidopsis.” *The Plant Cell* 24 (5): 2058–70. doi:10.1105/tpc.112.098459.

Kwek, Kon Yew, Shona Murphy, Andre Furger, Benjamin Thomas, William O’Gorman, Hiroshi Kimura, Nick J. Proudfoot, and Alexandre Akoulitchev. 2002. “U1 SnRNA Associates with TFIIH and Regulates Transcriptional Initiation.” *Nature Structural Biology* 9 (11). Springer Science and Business Media LLC: 800–805. doi:10.1038/nsb862.

Lambing, Christophe, Kim Osman, Komsun Nuntasoontorn, Allan West, James D. Higgins, Gregory P. Copenhaver, Jianhua Yang, et al. 2015. “Arabidopsis PCH2 Mediates Meiotic Chromosome Remodeling and Maturation of Crossovers.” *PLoS Genetics* 11 (7). Public Library of Science (PLoS): e1005372. doi:10.1371/journal.pgen.1005372.

Le Hir, H., D. Gatfield, E. Izaurralde, and M. J. Moore. 2001. “The Exon-Exon Junction Complex Provides a Binding Platform for Factors Involved in MRNA Export and Nonsense-Mediated MRNA Decay.” *The EMBO Journal* 20 (17). Wiley: 4987–97. doi:10.1093/emboj/20.17.4987.

Le Hir, Hervé, Ajit Nott, and Melissa J. Moore. 2003. “How Introns Influence and Enhance Eukaryotic Gene Expression.” *Trends in Biochemical Sciences* 28 (4). Elsevier BV: 215–20. doi:10.1016/S0968-0004(03)00052-5.

Lee, R. H., and S. M. Honigberg. 1996. “Nutritional Regulation of Late Meiotic Events in Saccharomyces Cerevisiae through a Pathway Distinct from Initiation.” *Molecular and Cellular Biology* 16 (6). Informa UK Limited: 3222–32. doi:10.1128/MCB.16.6.3222.

Lin, Shengrong, Gabriela Coutinho-Mansfield, Dong Wang, Shatakshi Pandit, and Xiang-Dong Fu. 2008. “The Splicing Factor SC35 Has an Active Role in Transcriptional Elongation.” *Nature Structural & Molecular Biology* 15 (8). Springer Science and Business Media LLC: 819–26. doi:10.1038/nsmb.1461.

Liu, Jingjing, and Li-Jia Qu. 2008. “Meiotic and Mitotic Cell Cycle Mutants Involved in Gametophyte Development in Arabidopsis.” *Molecular Plant* 1 (4). Elsevier BV: 564–74. doi:10.1093/mp/ssn033.

Londoño-Vásquez, Daniela, Katherine Rodriguez-Lukey, Susanta K. Behura, and Ahmed Z. Balboula. 2022. “Microtubule Organizing Centers Regulate Spindle Positioning in Mouse Oocytes.” *Developmental Cell* 57 (2). Elsevier BV: 197-211.e3. doi:10.1016/j.devcel.2021.12.011.

Luehrsen, K. R., and V. Walbot. 1991. “Intron Enhancement of Gene Expression and the Splicing Efficiency of Introns in Maize Cells.” *Molecular & General Genetics: MGG* 225 (1). Springer Science and Business Media LLC: 81–93. doi:10.1007/bf00282645.

Lutz, C. S., K. G. Murthy, N. Schek, J. P. O’Connor, J. L. Manley, and J. C. Alwine. 1996. “Interaction between the U1 SnRNP-A Protein and the 160-KD Subunit of Cleavage-Polyadenylation Specificity Factor Increases Polyadenylation Efficiency in Vitro.” *Genes & Development* 10 (3). Cold Spring Harbor Laboratory: 325–37. doi:10.1101/gad.10.3.325.

Makrantoni, Vasso, and Adele L. Marston. 2018. “Cohesin and Chromosome Segregation.” *Current Biology: CB* 28 (12). Elsevier BV: R688–93. doi:10.1016/j.cub.2018.05.019.

Mascarenhas, D., I. J. Mettler, D. A. Pierce, and H. W. Lowe. 1990. “Intron-Mediated Enhancement of Heterologous Gene Expression in Maize.” *Plant Molecular Biology* 15 (6). Springer Nature America, Inc: 913–20. doi:10.1007/bf00039430.

McCracken, Susan, Mark Lambermon, and Benjamin J. Blencowe. 2002. “SRm160 Splicing Coactivator Promotes Transcript 3’-End Cleavage.” *Molecular and Cellular Biology* 22 (1). American Society for Microbiology: 148–60. doi:10.1128/MCB.22.1.148-160.2002.

Mercier, Raphael, Susan J. Armstrong, Christine Horlow, Neil P. Jackson, Christopher A. Makaroff, Daniel Vezon, Georges Pelletier, Gareth H. Jones, and F. Christopher H. Franklin. 2003. “The Meiotic Protein SWI1 Is Required for Axial Element Formation and Recombination Initiation in Arabidopsis.” *Development (Cambridge, England)* 130 (14): 3309–18. doi:10.1242/dev.00550.

Millhouse, Scott, and James L. Manley. 2005. “The C-Terminal Domain of RNA Polymerase II Functions as a Phosphorylation-Dependent Splicing Activator in a Heterologous Protein.” *Molecular and Cellular Biology* 25 (2). Informa UK Limited: 533–44. doi:10.1128/MCB.25.2.533-544.2005.

Mimura, Manaki, Seijiro Ono, and Ken-Ichi Nonomura. 2021. “Rice MEL2 Regulates the Timing of Meiotic Transition as a Component of Cytoplasmic RNA Granules.” *BioRxiv*. bioRxiv. doi:10.1101/2021.03.24.433842.

Mimura, Manaki, Seijiro Ono, Harsha Somashekar, and Ken-Ichi Nonomura. 2024. “Impact of Protein Domains on the MEL2 Granule, a Cytoplasmic Ribonucleoprotein Complex Maintaining Faithful Meiosis Progression in Rice.” *The New Phytologist* 243 (6). Wiley: 2235–50. doi:10.1111/nph.19968.

Mitchell, A. P., and K. S. Bowdish. 1992. “Selection for Early Meiotic Mutants in Yeast.” *Genetics* 131 (1). Oxford University Press (OUP): 65–72. doi:10.1093/genetics/131.1.65.

Moabbi, Aboudi M., Neha Agarwal, Belal El Kaderi, and Athar Ansari. 2012. “Role for Gene Looping in Intron-Mediated Enhancement of Transcription.” *Proceedings of the National Academy of Sciences of the United States of America* 109 (22). Proceedings of the National Academy of Sciences: 8505–10. doi:10.1073/pnas.1112400109.

Morgan, Chris, John A. Fozard, Matthew Hartley, Ian R. Henderson, Kirsten Bomblies, and Martin Howard. 2021. “Diffusion-Mediated HEI10 Coarsening Can Explain Meiotic Crossover Positioning in Arabidopsis.” *Nature Communications* 12 (1). Springer Science and Business Media LLC: 4674. doi:10.1038/s41467-021-24827-w.

Nan, Guo-Ling, Arnaud Ronceret, Rachel C. Wang, John F. Fernandes, W. Zacheus Cande, and Virginia Walbot. 2011. “Global Transcriptome Analysis of Two Ameiotic1 Alleles in Maize Anthers: Defining Steps in Meiotic Entry and Progression through Prophase I.” *BMC Plant Biology* 11 (August): 120. doi:10.1186/1471-2229-11-120.

Nojima, Takayuki, Kenny Rebelo, Tomás Gomes, Ana Rita Grosso, Nicholas J. Proudfoot, and Maria Carmo-Fonseca. 2018. “RNA Polymerase II Phosphorylated on CTD Serine 5 Interacts with the Spliceosome during Co-Transcriptional Splicing.” *Molecular Cell* 72 (2). Elsevier BV: 369-379.e4. doi:10.1016/j.molcel.2018.09.004.

Nonomura, Ken-Ichi, Mitsugu Eiguchi, Mutsuko Nakano, Kazuya Takashima, Norio Komeda, Satoshi Fukuchi, Saori Miyazaki, Akio Miyao, Hirohiko Hirochika, and Nori Kurata. 2011. “A Novel RNA-Recognition-Motif Protein Is Required for Premeiotic G1/S-Phase Transition in Rice (Oryza Sativa L.).” *PLoS Genetics* 7 (1). Public Library of Science (PLoS): e1001265. doi:10.1371/journal.pgen.1001265.

Oatley, Jon M., and Michael D. Griswold. 2020. “MEIOSIN: A New Watchman of Meiotic Initiation in Mammalian Germ Cells.” *Developmental Cell*. Elsevier BV. doi:10.1016/j.devcel.2020.02.002.

Okkema, P. G., S. W. Harrison, V. Plunger, A. Aryana, and A. Fire. 1993. “Sequence Requirements for Myosin Gene Expression and Regulation in Caenorhabditis Elegans.” *Genetics* 135 (2). Oxford University Press (OUP): 385–404. doi:10.1093/genetics/135.2.385.

Palmiter, R. D., E. P. Sandgren, M. R. Avarbock, D. D. Allen, and R. L. Brinster. 1991. “Heterologous Introns Can Enhance Expression of Transgenes in Mice.” *Proceedings of the National Academy of Sciences of the United States of America* 88 (2). Proceedings of the National Academy of Sciences: 478–82. doi:10.1073/pnas.88.2.478.

Pfaltzgraff, Natalie G., Bingrun Liu, Dirk G. de Rooij, David C. Page, and Maria M. Mikedis. 2024. “Destabilization of MRNAs Enhances Competence to Initiate Meiosis in Mouse Spermatogenic Cells.” *Development (Cambridge, England)* 151 (14). The Company of Biologists. doi:10.1242/dev.202740.

Pochon, Gaetan, Isabelle M. Henry, Chao Yang, Niels Lory, Nadia Fernández-Jiménez, Franziska Böwer, Bingyan Hu, et al. 2023. “The Arabidopsis Hop1

Homolog ASY1 Mediates Cross-over Assurance and Interference." *PNAS Nexus* 2 (3). Oxford University Press (OUP): gac302. doi:10.1093/pnasnexus/pgac302.

Pradillo, Mónica, Eva López, Concepción Romero, Eugenio Sánchez-Morán, Nieves Cuñado, and Juan L. Santos. 2007. "An Analysis of Univalent Segregation in Meiotic Mutants of Arabidopsis Thaliana: A Possible Role for Synaptonemal Complex." *Genetics* 175 (2). Oxford University Press (OUP): 505–11. doi:10.1534/genetics.106.067595.

Rose, A. B., and R. L. Last. 1997. "Introns Act Post-Transcriptionally to Increase Expression of the Arabidopsis Thaliana Tryptophan Pathway Gene PAT1." *The Plant Journal: For Cell and Molecular Biology* 11 (3). Wiley: 455–64. doi:10.1046/j.1365-313x.1997.11030455.x.

Rose, Alan B. 2004. "The Effect of Intron Location on Intron-Mediated Enhancement of Gene Expression in Arabidopsis." *The Plant Journal: For Cell and Molecular Biology* 40 (5). Wiley: 744–51. doi:10.1111/j.1365-313X.2004.02247.x.

Sanchez-Moran, Eugenio, Juan-Luis Santos, Gareth H. Jones, and F. Christopher H. Franklin. 2007. "ASY1 Mediates AtDMC1-Dependent Interhomolog Recombination during Meiosis in Arabidopsis." *Genes & Development* 21 (17). Cold Spring Harbor Laboratory: 2220–33. doi:10.1101/gad.439007.

Shimada, Ryuki, and Kei-Ichiro Ishiguro. 2024. "Female-Specific Mechanisms of Meiotic Initiation and Progression in Mammalian Oocyte Development." *Genes to Cells: Devoted to Molecular & Cellular Mechanisms* 29 (10). Wiley: 797–807. doi:10.1111/gtc.13152.

Shingu, Yoshinori, Tsutomu Mikawa, Mariko Onuma, Takashi Hirayama, and Takehiko Shibata. 2010. "A DNA-Binding Surface of SPO11-1, an Arabidopsis SPO11 Orthologue Required for Normal Meiosis." *The FEBS Journal* 277 (10). Wiley: 2360–74. doi:10.1111/j.1742-4658.2010.07651.x.

Solc, Petr, Richard M. Schultz, and Jan Motlik. 2010. "Prophase I Arrest and Progression to Metaphase I in Mouse Oocytes: Comparison of Resumption of Meiosis and Recovery from G2-Arrest in Somatic Cells." *Molecular Human Reproduction* 16 (9). Oxford University Press (OUP): 654–64. doi:10.1093/molehr/gaq034.

Stacey, Nicola J., Takashi Kuromori, Yoshitaka Azumi, Gethin Roberts, Christian Breuer, Takuji Wada, Anthony Maxwell, Keith Roberts, and Keiko Sugimoto-

Shirasu. 2006. “Arabidopsis SPO11-2 Functions with SPO11-1 in Meiotic Recombination.” *The Plant Journal: For Cell and Molecular Biology* 48 (2). Wiley: 206–16. doi:10.1111/j.1365-313X.2006.02867.x.

Tan-Wong, Sue Mei, Judith B. Zaugg, Jurgi Camblong, Zhenyu Xu, David W. Zhang, Hannah E. Mischo, Aseem Z. Ansari, Nicholas M. Luscombe, Lars M. Steinmetz, and Nick J. Proudfoot. 2012. “Gene Loops Enhance Transcriptional Directionality.” *Science (New York, N.Y.)* 338 (6107). American Association for the Advancement of Science (AAAS): 671–75. doi:10.1126/science.1224350.

Tian, H. 2001. “RNA Ligands Generated against Complex Nuclear Targets Indicate a Role for U1 SnRNP in Co-Ordinating Transcription and RNA Splicing.” *FEBS Letters* 509 (2). Wiley: 282–86. doi:10.1016/s0014-5793(01)03188-x.

Ueki, J., S. Ohta, S. Morioka, T. Komari, S. Kuwata, T. Kubo, and H. Imaseki. 1999. “The Synergistic Effects of Two-Intron Insertions on Heterologous Gene Expression and Advantages of the First Intron of a Rice Gene for Phospholipase D.” *Plant & Cell Physiology* 40 (6). Oxford University Press (OUP): 618–23. doi:10.1093/oxfordjournals.pcp.a029585.

Vrielynck, Nathalie, Marion Peuch, Stéphanie Durand, Qichao Lian, Aurélie Chambon, Aurélie Hurel, Julie Guérin, et al. 2023. “SCEP1 and SCEP2 Are Two New Components of the Synaptonemal Complex Central Element.” *Nature Plants* 9 (12). Springer Science and Business Media LLC: 2016–30. doi:10.1038/s41477-023-01558-y.

Wang, Haiyang, Yizeng Li, Jing Yang, Xing Duan, Petr Kalab, Sean X. Sun, and Rong Li. 2020. “Symmetry Breaking in Hydrodynamic Forces Drives Meiotic Spindle Rotation in Mammalian Oocytes.” *Science Advances* 6 (14). American Association for the Advancement of Science (AAAS): eaaz5004. doi:10.1126/sciadv.aaz5004.

Wang, Yazhong, Willem M. J. van Rengs, Mohd Waznul Adly Mohd Zaidan, and Charles J. Underwood. 2021. “Meiosis in Crops: From Genes to Genomes.” *Journal of Experimental Botany* 72 (18). Oxford University Press (OUP): 6091–6109. doi:10.1093/jxb/erab217.

Watanabe, Yoshinori. 2012. “Geometry and Force behind Kinetochore Orientation: Lessons from Meiosis.” *Nature Reviews. Molecular Cell Biology* 13 (6). Springer Science and Business Media LLC: 370–82. doi:10.1038/nrm3349.

Wiegand, Heather L., Shihua Lu, and Bryan R. Cullen. 2003. “Exon Junction Complexes Mediate the Enhancing Effect of Splicing on MRNA Expression.” *Proceedings of the National Academy of Sciences of the United States of America* 100 (20). Proceedings of the National Academy of Sciences: 11327–32. doi:10.1073/pnas.1934877100.

Xu, Y., H. Yu, and T. C. Hall. 1994. “Rice Triosephosphate Isomerase Gene 5[Prime] Sequence Directs [Beta]-Glucuronidase Activity in Transgenic Tobacco but Requires an Intron for Expression in Rice.” *Plant Physiology* 106 (2). Oxford University Press (OUP): 459–67. doi:10.1104/pp.106.2.459.

Yang, Chao, Yuki Hamamura, Kostika Sofroni, Franziska Böwer, Sara Christina Stolze, Hirofumi Nakagami, and Arp Schnittger. 2019. “SWITCH 1/DYAD Is a WINGS APART-LIKE Antagonist That Maintains Sister Chromatid Cohesion in Meiosis.” *Nature Communications* 10 (1). Springer Science and Business Media LLC: 1755. doi:10.1038/s41467-019-09759-w.

Yang, Chao, Bingyan Hu, Stephan Michael Portheine, Pichaporn Chuenban, and Arp Schnittger. 2020. “State Changes of the HORMA Protein ASY1 Are Mediated by an Interplay between Its Closure Motif and PCH2.” *Nucleic Acids Research* 48 (20). Oxford University Press (OUP): 11521–35. doi:10.1093/nar/gkaa527.

Yang, Chao, Kostika Sofroni, Yuki Hamamura, Bingyan Hu, Hasibe Tunçay Elbasi, Martina Balboni, Lei Chu, Dagmar Stang, Maren Heese, and Arp Schnittger. 2022. “ZYP1-Mediated Recruitment of PCH2 to the Synaptonemal Complex Remodels the Chromosome Axis Leading to Crossover Restriction.” *Nucleic Acids Research* 50 (22). Oxford University Press (OUP): 12924–37. doi:10.1093/nar/gkac1160.

Yang, W. C., D. Ye, J. Xu, and V. Sundaresan. 1999. “The SPOROCYTELESS Gene of Arabidopsis Is Required for Initiation of Sporogenesis and Encodes a Novel Nuclear Protein.” *Genes & Development* 13 (16). Cold Spring Harbor Laboratory: 2108–17. doi:10.1101/gad.13.16.2108.

Yang, Xiaohui, Kingsley A. Boateng, Lara Strittmatter, Rebecca Burgess, and Christopher A. Makaroff. 2009. “Arabidopsis Separase Functions beyond the Removal of Sister Chromatid Cohesion during Meiosis.” *Plant Physiology* 151 (1). American Society of Plant Biologists (ASPB): 323–33. doi:10.1104/pp.109.140699.

Yuan, Xinjie, Bowei Cai, Yuki Hamamura, Arp Schnittger, and Chao Yang. 2025. “SCFRMF-Dependent Degradation of the Nuclear Lamina Releases the Somatic Chromatin Mobility Restriction for Meiotic Recombination.” *Science Advances* 11 (8). American Association for the Advancement of Science (AAAS): eadr4567. doi:10.1126/sciadv.adr4567.

Zamariola, Linda, Nico De Storme, Katrijn Vannerum, Klaas Vandepoele, Susan J. Armstrong, F. Christopher H. Franklin, and Danny Geelen. 2014. “SHUGOSHINs and PATRONUS Protect Meiotic Centromere Cohesion in Arabidopsis Thaliana.” *The Plant Journal: For Cell and Molecular Biology* 77 (5). Wiley: 782–94. doi:10.1111/tpj.12432.

Zhang, Qian, Wenzhe Zhang, Xinyi Wu, Hanni Ke, Yingying Qin, Shidou Zhao, and Ting Guo. 2023. “Homozygous Missense Variant in MEIOSIN Causes Premature Ovarian Insufficiency.” *Human Reproduction (Oxford, England)* 38 (Suppl 2). Oxford University Press (OUP): ii47–56. doi:10.1093/humrep/dead084.

Zickler, D., and N. Kleckner. 1999. “Meiotic Chromosomes: Integrating Structure and Function.” *Annual Review of Genetics* 33: 603–754. doi:10.1146/annurev.genet.33.1.603.

Research Aim

Meiosis is a fundamental process in sexual reproduction, involving one round of DNA replication followed by two rounds of cell division, ensuring genome stability and genetic diversity across generations. Although significant progress has been made in understanding meiosis in plants, many regulatory and cellular aspects remain less explored. In this dissertation, two different aspects of meiosis were investigated in *Arabidopsis thaliana.*

In the first chapter, I focused on how meiosis-specific gene expression is regulated, using the chromosome axis gene *ASY1* as a model. While over 100 meiotic genes have been functionally characterized, the regulatory elements controlling their expression are still poorly understood. The central question of this chapter is whether regulatory mechanisms beyond promoters, particularly whether introns contribute to meiotic gene regulation. This study aims to investigate the role of intron-mediated transcriptional regulation and transcription factors in meiotic gene expression, including potential sex-specific regulatory mechanisms related to female fertility. This work advances our understanding of transcriptional control in meiosis and offers tools for manipulating meiotic gene expression in both basic research and applied science.

The second chapter presents a cytological framework of female meiosis in Arabidopsis by live-cell imaging. While male meiosis has been relatively well studied, female meiosis remains less explored due to the biological complexity and technical limitations. This study aims to develop a live-cell imaging system for visualizing and tracking the progression of female meiosis in real-time. By integrating fluorescent reporters and advanced microscopy techniques, key cytological features and stage-specific landmarks were identified. This framework not only contributes to our understanding of female meiosis but also serves as a practical reference for future study into female meiosis.

Chapter I

Analysis of meiosis-specific gene expression regulation in *Arabidopsis thaliana*

Bingyan Hu[1], Seijiro Ono[1], Mengmeng Chen[1], Yingqi Wang[1], Silja Seemann[1], Maren Hesse[1] and Arp Schnittger[1]*

[1] Department of Developmental Biology, Institute of Plant Science and Microbiology, University of Hamburg, Hamburg, Germany

* Corresponding author. Email: arp.schnittger@uni-hamburg.de

Contributions of authors

All experiments and analyses presented in this chapter were performed exclusively by me, Bingyan Hu, except for those indicated below. I am sincerely grateful to all collaborators for their invaluable contributions to this work.

Dr. Seijiro Ono has generated four empty level-1 modules for the four amiRNAs and the level-2 entry vector to assemble the multiplex amiRNA in a single expression cassette, contributing to Figures 4A and 4 B.

Mengmeng Chen has counted the seed set and pollen viability for several amiREMs lines in *PRO_{ASY1}:intron1-8:CDS_{ASY1}:GFP* reporter, contributing to Figures 5A-B and S7B.

Yingqi Wang has performed the chromosome spreads for the WT and the *PRO_{ASY1}:intron1-8:GFP:CDS_{KNO1}* reporter, partially contributing to Figure 7F.

Silja Seemann has generated the constructs of *PRO_{ASY1}:intron3,5:GFP* and *PRO_{ASY1}:intron3-4:GFP* under my supervision, contributing to Figure S4A.

Maren Hesse contributed to the selection of transcription factors identified by a yeast one-hybrid screen, as shown in Figures S6C and D.

Analysis of meiosis-specific gene expression regulation in *Arabidopsis thaliana*

Abstract

Although meiosis is fundamental to sexual reproduction in eukaryotes, including plants, the regulatory mechanisms governing meiotic gene expression remain poorly understood. In *Arabidopsis thaliana*, the expression patterns of meiotic genes have been characterized using genomic reporter lines, but the contribution of transcriptional control remains unclear. In this study, the regulatory elements required for the meiocyte-specific expression of *ASY1*, a gene encoding a key component of the meiotic chromosome axis, were investigated. It was found that the *ASY1* promoter alone was insufficient to drive meiotic expression. Instead, intron 3-5 and the *ASY1* terminator were required for expression in meiocytes, and further enhanced by the addition of intron 1-2 and intron 6-8. These results suggest that intron-mediated transcriptional regulation may serve as a general principle for the transcriptional control of meiotic genes, which are often intron-rich.

To further investigate the regulatory network controlling *ASY1* expression, a yeast one-hybrid screening was performed. Members of the *REPRODUCTIVE MERISTEM (REM)* gene family were identified as potential regulators of *ASY1*. While single *rem* mutants did not exhibit obvious meiotic defects, multiplex artificial microRNA (amiRNA) was used to silence *REM35*, *REM34*, *REM36*, and *REM37* simultaneously at the time of meiosis. This knockdown led to fertility defects mainly on the female side, suggesting that *REM* genes play an important and previously unrecognized role in *ASY1* expression during female meiosis.

As a proof of concept that misexpression of a protein by an *ASY1*-derived regulatory unit can alter the course of meiosis, KNO1, an interactor of the RTR complex in mitosis, was misexpressed in meiosis using the *ASY1* promoter combined with intron 1-8. The RTR complex acts as an inhibitor of recombination, and *rtr* mutants exhibit reduced fertility and/or chromosome entanglement. Analysis of the transgenic lines showed accumulation of KNO1-GFP in meiocytes, as well as a reduction in fertility and entangled chromosomes, indicating RTR complex reduction or dysfunction in meiocytes due to KNO1 misexpression.

Introduction

Meiosis is a fundamental process for sexual reproduction in eukaryotes, creating genetic diversity through chromosome recombination and ensuring genetic stability across generations by reduction division. Although the process of meiosis is highly conserved, the developmental strategies that govern germline differentiation vary a lot across different species. Unlike animals, where the germline is usually established early in embryogenesis, flowering plants generate the reproductive lineage late in development from somatic cells of the floral organs. At one point, cells of the germline differentiate into pollen mother cells (PMCs) or megaspore mother cells (MMCs) and undergo meiosis, resulting in cells with half the genetic material (spores) that then progress with gametophyte development, forming male and female gametes. This remarkable developmental process requires exact regulation of meiotic genes. Over the past decades of research, more than 100 plant genes involved in meiosis have been functionally studied, including genes involved in sister chromatid cohesion and separation, chromosome pairing and synapsis, recombination, cell cycle control and chromosome distribution (L. Zhang et al. 2018; Thangavel et al. 2023). Understanding how meiotic genes are regulated is crucial for understanding the process of meiosis. However, in plant meiosis, no transcriptional master regulator comparable to yeast IME1 (Kassir, Granot, and Simchen 1988; Nachman, Regev, and Ramanathan 2007; Tam and van Werven 2020), mammalian meiosis initiator (MEIOSIN, Ishiguro et al. 2020; Oatley and Griswold 2020) or Stimulated by Retinoic Acid8 (STRA8, Anderson et al. 2008; Desimio et al. 2021) has yet been identified, highlighting significant gaps in our understanding of how plants initiate meiotic gene expression. This suggests that the transcriptional control of meiotic genes in plants may have evolved differently from that in other organisms.

The first step of gene expression is to initiate transcription, which requires the recruitment of the basal transcription factors (TFs) and RNA polymerase II to the core promoter, where the transcription start site (TSS) is defined (Thomas and Chiang 2006; Danino et al. 2015; Jores et al. 2021). However, the core promoter could usually only activate relatively low expression (Smale and Kadonaga 2003; Andersson and Sandelin 2020). The transcription level can be significantly increased through interactions with transcriptional activators, which bind to regulatory DNA sequences located upstream or downstream of the TSS, and may act across variable genomic

distances (Banerji, Rusconi, and Schaffner 1981; Vernimmen and Bickmore 2015; Ricci et al. 2019; Jores et al. 2021). The promoter is defined as the regulatory region upstream of a gene, and for a long time has been thought to define the expression pattern. However, some studies have shown that for some genes even a complete promoter containing all necessary transcription factor binding sites is not active unless one or more endogenous introns of the gene are present (Callis, Fromm, and Walbot 1987; Emami et al. 2013). This indicates that Introns can enhance transcription in some contexts. For example, there is a conserved intron in the 5' untranslated region (5'UTR) of *Arabidopsis Thaliana* UBIQUITIN 10 (UBQ10) that significantly boosts gene expression (Norris, Meyer, and Callis 1993). Furthermore, when introducing this intron sequence into other gene contexts, it also boosts expression and sometimes even alters tissue specificity (Gallegos and Rose 2019). This is consistent with a previous study analyzing the chromosome axis protein ASY1 in Arabidopsis, which showed that the *ASY1* promoter alone is not sufficient to drive protein expression in meiocytes (Yang, Hu, et al. 2020). Notably, the gene structure of *ASY1* shows it has 21 introns, which is much more than the average of four introns per gene in Arabidopsis (Reddy 2007; Li et al. 2020). Interestingly, other meiotic genes are also characterized by a large number of introns, such as 20 introns in *REC8*, 23 introns in *MSH4*, and 33 introns in *MSH5*. Taken together, these findings suggest that meiotic genes may not only be controlled by promoter-binding transcription factors but might also rely on intron-mediated effects.

Introns can enhance gene expression by acting as classical intragenic enhancers, containing regulatory DNA sequences that recruit transcription factors, which interact with the basal transcription complex to promote gene transcription in specific cell types (Palstra and Grosveld 2012; Kyrchanova and Georgiev 2021; Borsari et al. 2021). This enhancement relies on transcription factors (TFs) binding to DNA segments within introns, known as intronic enhancers, which are similar to classical enhancers and can act independently of genomic distance and orientation relative to the target gene promoter.

In addition to acting as classical enhancers, introns can enhance gene expression through a TF-independent mechanism known as intron-mediated enhancement (IME). In most cases, IME recruits the splicing factors like U1-snRNP to the intron, which binds to the 5' splice site, interacts with RNA polymerase II and other general transcription factors like TFIIH during cotranscriptional splicing to facilitate

initiation and reinitiation of transcription (Tian 2001; Das et al. 2007; Nojima et al. 2018). Beyond promoting transcription initiation, introns also contribute to transcriptional elongation. Splicing factors such as U1-snRNP, SKIP, and SC35, have been found to interact with elongation factors to promote transcriptional elongation (Fong and Zhou 2001; Brès et al. 2005; Lin et al. 2008). The splicing-dependent IME can also be achieved by forming a looped gene structure during transcription. A looped gene architecture formed by the physical interaction between the promoter and terminator in yeast has been proven to enhance transcription by direct recycling of RNA polymerase from the terminator back to the promoter for reinitiation, as well as by reinforcing promoter directionality (Ansari and Hampsey 2005; Tan-Wong et al. 2012; Al Husini, Kudla, and Ansari 2013). In the case of IME, the physical interaction of the promoter-terminator, promoter-5' splice site, and terminator-3' splice site during splicing results in a looped gene architecture, enhancing transcription (Moabbi et al. 2012; Dwyer et al. 2021). Therefore, the IME is a splicing-dependent mechanism mediated by the recruitment of splicing factors or the formation of gene loops to facilitate transcription initiation, elongation, and reinitiation (Moabbi et al. 2012; Shaul 2017).

IME can also be achieved by another poorly understood splicing-independent mechanism related to specific intronic motifs, e.g., TTNGATYTG in Arabidopsis, to enhance mRNA accumulation independent of transcription factors (Gallegos and Rose 2019). This motif only boosts expression when located less than 1 kb downstream of the TSS, not when it is located upstream or far downstream of the TSS. This location-dependency suggests that it does not represent a TF-binding enhancer. Interestingly, the motif enhances mRNA accumulation in a dose-dependent manner, i.e., each copy adds up to 1.5-fold more mRNA, suggesting a cumulative, modular effect (Gallegos and Rose 2019). The motif still enhances mRNA accumulation even if placed in the exons of an intronless construct, which indicates splicing is not required for enhancement (Gallegos and Rose 2019). The activity is from the DNA sequence itself, not the splicing process (Gallegos and Rose 2019). There are some hypotheses about the possible mechanisms, but the exact molecular mechanism remains unclear (Gallegos and Rose 2019).

According to current research, there is no single, universal explanation for how introns influence gene expression. Instead, each intron may follow its unique mixture of mechanisms that together lead to the observed effect (Shaul 2017).

Given the well-described expression pattern of *ASY1* in meiosis, its intron-rich gene structure and the observation that its promoter is insufficient to drive expression in meiosis, ASY1 was chosen in this study as a model to investigate if and to what degree introns are relevant for gene regulation in meiocytes.

To test the role of *ASY1* introns in meiotic expression, various *ASY1* constructs with different intron combinations were generated. While deleting the first eight introns disrupted *ASY1* meiotic expression and function, the single deletion of these eight introns had little effect, indicating a cumulative function of the introns. The *ASY1* promoter plus the 5'UTR in combination with intron 3-5 and *ASY1* terminator was identified as the shortest functional combination that restored GFP expression in male meiocytes. However, the construct only worked when the introns were within the transcribed region. Yeast one-hybrid screens identified REM transcription factors, particularly REM35 and its homologs, as potential regulators of intron-mediated expression in meiocytes. Silencing REMs in a partially rescued *asy1* background significantly reduced fertility, especially in female development, suggesting an important role of REMs in female meiosis. These results indicate that *ASY1* introns function through both IME and enhancer-like mechanisms to drive robust meiotic expression. Furthermore, I used this meiotic expression system to mis-express the mitotic gene *KNO1* in meiocytes. KNO1 is an interactor of the RTR-complex, an inhibitor of homologous recombination, and its expression in meiosis resulted in fertility defects with slightly increased crossovers and chromosome entanglement, resembling the phenotypes of RTR-complex mutants such as *rmi1* and *top3a*, suggesting the reduction or dysfunction of the RTR-complex in meiocytes.

Results

Introns contribute to *ASY1* expression

A previous study on the closure motif of ASY1, a region needed for protein-protein interaction, demonstrated that using the *ASY1* promoter including the 5'UTR (here PRO_{ASY1} for short) to drive expression of an ASY1closure motif-GFP fusion (PRO_{ASY1}*:closure:GFP*) did not result in GFP fluorescence in the male meiocytes (Yang, Hu, et al. 2020). To determine if this lack of signal was related to the motif being out of context, two reporters were created: PRO_{ASY1}*:*CDS_{ASY1}*:GFP*, a C-terminal fusion of *GFP* to the coding sequence of *ASY1* under control of the *ASY1* promoter, and PRO_{ASY}*:GFP*, where the *ASY1* promoter was used to drive *GFP* only. However, neither of these constructs showed any visible *GFP* expression in male meiocytes (Figure 1B, 2B), and introducing PRO_{ASY1}*:*CDS_{ASY1}*:GFP* into the *asy1* null mutant failed to rescue the *asy1* mutant phenotype (Figure 1C). Since the genomic reporter of *ASY1*, PRO_{ASY1}*:ASY1:GFP,* is functional and produces a strong ASY1-GFP signal in male meiocytes (Yang et al. 2019, Figure 1B), these results suggest that introns are essential for proper ASY1 expression.

A previous study demonstrated that introns located near the transcriptional start site (TSS) can increase mRNA accumulation, resulting in enhanced gene expression compared to introns positioned farther away (Rose 2004). The *ASY1* genomic sequence contains 21 introns, with intron 8 being the largest and intron 2 the second largest. To determine which intron or introns contribute to ASY1 expression in the meiocyte, intron 1 to intron 8 were individually deleted from the *ASY1* genomic sequence. The imaging results, showing strong ASY1-GFP fluorescence in male meiocytes for all constructs, indicate that *ASY1* expression remains unaffected. All single intron deletion constructs can rescue the *asy1* fertility defect, confirming that sufficient functional ASY1 can be produced even when one of these introns is absent (Figure S1, Table 1).

Since deletion of a single intron was insufficient to affect ASY1 function, both intron 1 and intron 2 were deleted from the *ASY1* genomic sequence as well. Nevertheless, the resulting construct was still able to rescue the *asy1* mutant phenotype, and the fluorescence of ASY1-GFP remained unaffected (Figure 1A-C, Table 1). However, when all eight introns were deleted simultaneously, the expression

of ASY1 was lost, and the construct could no longer rescue the asy1 fertility defect (Figure 1A-C, Table 1). These results indicate that some introns of intron 1-8 work together to support *ASY1* expression in the male meiocyte.

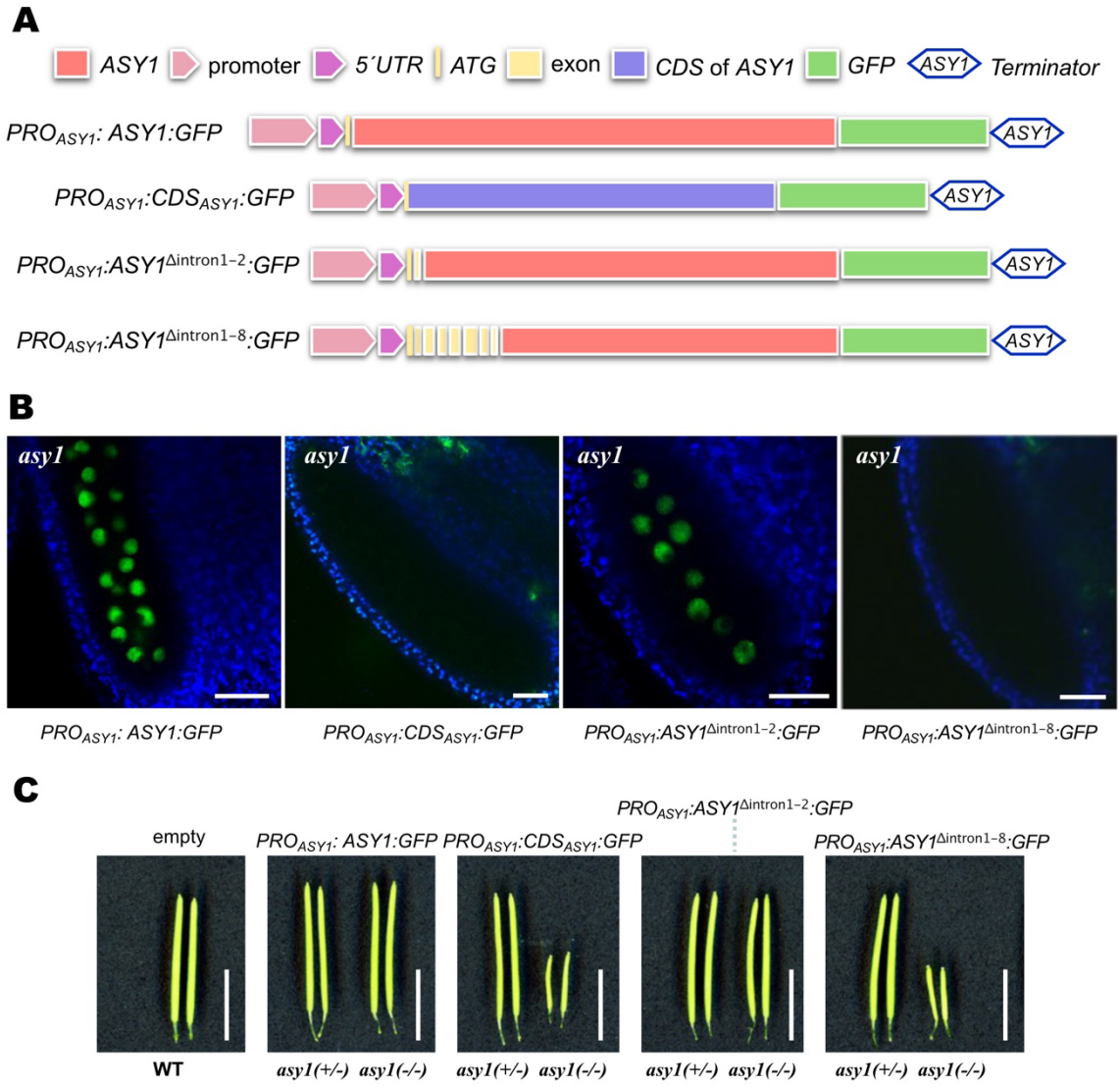

Figure 1. Intron 1-8 contributes to the *ASY1* expression in the male meiocyte. (A) Schematic representation of four different *ASY1-GFP* constructs. For simplicity the exon-intron structure of the genomic fragments is not indicated. Yellow boxes indicate fused exons, i.e., where the intervening introns have been deleted **(B)** GFP-signal in anthers of *asy1* mutants expressing *ASY1:GFP, PRO_{ASY1}:CDS_{ASY1}:GFP, PRO_{ASY1}:$ASY1^{\Delta intron1-2}$:GFP, and PRO_{ASY1}:$ASY1^{\Delta intron1-8}$:GFP*, respectively, detected by confocal microscopy. Scale bar: 20 µm. **(C)** Siliques of WT and siliques of plants expressing *PRO_{ASY1}:ASY1:GFP, PRO_{ASY1}:CDS_{ASY1}:GFP, PRO_{ASY1}:$ASY1^{\Delta intron1-2}$:GFP, and PRO_{ASY1}:$ASY1^{\Delta intron1-8}$:GFP* in both *asy1+/-* and *asy1-/-* background. Scale bar: 1 cm.

A combination of *ASY1* promoter, 5'UTR/ATG, intron 3-5, and *ASY1* terminator is sufficient for *GFP* expression in meiocytes

To test if intron 1-8 instead of a promoter would even be sufficient to promote gene expression in meiocytes, the construct *5'UTR$_{ASY1}$: intron1-8: GFP* was generated and transformed into WT plants. However, no GFP could be detected in the male meiocyte (Figure 2A-B, Table 2). Only after adding 318 bp promoter sequence to the construct, *GFP* expression could be observed in both the cytoplasm and the nucleus of meiocytes, reflecting the behavior of free unfused GFP (Figure 2A-B, Table 2). The respective construct was called *PRO$_{ASY1}$:intron1-8:GFP*. It is to note that the exon coding for the *5'UTR* also included the *ATG* of *ASY1*, i.e., *PRO$_{ASY}$* in this study designates a 318 bp promoter fragment plus the *5'UTR* and the *ATG* of *ASY1*.

Next, I wondered if the concatenated introns in construct *PRO$_{ASY}$:intron1-8:GFP* would be removed from precursor mRNA (pre-mRNA) during splicing. To find out the mRNA structure of this meiosis-specific reporter, I performed 5'RACE (Rapid Amplification of cDNA Ends) on *PRO$_{ASY1}$:intron1-8:GFP* transcripts. After sequencing the RACE products and aligning them to genomic DNA (gDNA), we identified different 5' end locations and different mRNA structures. Only 11 out of 26 fragments indicated that transcription started from the beginning of the *5'UTR* as expected (Figure S2), while the latter RACE products were shorter, which might reflect the actual transcripts or technical problems. However, in none of the 26 transcripts all introns were spliced out completely, but the splicing pattern was rather diverse. For example, 9 transcripts retained the same part of intron 3, and in 16 transcripts, intron 6 was still present. However, also parts of other introns occasionally seemed to be part of the mature mRNA (Figure S2). These results indicate that the splicing machinery generates a plethora of different mRNAs from the *PRO$_{ASY1}$:intron1-8:GFP,* at least some of which get translated into functional GFP.

Seeing that half of the RACE fragments that did not contain the known *5'UTR* of *ASY1*, I wondered if hidden promoter sequences might be present in the intron regions. In plants, several short motifs in the core promoter region are known to enhance gene expression, such as the TC motif and the Y patch (pyrimidine patch). By sequence analysis, I found out that there is a sequence with similarity to a Y patch in intron 5. Therefore, I deleted the Y patch in intron 5 from the *PRO$_{ASY1}$:intron1-8:GFP*

reporter. However, this deletion did not change the *GFP* expression in meiocytes (Figure S3A-B, Table 2).

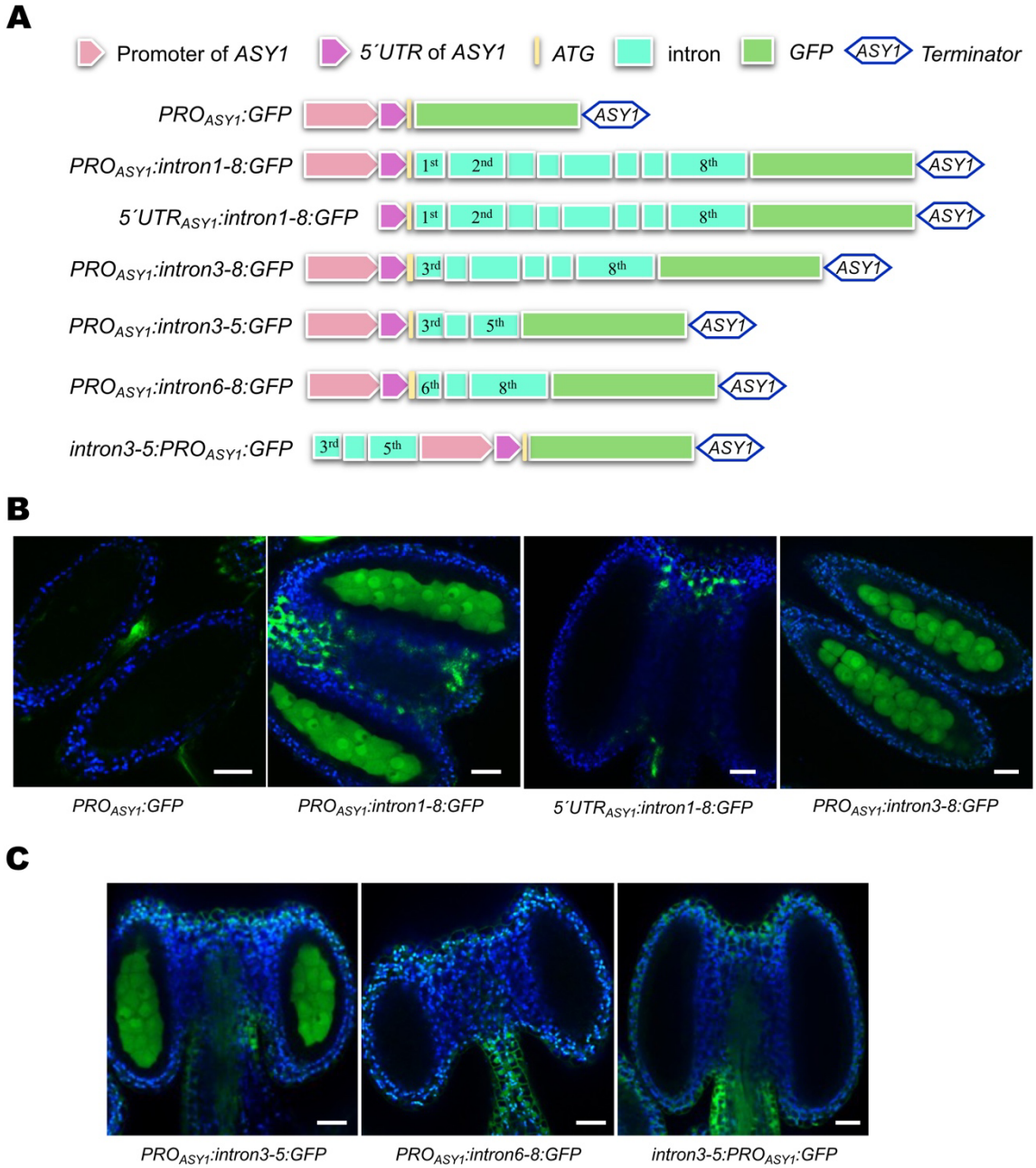

Figure 2. Intron3-5 promote *GFP* expression in the meiocyte and need to be positioned after the *ASY1* promoter. (A) Schematic representation of 7 different constructs where *GFP* was combined with the *ASY1* promoter and introns in different arrangements. **(B)** Expression of *PROASY1:GFP, PROASY1:intron1-8:GFP, 5'UTRASY1:intron1-8:GFP,* and *PROASY1:intron3-8:GFP* in the male meiocytes of WT background using confocal microscopy. Scale bar: 20 μm. **(C)** Expression of *PROASY1:intron3-5:GFP, PROASY1:intron6-8:GFP*, and *intron3-5:PROASY1:GFP* in the anthers of WT background using confocal microscopy. Scale bar: 20 μm.

To determine the shortest combination of introns that contributes to *ASY1* meiocyte expression, intron 1 and intron 2 were further deleted from the *PRO$_{ASY1}$:intron1-8:GFP* construct. The *GFP* expression pattern of *PRO$_{ASY1}$:intron3-8:GFP* remained unchanged. However, when the remaining construct *PRO$_{ASY1}$:intron3-8:GFP* was further divided into *PRO$_{ASY1}$:intron3-5:GFP* and *PRO$_{ASY1}$:intron6-8:GFP*, the free GFP expression in the male meiocyte was retained in the *PRO$_{ASY1}$:intron3-5:GFP* expressing plants, while no GFP signal was detected using the *PRO$_{ASY1}$:intron6-8:GFP* reporter (Figure 2C, Table 2). Furthermore, intron 3, intron 4, and intron 5 were deleted individually from the *PRO$_{ASY1}$: intron3-5: GFP* reporter construct. All three of the resulting constructs expressed GFP extremely weakly in the meiocyte (Figure S4, Table 2), which implies that all three introns contribute to enhancing gene expression in the meiocyte. In an attempt to further minimize the expression construct, I also generated a reporter using only a minimal promoter with only one CAAT box combined with the introns 3-5, i.e., *CAAT:5´UTR$_{ASY1}$:intron3-5:GFP*, but no GFP was detectable in the male meiocyte of plants expressing this construct (Figure S5A-B). Since all the constructs we generated so far were using the same *ASY1* terminator, the terminator of *ASY1* from *PRO$_{ASY1}$:intron3-5:GFP* was changed to the NOS terminator, and the *PRO$_{ASY1}$:intron3-5:GFP:TER$_{NOS}$* reporter was transformed into WT, resulting in extremely weak GFP expression in the anthers (Figure S5A-B). This implies the ASY1 terminator also contributes to the enhancement of meiotic expression.

Finally, I also deleted the Y patch from intron 5 of *PRO$_{ASY1}$:intron3-5:GFP* reporters. However, the expression of GFP remained unchanged in the meiocytes in the respective transgenic plants (Figure S3A-B, Table 2).

The position of introns is essential for meiosis-specific expression

After having defined the minimal number of introns needed for strong *GFP* expression in meiocytes, I wondered if the position of introns would affect gene expression. Thus, the intron and promoter position of *PRO$_{ASY1}$:intron3-5:GFP* was swapped and the resulting vector *intron3-5:PRO$_{ASY1}$:GFP* was analyzed in WT plants. The transformants did not show any GFP expression in the meiocyte, but the anther filament and epidermis cells showed residual GFP expression, which is occasionally also seen in the other lines (Figure 2C). This indicates that the meiocyte-specific gene

expression regulated by introns is dependent on the position of the introns. The introns do not function as meiosis-specific expression elements when placed upstream of the promoter, i.e. outside of the transcribed region, which is consistent with the nature of IME (Gallegos and Rose 2017). Thus, the shortest regulatory unit identified, conferring meiocyte expression of GFP is *ASY1* intron 3-5 placed downstream of a fragment consisting of 318 bp *ASY1* promotor plus *ASY1*'s first exon (*5'UTR* + ATG) and the *ASY1* terminator.

Inton1-8 and intron3-5 meditated *ASY1* expression rescue the *asy1* fertility defects to different degrees

When comparing the fluorescence strength of the different reporter lines, the GFP expression level in PRO_{ASY1}*:intron3-5:GFP* lines was notably lower than that in PRO_{ASY1}*:intron1-8:GFP* lines (Figure 2B-C). This suggests that introns 1-2 and/or 6-8 contribute to increased gene expression. At this point, I wondered which artificial regulatory unit would be sufficient to drive *ASY1* expression strong enough for *asy1* mutant rescue. To test this, the coding sequence of *ASY1* was added before *GFP*, resulting in the reporter PRO_{ASY1}*:intron1-8:*CDS_{ASY1}*:GFP* which I then expressed in the *asy1* mutant background. Indeed, despite the introns not being in their original positions within the *ASY1* sequence, the construct still produced enough functional ASY1 in meiocytes to significantly rescue the fertility defects associated with the *asy1* mutation (Figure 3B-F). Also the shorter version PRO_{ASY1}*:intron3-5:*CDS_{ASY1}*:GFP* could restore ASY1-GFP expression in the nucleus, however a visibly lower GFP signal in these transgenic plants indicated a lower ASY1 level, and consistently the fertility defects of the *asy1* mutant were rescued to a lower extend compared to PRO_{ASY1}*:intron1-8:*CDS_{ASY1}*:GFP* expressing plants as measured by fluorescence intensity and seed setting rate, respectively (Figure 3B-F).

Table 1. Summary of different versions of *ASY1* coding sequence containing constructs used in this study.

Constructs	Background	Source	Subcellular localization	Functionality
PRO_{ASY1}*:ASY1:GFP*	WT and *asy1*	From (Yang et al. 2020)	Nucleus	Functional
PRO_{ASY1}*:*CDS_{ASY1}*:GFP*	*asy1*	This study	Nucleus	Non-functional
PRO_{ASY1}*:ASY1*$^{\Delta intron1}$*:GFP*	*asy1*	This study	No expression	Non-functional
PRO_{ASY1}*:ASY1*$^{\Delta intron2}$*:GFP*	*asy1*	This study	Nucleus	Functional
PRO_{ASY1}*:ASY1*$^{\Delta intron3}$*:GFP*	*asy1*	This study	Nucleus	Functional
PRO_{ASY1}*:ASY1*$^{\Delta intron4}$*:GFP*	*asy1*	This study	Nucleus	Functional
PRO_{ASY1}*:ASY1*$^{\Delta intron5}$*:GFP*	*asy1*	This study	Nucleus	Functional
PRO_{ASY1}*:ASY1*$^{\Delta intron6}$*:GFP*	*asy1*	This study	Nucleus	Functional
PRO_{ASY1}*:ASY1*$^{\Delta intron7}$*:GFP*	*asy1*	This study	Nucleus	Functional
PRO_{ASY1}*:ASY1*$^{\Delta intron8}$*:GFP*	*asy1*	This study	Nucleus	Functional
PRO_{ASY1}*:ASY1*$^{\Delta intron1\text{-}2}$*:GFP*	*asy1*	This study	Nucleus	Functional
PRO_{ASY1}*:ASY1*$^{\Delta intron1\text{-}8}$*:GFP*	*asy1*	This study	No expression	Non-functional
PRO_{ASY1}*:intron1-8:*CDS_{ASY1}*:GFP*	*asy1*	This study	Nucleus	Functional
PRO_{ASY1}*:intron3-5:*CDS_{ASY1}*:GFP*	*asy1*	This study	Nucleus	Functional

Table 2. Summary of different versions of GFP-only constructs used in this study.

Constructs	Background	Source	GFP subcellular localization in meiocytes
PRO_{ASY1}:GFP	WT	This study	No expression
PRO_{ASY1}:intron1-8:GFP	WT	This study	Nucleus and cytoplasm
PRO_{ASY1}:intron3-8:GFP	WT	This study	Nucleus and cytoplasm
PRO_{ASY1}:intron3-5:GFP	WT	This study	Nucleus and cytoplasm
PRO_{ASY1}:intron6-8:GFP	WT	This study	No expression
PRO_{ASY1}:intron3-5$^{\Delta Y\ patch}$:GFP	WT	This study	Nucleus and cytoplasm
PRO_{ASY1}:intron1-8$^{\Delta Y\ patch}$:GFP	WT	This study	Nucleus and cytoplasm
Intron3-5:PRO_{ASY1}:GFP	WT	This study	No expression
PRO_{ASY1}:intron4-5:GFP	WT	This study	Extremely weak nucleus and cytoplasm
PRO_{ASY1}:intron3,5:GFP	WT	This study	Extremely weak nucleus and cytoplasm
PRO_{ASY1}:intron3-4:GFP	WT	This study	Extremely weak nucleus and cytoplasm
5´UTR_{ASY1}:intron1-8:GFP	WT	This study	No expression
$CAAT_{ASY1}$:5'UTR_{ASY1}:intron3-5:GFP	WT	This study	Extremely weak nucleus and cytoplasm
PRO_{ASY1}:intron3-5:GFP:TER_{NOS}	WT	This study	Extremely weak nucleus and cytoplasm

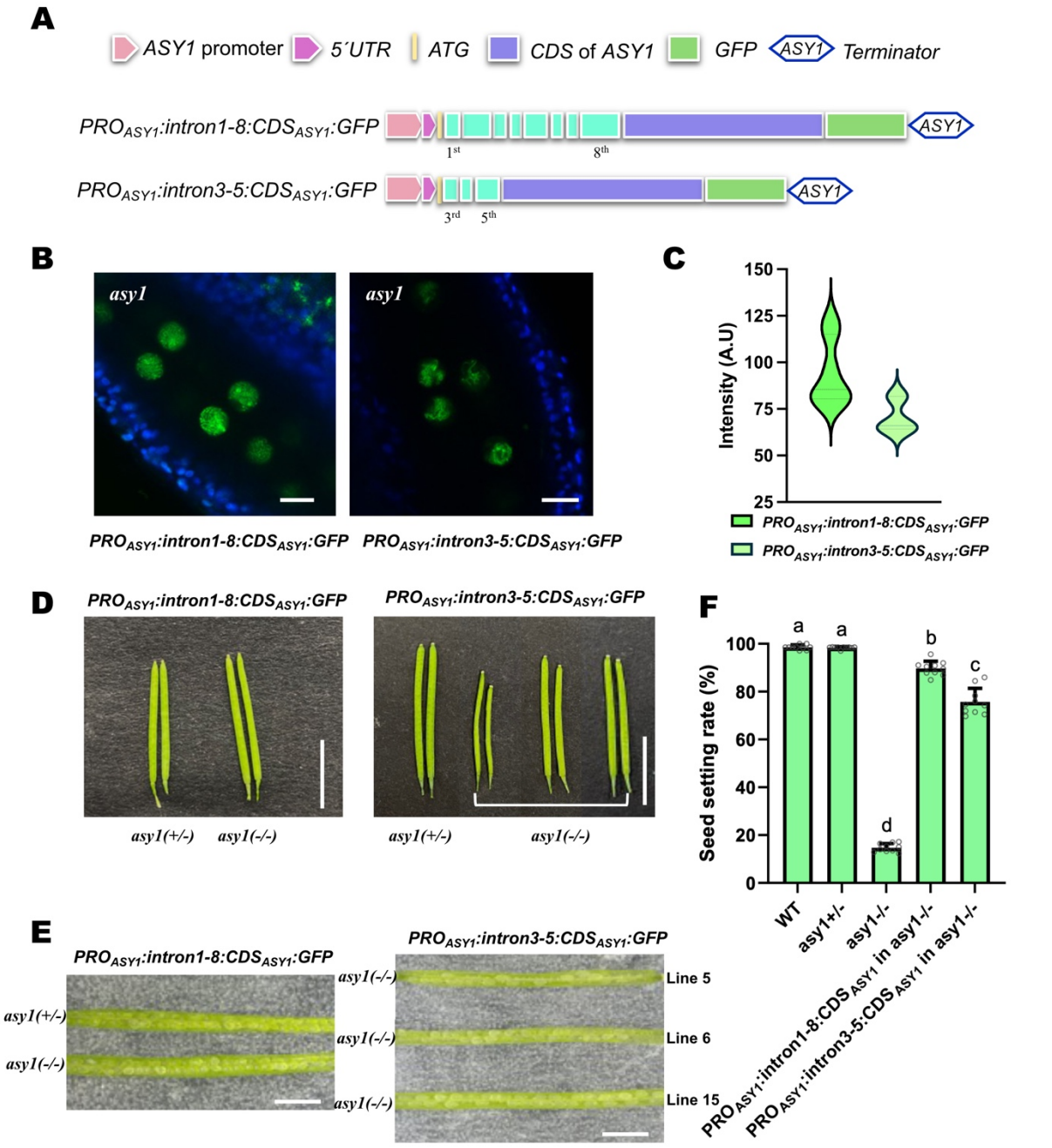

Figure 3. Partial rescue of the *asy1* fertility defect by *PRO$_{ASY1}$:intron1-8:CDS$_{ASY1}$:GFP* and *PRO$_{ASY1}$:intron3-5:CDS$_{ASY1}$:GFP*. **(A)** Schematic representation of 2 constructs where *ASY1-GFP* was driven by different *ASY1* promoter-intron combinations. **(B)** Localization of GFP in anthers of *PRO$_{ASY1}$:intron1-8:CDS$_{ASY1}$:GFP* and *PRO$_{ASY1}$:intron3-5:CDS$_{ASY1}$:GFP* transgenic plants in *asy1* background as detected by confocal microscopy. Scale bar: 10 μm. **(C)** Fluorescence intensity measurements of male meiocyte nuclei as shown in (B). Seven nuclei were measured per line. Scale bar: 10 μm. **(D)** Siliques of plants expressing *PRO$_{ASY1}$:intron1-8:CDS$_{ASY1}$:GFP* and *PRO$_{ASY1}$:intron3-5:CDS$_{ASY1}$:GFP* in both *asy1+/-* and *asy1-/-* background. Scale bar: 1cm. **(E)** Seeds/non-fertilized ovules of plants expressing *PRO$_{ASY1}$:intron1-8:CDS$_{ASY1}$:GFP* and *PRO$_{ASY1}$:intron3-5:CDS$_{ASY1}$:GFP* in both *asy1+/-* and *asy1-/-* background. Scale bar: 2 mm. **(F)** Seed setting rate of Arabidopsis WT, *asy1+/-*, *asy1-/-*, *PRO$_{ASY1}$:intron1-8:CDS$_{ASY1}$:GFP* in *asy1-/-* background and *PRO$_{ASY1}$:intron3-5:CDS$_{ASY1}$:GFP*

in *asy1-/-* background. Data are presented as individual values (dots) and mean ± SD. Ten individual plants were counted per line. Groups labeled with different lowercase letters are significantly different ($P < 0.05$) by one-way ANOVA followed by Tukey's HSD test.

Identification of *ASY1* intron-binding TFs

To identify transcription factors that potentially regulate *ASY1* expression by binding to intron sequences, different promoter/intron constructs were cloned to be used in a yeast one-hybrid screening analyzing the binding of 2166 Arabidopsis transcription factors, i.e., $PRO_{ASY1,}$ PRO_{ASY1}*:intron3-8,* PRO_{ASY1}*:intron3-5*, and PRO_{ASY1}*:intron6-8*. The yeast one-hybrid assays were performed in Siobhan Brady´s lab (Gaudinier et al. 2011; Pruneda-Paz et al. 2014). In the yeast one-hybrid screening, 38 TFs interacted with the PRO_{ASY1}*:intron3-8* bait construct, 51 TFs with the PRO_{ASY1}*:intron3-5* construct, and 86 TFs interacted with the PRO_{ASY1}*:intron6-8* (Figure S6A, Table S2-4). To reduce the number of candidates for further analysis, we checked public transcription databases (Genevestigator), if the transcript was present in meiocytes and if the developmental expression pattern was similar to *ASY1* expression during flower development, i.e., the expression of the TF should slightly precede and/or overlap with *ASY1* expression (Figure S6C-D). Nine candidate genes were selected for further analysis, i.e., *AT5G24050*, *AT5G38490*, *AT1G02030*, *ATHB4*, *AGL77*, *REM35*, *BT3*, *TAF9/TAFII21*, and *TRFL10*. T-DNA insertion mutants were ordered and screened for fertility defects, but none of the single mutants showed any developmental phenotype (Seemann 2022).

Knockdown of four highly homologous REMs leads to reduced seed set in PRO_{ASY1}*:intron1-8:*CDS_{ASY1}*:GFP* expressing *asy1* plants

Functional redundancy among genes is one of the possible explanations for the absence of mutant phenotypes in a single mutant. *REM34, REM36*, and *REM37* are very close homologs of *REM35*, which was one of the candidate TFs identified in the Y1H screen. Therefore, an artificial microRNA (amiRNA) approach was adopted to investigate their possibly redundant role during meiosis progression in Arabidopsis. Due to sequence divergence, designing a single artificial microRNA fragment to silence the four *REM* genes simultaneously was not possible. Therefore, multiple *amiRNAs* for multiplex gene silencing using the polycistronic tRNA-pre-amiRNA

strategy were utilized to co-silence four *REM* genes during meiosis (Carbonell et al. 2014; Xie, Minkenberg, and Yang 2015; N. Zhang et al. 2018). Because of sequence similarity, it was feasible to design *amiRNA* fragments simultaneously targeting two of the *REM* genes. Two regions specific to the coding sequences of both *REM34* and *REM36*, and two regions for both *REM35* and *REM37* were selected (Figure 4A). The targeted regions are highly specific for the genes of interest; thus they were expected not to have any off-target effects. The multiple *amiRNA* knockdown expression vector with all four *amiRNA* sequences was cloned based on the *miR390a* backbone (Carbonell et al. 2014) and tRNA-processing systems (Xie, Minkenberg, and Yang 2015; N. Zhang et al. 2018) using the meiosis-specific *DMC1* promoter (Figure 4B). The silencing construct was transformed into WT plants, *asy1* homozygous mutants, *asy1* heterozygous mutants, as well as *asy1* homozygous mutant plants carrying either the *ASY1-GFP* genomic reporter or the PRO_{ASY1}*:intron1-8:*CDS_{ASY1}*:GFP* construct. It is worth noting that two different lines of *ASY1-GFP* genomic reporters with different levels of ASY1 were used in these experiments. One PRO_{ASY1}*:ASY1:GFP* genomic reporter line fully rescued the *asy1* phenotype while another line only rescued the *asy1* phenotype partially and will be referred to as PRO_{ASY1}*:*$ASY1^{partial}$*:GFP*. Finally, the *amiRNA* construct was also transformed into a *rem34rem35* double mutant (Figure S6).

To evaluate the function of *REM* genes in meiosis, 10 independent T1 lines carry the *amiRNA* construct targeting *REM34, REM35, REM36*, and *REM37* expressed under the *DMC1* promoter (referred to as amiREMs hereafter) were checked in each genetic background. The knockdown of *REMs* did not affect the fertility in backgrounds that show WT-like fertility levels, i.e., WT plants, *rem34rem35* double mutants, *asy1* heterozygotes, and *asy1* mutants fully rescued by the genomic *ASY1-GFP* reporter (Figure S6A, C).

However, in plant lines where the *asy1* phenotype was only partially rescued by either *ASY1:GFP* or PRO_{ASY}*:intron1-8:*CDS_{ASY1}*:GFP*, the knockdown of *REMs* resulted in a clear reduction of viable seeds compared to the corresponding backgrounds without amiREMs expression (Figure 4C-D, S6D). Especially in the PRO_{ASY1}*:intron1-8:*CDS_{ASY1}*:GFP* expressing *asy1* plants, 7 out of 10 lines showed significantly decreased seed setting rate (Figure 4D).

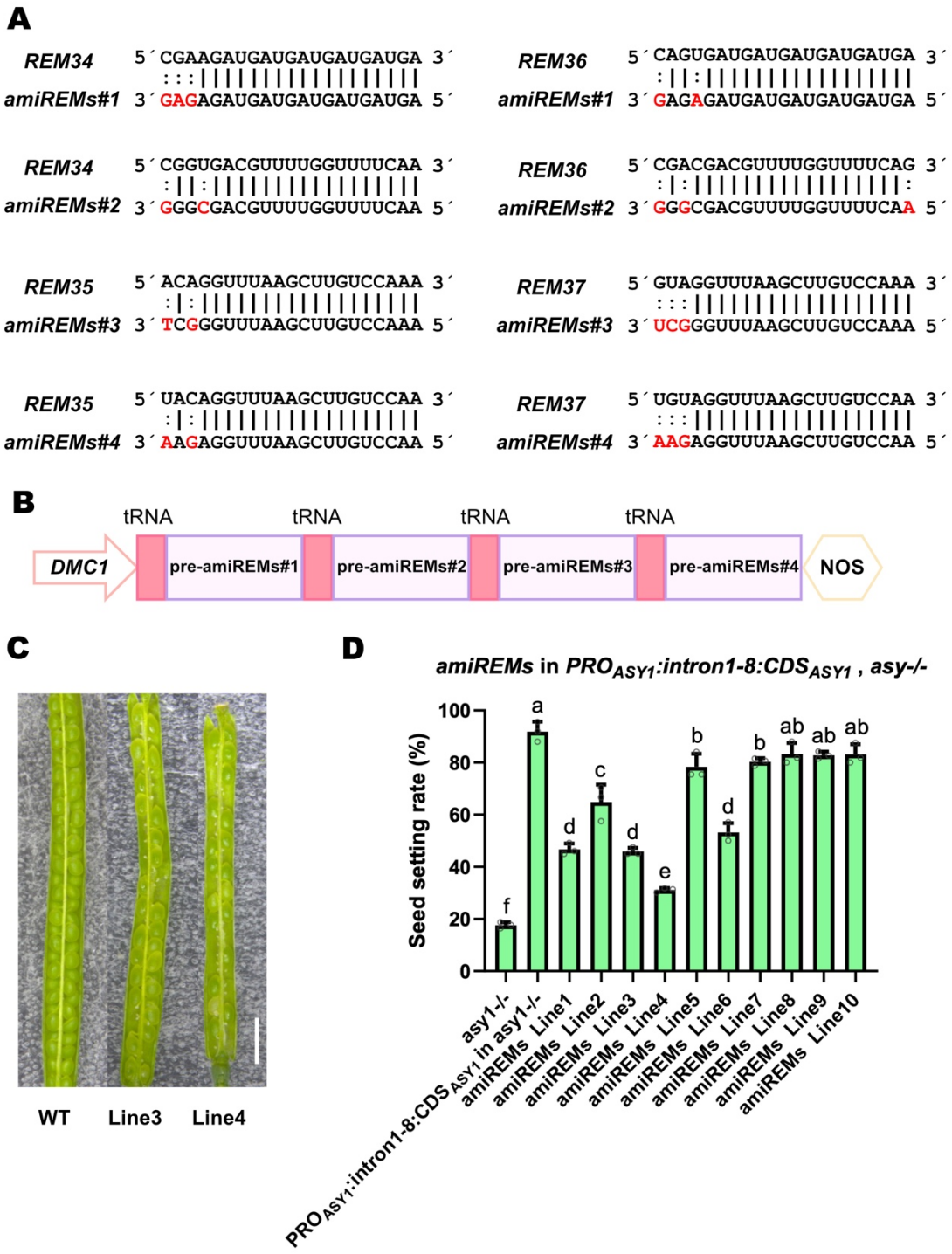

Figure 4. Phenotypic analysis of amiRNA-mediated *REM34, REM35, REM36*, and *REM37* knockdown plants in WT, and *PRO$_{ASY1}$:intron1-8:CDS$_{ASY1}$ rescued asy1-/-* background. (A) Sequence alignment of *amiRNAs* and their target sites on *REM34*, *REM35, REM36*, and *REM37* mRNA. **(B)** Schematic representation of the amiRNA construct. **(C)** Siliques of WT, *amiREMs* in *PRO$_{ASY1}$:intron1-8:CDS$_{ASY1}$:GFP* rescued *asy1-/-* background line 3 and line 4. Scale bar: 2 mm **(D)** Seed setting rate of Arabidopsis in *asy1-/-*, *PRO$_{ASY1}$:intron1-8:CDS$_{ASY1}$ rescued asy1-/-*, and 10 lines of *amiREMs* in *PRO$_{ASY1}$:intron1-8:CDS$_{ASY1}$* rescued *asy1-/-* (amiREMs). Data are presented as individual values per silique (dots) and mean ± SD. Three individual plants were counted for *asy1-/-* and

PRO$_{ASY1}$:intron1-8:CDS$_{ASY1}$ rescued asy1-/-. Three indicidual siliques were counted per plant. Groups labeled with different lowercase letters are significantly different ($P < 0.05$) by one-way ANOVA followed by Tukey's HSD test.

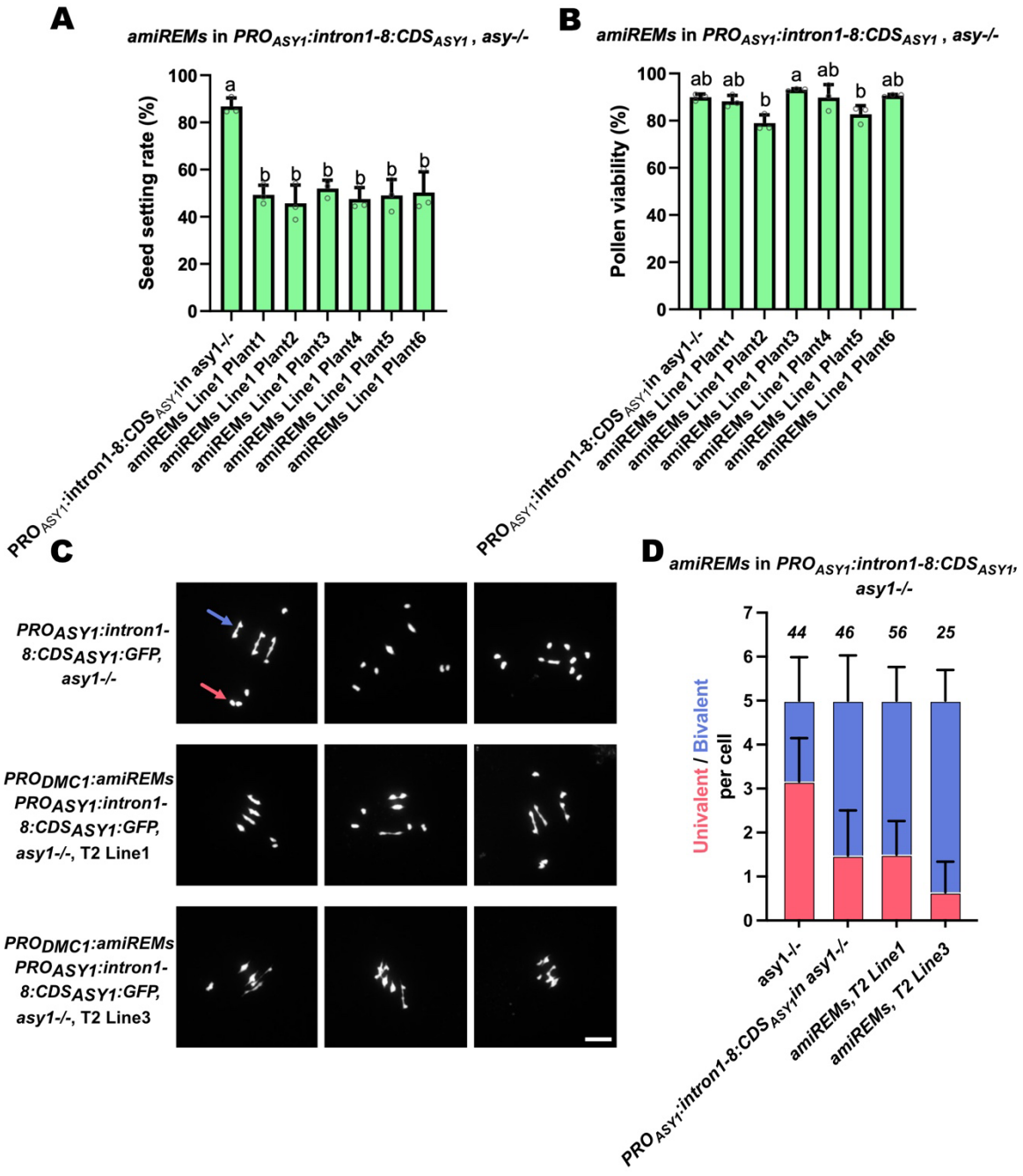

Figure5. Phenotypic analysis of *amiREMs* in *PRO$_{ASY}$:intron1-8:CDS$_{ASY1}$:GFP* rescued *asy1* plants. **(A)** Seed setting rate of Arabidopsis of *PRO$_{ASY1}$:intron1-8:CDS$_{ASY1}$* rescued *asy1-/-* plants compared to 6 plants from the T2 of line1 of *amiREMs* in *PRO$_{ASY1}$:intron1-8:CDS$_{ASY1}$* rescued *asy1-/-* background (amiREMs). Data are presented as individual values per silique (dots) and mean ± SD. Three individual siliques were counted per plant. Groups labeled with different lowercase letters are significantly different ($P < 0.05$) by one-way ANOVA followed by Tukey's HSD test. **(B)** Pollen viability of *PRO$_{ASY1}$:intron1-8:CDS$_{ASY1}$* rescued *asy1-/-* and 6 plants from the T2 of line1 of *amiREMs* in *PRO$_{ASY1}$:intron1-8:CDS$_{ASY1}$*

rescued *asy1-/-* background (amiREMs). Data are presented as individual values per flower (dots) and mean ± SD. Three individual flowers were used per line. Groups labeled with different lowercase letters are significantly different ($P < 0.05$) by one-way ANOVA followed by Tukey's HSD test. **(C)** Chromosome spread analysis of male meiocytes at metaphase I stage in PRO_{ASY1}*:intron1-8:*CDS_{ASY1} rescued *asy1-/-* and *amiREMs* in PRO_{ASY1}*:intron1-8:*CDS_{ASY1} rescued *asy1-/-* from T2 of line 1 and line 3. Blue arrow: bivalent. Red arrow: univalent. Scale bar: 10 μm. **(D)** Average number of bivalents and univalents per male meiocyte from *asy1-/-*, PRO_{ASY1}*:intron1-8:*CDS_{ASY1} rescued *asy1-/-*, and two T2 lines of *amiREMs* in PRO_{ASY1}*:intron1-8:*CDS_{ASY1} rescued *asy1-/-*. Bule bars represent bivalents while red bars indicate pairs of univalents. The number of metaphase I cells analyzed is indicated above each bar.

The knockdown of *REMs* has little effect on male meiosis

To analyse more closely the reason for the reduced seed set in the T1 of the *amiREMs* in PRO_{ASY1}*:intron1-8:*CDS_{ASY1}*:GFP*, *asy1-/-* background, 2 lines were selected for further investigation. In the T2 generation, the seed setting rate and pollen viability were evaluated. Line 1 showed nearly 50% seed abortion, consistent with the result in the T1 generation (Figure 4D), while pollen viability only exhibited a slight decrease compared to the background (Figure 5A-B). To analyse chromosome behavior in meiosis, chromosome spreads were performed for line 1 and line 3 to check if meiosis was affected after knockdown of *REMs* in the PRO_{ASY1}*:intron1-8:*CDS_{ASY1} rescued *asy1* lines (Figure 5C). Despite the slight pollen defects seen in line 1, the univalent number caused by the ASY1 reduction in the background was not enhanced in the *amiREMs* lines (Figure 5), which suggests that the seed abortion was caused by problems on the female side, which may relate to a disruption of female meiosis.

The female meiosis is difficult to observe, since single meiocytes are surrounded by ovule tissue and the ovules are deeply embedded in the pistil. Thus, instead of performing chromosome spreads, ASY1 expression levels were evaluated by fluorescence microscopy. In the PRO_{ASY1}*:intron1-8:*CDS_{ASY1}*:GFP* rescued *asy1* lines, *ASY1* expression level in the female meiocyte was significantly higher than in the male meiocyte (Figure 6 A-B). However, after the knockdown of the *REMs* in the meiocyte, this situation changed, i.e. the fluorescent intensity of ASY1-GFP in meiotic nuclei on the female side was significantly lower than on the male side (Figure 6C-D). The absolute values of ASY1-GFP intensity could not be compared between lines since the images were captured on different days, and the laser condition might have been different during the acquisition. However, comparing the intensity difference between male and female, we suspected that knockdown of REMs leads to reduced

expression of ASY1 in the female meiosis, which would mean that ASY1 in the female meiosis is more sensitive to REM regulation than in male meiosis.

The observation that the fertility problem in the *amiREMs* originates on the female side was confirmed by a backcross with WT. Three lines of *amiREMs* in *PRO$_{ASY1}$:intron1-8:CDS$_{ASY1}$:GFP* rescued the *asy1* background as female, were backcrossed with the pollen from WT. The resulting siliques showed no significant seedset changes compared to the *amiREMs* mother plants (Figure 6E-F). This indicates that the fertility defects in the *amiREMs* were caused primarily by defects on the female side.

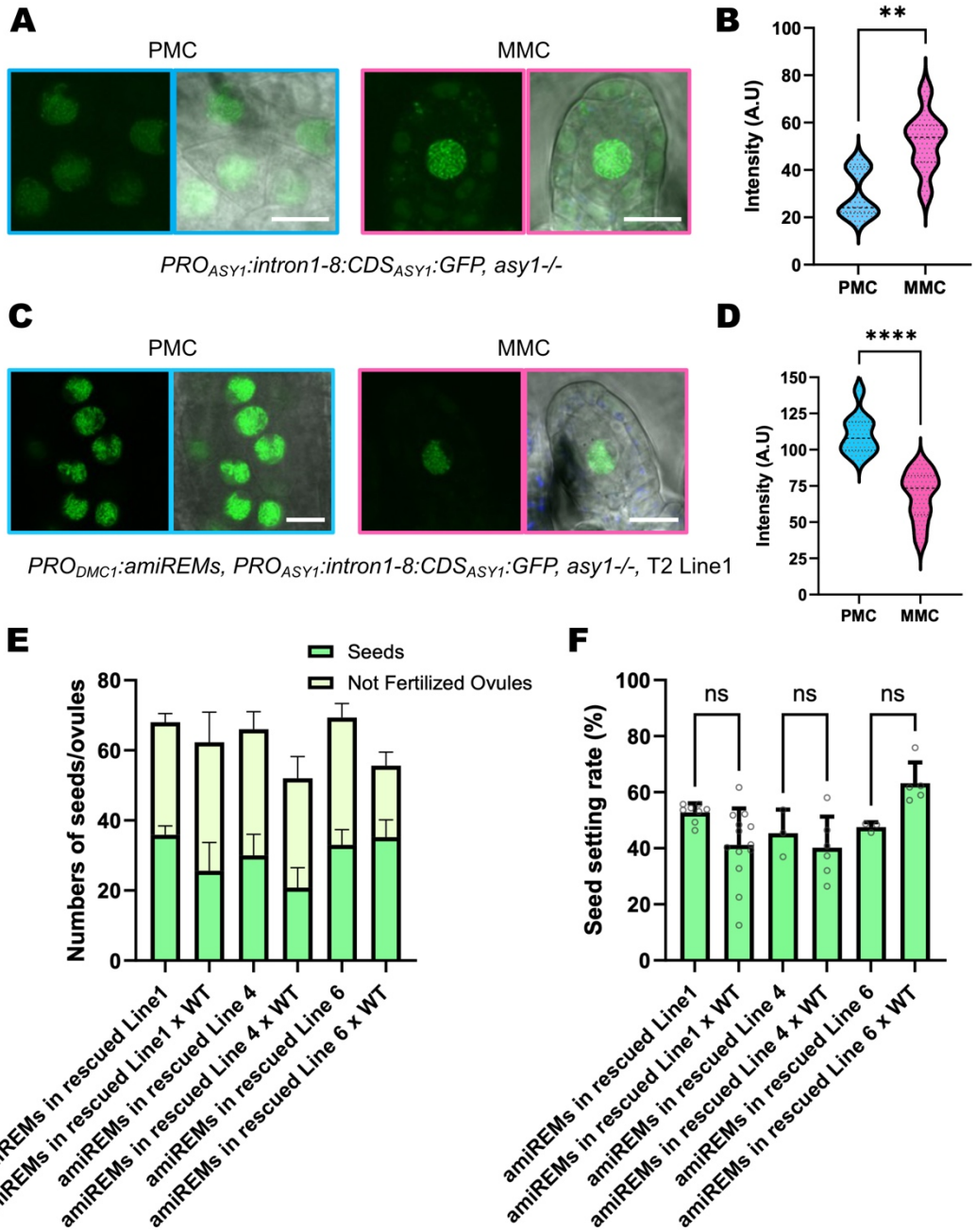

Figure6. *ASY1* expression level analysis in male and female meiocytes. (A) Analysis of ASY1-GFP localization in the PMC (pollen mother cell) and MMC (megaspore mother cell) of *PRO$_{ASY1}$:intron1-8:CDS$_{ASY1}$:GFP* rescued *asy1* plants using confocal microscopy. Scale bar: 10 µm. **(B)** The fluorescence intensity of ASY1-GFP in the nuclei of PMCs and MMCs in *PRO$_{ASY1}$:intron1-8:CDS$_{ASY1}$:GFP* rescued *asy1* background. Data are based on the analysis of eight PMCs and eight MMCs. ***P* < 0.01, determined by two-tailed Student's *t*-test. **(C)** Analysis of ASY1-GFP localization in the nuclei of PMCs and MMCs of *amiREMs* in *PRO$_{ASY1}$:intron1-8:CDS$_{ASY1}$:GFP* rescued *asy1* background. Scale bar: 10 µm. **(D)** The fluorescence intensity of ASY1-GFP in nuclei of PMCs and MMCs of *amiREMs* in *PRO$_{ASY1}$:intron1-8:CDS$_{ASY1}$:GFP* rescued *asy1* background. Data are based on the analysis of ten PMCs and ten MMCs. *****P* < 0.0001, determined by two-tailed Student's *t*-test. **(E)** Numbers of seeds and unfertilized ovules in line1, line4, and line6 of amiREMs in *PRO$_{ASY1}$:intron1-8:CDS$_{ASY1}$:GFP* rescued *asy1* plants and their individual backcrosses with WT plants (WT as male). **(F)** Seed setting rate of three lines of *amiREMs* reporters in *PRO$_{ASY1}$:intron1-8:CDS$_{ASY1}$* rescued *asy1-/-* plants compared to their respective backcrosses. Data are presented as individual values (dots) and mean ± SD. Three individual plants were used per line and three siliques were used per plant. ns, not significant, determined by two-tailed Student's *t*-test.

Analysis of *ASY1* regulatory region-mediated *KNO1* expression

The here identified regulatory regions of ASY1 could be used as a tool to drive gene expression or to knock down genes e.g., by *amiRNA* constructs primarily in the meiocyte. As a test case, we decided on overexpression of *KNOTEN1* (*KNO1*), a known interactor of the RTR-complex (Westphal 2024). The RTR-complex has been described as a repressor of homologous recombination with a function in somatic and meiotic cells (Knoll, Schröpfer, and Puchta 2014), while KNO1 seems to be only marginally present in meiotic cells (Figure 7A). Therefore, we wondered if enhancing *KNO1* expression in meiosis would lead to a recombination-related mutant phenotype.

Here, the *PRO$_{ASY1}$:intron1-8* fragment was used to drive *KNO1* expression in the meiocyte. The *PRO$_{ASY1}$:intron1-8:GFP:CDS$_{KNO1}$* construct was transformed into the WT and *msh4* mutant background. The *msh4* mutant was chosen as combined with some mutants in components of the RTR complex, e.g., *msh4recq4a-4recq4b-2* the *msh4* sterility phenotype is rescued (Séguéla-Arnaud et al. 2015). Ten different T1 carrying the *PRO$_{ASY1}$:intron1-8:GFP:CDS$_{KNO1}$* construct were evaluated for both WT and *msh4* mutant backgrounds. As determined by confocal microscopy, the expression level of *KNO1* in the meiocytes was significantly increased by the *PRO$_{ASY1}$:intron1-8:GFP:CDS$_{KNO1}$* construct in the WT background (Figure 7A-B). The GFP-KNO1 protein accumulated in the nucleoplasm and more strongly in the

nucleolus. Interestingly, overexpression of *KNO1* in the meiocytes led to significant fertility defects in half of the WT background lines, while the *msh4* sterility phenotype was not changed significantly (Figure 7C-E). Notably, the crossover numbers were slightly increased in the WT upon overexpression of KNO1 (Figure 7F-G). At the same time, we observed a significantly higher amount of chromosome entanglements in the PRO_{ASY1}*:intron1-8:GFP:*CDS_{KNO1} lines than in WT, which may be the reason for the observed fertility defects (Figure 7F, H).

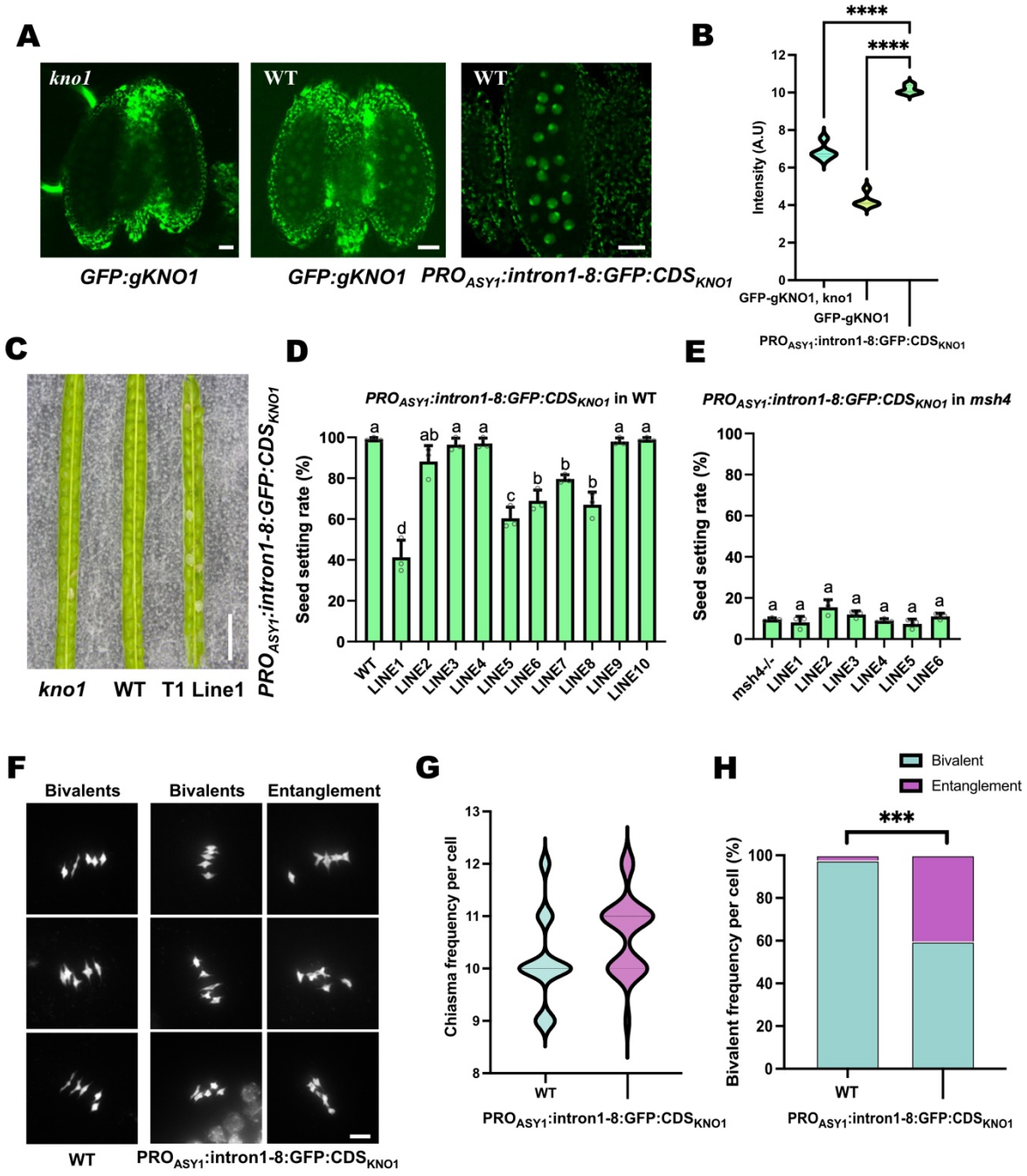

Figure7. Analysis of *KNO1* overexpression in male meiocytes. (A) Analysis of *GFP:gKNO1* expression in *kno1* and WT background as well as PRO_{ASY1}*:intron1-8:GFP:*CDS_{KNO1} in WT in male

meiocytes using confocal microscopy. Note that the confocal settings are not comparable, but the laser power was adjusted to see residual signal in each case. Scale bar: 20 µm. **(B)** Quantification of GFP-KNO1 signal in male meiocytes comparing the lines shown in (A), but using the same confocal settings. Five meiocytes were analyzed per line. ****$P < 0.0001$, determined by one-way ANOVA followed by Tukey's HSD test. **(C)** Siliques of *kno1*, WT, and the T2 of line 1 of PRO_{ASY1}*:intron1-8:GFP:*CDS_{KNO1} in WT. Scale bar: 2mm **(D)** Seed setting rate of WT and 10 lines of PRO_{ASY1}*:intron1-8:GFP:*CDS_{KNO1} in WT. Data are presented as individual values (dots) and mean ± SD. Three individual plants were used per line. Groups labeled with different lowercase letters are significantly different ($P < 0.05$) by one-way ANOVA followed by Tukey's HSD test. **(E)** Seed setting rate of *msh4* and 6 lines of PRO_{ASY1}*:intron1-8:GFP:*CDS_{KNO1} in *msh4*. Data are presented as individual values (dots) and mean ± SD. Three individual siliques were counted per line. Groups labeled with different lowercase letters are significantly different ($P < 0.05$) by one-way ANOVA followed by Tukey's HSD test. **(F)** Chromosome spread analysis of male meiocytes at metaphase I stage in WT and PRO_{ASY1}*:intron1-8:GFP:*CDS_{KNO1} lines. Scale bar: 10 µm. **(G)** Chiasma frequency per cell in WT and PRO_{ASY1}*:intron1-8:GFP:*CDS_{KNO1} lines. **(H)** Bivalent and entanglement frequency per male meiocyte from WT and PRO_{ASY1}*:intron1-8:GFP:*CDS_{KNO1} reporter. Fifty meiocytes during metaphase I were used per line. ***$P < 0.001$, determined by two-tailed Student's *t*-test.

Discussion

Our work focusing on the chromosome axis protein ASY1, reveals insights into meiosis-specific gene expression in *Arabidopsis thaliana*. We demonstrate that *ASY1* expression in meiocytes is not driven by promoter sequence alone but requires specific introns as well as the terminator to ensure robust expression.

Consistent with expectations, our findings demonstrate that the *ASY1* promoter, despite its short length, is essential for driving gene expression in meiocytes. However, the promoter plus terminator alone are insufficient for full meiotic expression. Introns 3-5 are the minimal functional unit that needs to be added to reconstitute the meiotic expression of *ASY1*. Further addition of intron1-2 and 6-8 further resulted in a cumulative increase of expression and, importantly, conferred a greater ability to rescue the fertility defects of *asy1* mutants. This additive effect of multiple introns aligns with the principles of intron-mediated enhancement (IME) but might also reflect potential synergistic contributions from associated transcription factors. Notably, the meiotic expression was lost when the introns were placed upstream of the promoter, i.e., outside of the transcript, indicating that a position-sensitive IME mechanism is involved. 5'RACE showed excessive, but non-native splicing of the region of the

concatenated introns. However, we cannot decide at this point if this splicing activity is relevant for expression strength, i.e., if some splicing-dependent IME is at play. On the other hand, the introns function outside of their native position, i.e., concatenated after the first exon, more in line with classical intronic transcription factors.

Given that many meiotic genes in Arabidopsis are highly intron-rich and we also know from other genes, e.g., *REC8* and *DMC1*, that introns are essential for expression in meiocytes (unpublished results), it is possible that intron-mediated regulation plays a widespread role in controlling the meiotic transcriptional program.

As we observed that the minimal promoter construct with one CAAT box, i.e. *CAAT:5´UTR$_{ASY1}$:intron3-5:GFP*, resulted in no detectable GFP in the male meiocyte (Figure S5A-B), we conclude that the 183 bp sequence upstream of the minimal promoter is also needed for meiotic expression. Using the PLACE online tool to detect known *cis*-regulatory elements in plant promoter sequences, two more CAAT boxes were found similarly spaced with the third CAAT box. The presence of multiple, evenly spaced CAAT boxes might allow for cooperative or additive binding of transcription factors, which then can facilitate efficient recruitment of RNA polymerase II and stabilize the transcriptional machinery, leading to robust gene expression (Song and Young 1998; Bates et al. 2001).

Last but not least, the ASY1 terminator could not be replaced by the generic NOS terminator without losing expression of the reporter construct, thereby adding a third region to the genomic elements required for meiocyte expression of ASY1. Chromatin conformations such as enhancer-promoter and promoter-terminator interactions play a crucial role in transcription by forming looped gene architectures (Ansari and Hampsey 2005; Misteli 2007). In budding yeast, introns can promote the formation of a loop, where the promoter contacts the 5' splice site and the terminator interacts with the 3' splice site (Moabbi et al. 2012; Tan-Wong et al. 2012). This splicing-dependent loop is thought to stabilize the preinitiation complex and facilitate RNA polymerase recycling, thereby enhancing transcription through IME (Damgaard et al. 2008; Al Husini, Kudla, and Ansari 2013). Notably, the IME effect is lost in looping-defective yeast mutants despite normal splicing, suggesting that transcriptional enhancement depends on loop formation rather than splicing itself (Dwyer et al. 2021). Here, the ASY1 terminator might contain sequence elements or chromatin features that favor a looping mechanism in combination with the *ASY1*

promoter and/or *ASY1* introns while the generic NOS terminator may lack these features and thus fail to enhance the expression.

In search of a regulatory input via specific transcription factors, yeast one-hybrid screens were performed using different promoter-intron fragments as a bait. Interestingly, using the fragment *PRO$_{ASY1}$:intron3-8* as bait construct yielded only 38 binding TFs, while 51 TFs bound to the shorter *PRO$_{ASY1}$:intron3-5* fragment. Thus, we assume that the DNA fragments in yeast likely adopt some construct-specific, non-native configurations that foster or inhibit the binding of certain TFs. This could explain why the longer bait construct does not bind all the TFs that are bound by an even more truncated version. Thus, the sum of identified TFs should be rather seen as a pool of possible interactors, and we added additional criteria, like meiocyte expression and ASY1-like expression, to choose the most promising candidates.

REM35 and its close homologs, *REM34, REM36*, and *REM37,* were most extensively examined due to their known roles in reproduction, more precisely gametophyte development, as described in a previous study (Caselli et al. 2019). The authors demonstrate that in the *35S::REM_RNAi* lines, which knock down *REM34, REM35*, and *REM36*, neither the male nor female gametophytes develop normally. What drew our attention was the fact that they used the CaMV35S promoter to drive the RNAi production, which is known not to function well in the meiocytes (Fauser, Schiml, and Puchta 2014; Xu et al. 2018). Therefore, we assumed that the REMs expressed in the meiocyte were not knocked down, which could explain why no meiotic phenotype was observed in that study. To circumvent this problem and check the function of the REMs in meiosis, we use the *DMC1* promoter to generate a meiosis-specific multiplex amiRNA system targeting the *REM34, REM35, REM36*, and *REM37* genes. When we applied the *amiREMs* in the background of *asy1-/-*, which was partially rescued by *PRO$_{ASY}$:intron1-8:CDS$_{ASY1}$:GFP* expression, we observed significant fertility defects (Figures 4C-D). This effect was not visible in WT background, *asy1* heterozygous plants, or in fully rescued genomic *ASY1* reporter lines (Figure S7A-C). Thus, we assume that we observe an effect only when the ASY1 level or expression timing is already perturbed to a point where any additional reduction in expression cannot be compensated.

The fertility defects caused by amiREMs were more pronounced in female than in male meiocytes. This is consistent with a previous study showing that chromosome 1 and chromosome 3 of Arabidopsis tend to have a more pronounced reduction in

crossovers (COs) during female compared to male meiosis in *asy1* mutants (Pochon et al. 2023). These results suggest that *REMs* play an essential role in the transcriptional activation of *ASY1*, potentially reflecting a sex-specific transcriptional regulation machinery in meiosis.

However, the silencing of the four target *REM* genes needs to be confirmed by qRT-PCR in the T2 generation, and binding of *REMs* to the regulatory regions of *ASY1* needs to be verified by an additional method. As the knockdown of the REMs only occurs in the meiocytes, a decrease in expression will be challenging to detect by qRT-PCR, as the REMs are also expressed in other floral tissues, which may mask the decrease in expression in the meiocytes. A similar situation applies to the quantification of ASY1 expression, which also should be analyzed at the RNA level after knocking down the REMs in the meiocyte. Future approaches, such as cell sorting or single-cell RNA sequencing, may be effective in tackling these questions.

As demonstrated by the mis-expression of *KNO1* in meiocytes, the characterized regulatory sequences of *ASY1* can be used as a tool to manipulate meiosis. In the *KNO1* mis-expression lines, we observed a mild increase in crossover frequency, chromosome entanglements, and fertility defects, which correspond to phenotypes seen in mutants of the RTR complex (Figure 7F-H). This not only indicates that KNO1 is an RTR antagonist but also suggests potential applications in manipulating gene expression in meiotic cells, specifically to alter recombination frequency, which could be beneficial for plant breeding.

In summary, our study identified *ASY1* introns as essential, position-sensitive regulators of meiosis-specific gene expression in Arabidopsis. I suggest that together with the promoter and terminator, intron 3-5 convey meiotic-specific information, while they also significantly enhance expression supported by additional introns of *ASY1.* In addition to binding of classical transcription factors, possibly sex specific, also adds to the final pattern. Still, several key questions remain. The mechanisms of how the introns enhance transcription by IME, i.e., whether they act by enhancing mRNA stability, by facilitating splicing, or if intron retention even affects translation, require deeper investigation. Long-read RNA sequencing will be useful to understand how intron architecture and retention affect RNA processing and stability. Our observations raise the possibility that other intron-rich meiotic genes may be regulated through similar mechanisms. Systematic testing of intronic regions from other meiotic genes using similar reporter constructs will help determine whether this is a general strategy.

In this respect, it will also be interesting to see if the *ASY1* promoter only works in combination with *ASY1* introns and *ASY1* terminator, or if regulatory regions of different meiotic genes can be mixed, and if so, which element is relevant for the exact timing of expression.

Although we are still at the beginning of understanding the mechanics of meiotic gene expression control, this work adds to the puzzle by providing evidence for intron-mediated gene regulation in plant reproduction and opens doors for precise control of meiotic gene expression in both basic and applied science.

Materials and Methods

Plant material and growth conditions

All *Arabidopsis thaliana* plants used in this study were of the Columbia-0 background. The genomic *ASY1* reporter has been previously described (Yang et al. 2019). The T-DNA insertion lines *asy1-4* (At1g67370, Salk_046272) and *msh4* (At4g17380, Salk_136296) were obtained from the collection of T-DNA mutants at the Salk Institute Genomic Analysis Laboratory (SIGnAL, http://signal.salk.edu/cgi-bin/tdnaexpress).

All the seeds were first surface sterilized with chlorine gas and then stored overnight in a 4°C fridge. After that, the seeds were sown on a 1% plant agar plate containing half-strength Murashige and Skoog (MS) medium and 1% sucrose. Antibiotics were added to the plate for selection as needed. The plates with seeds were then placed in growth chambers at 21°C for 16 hours of light and 18°C for 8 hours of dark cycle for germination. Ten days later, the seedlings were transferred to soil and grown in the growth chamber under the same long-day conditions mentioned above, with 70% humidity.

Plasmids and plant transformation

All the *ASY1*-related constructs were based on the PRO_{ASY1}*:ASY1:GFP* genomic construct and PRO_{ASY1}*:*CDS_{ASY1}*:GFP* construct provided by Dr. Chao Yang. The seamless ligation cloning extract (SLiCE) method was employed for almost all the intron deletion and insertion work done with the entry vectors in this study. The gateway system was used for creating gene expression constructs, i.e., all the entry

clones were recombined with the destination vector pGWB501. A single intron deletion from the *ASY1* genomic sequence was achieved by using PCR to amplify the backbone sequence without the intron, which was then self-ligated to obtain the respective entry clone. For example, to clone PRO_{ASY1}*:ASY1*$^{\Delta intron1}$*:GFP* construct, exon 2-F and exon 1-R primers were combined to amplify the whole entry vector without intron 1. For the continuous deletion of intron 1-8, using the same strategy as single intron deletion, exon 9-F and exon 2-R primers were combined to clone the *ASY1* genomic sequence without the sequence from exon 1 until intron 8 from PRO_{ASY1}*:ASY1:GFP* as the backbone for later SLiCE reaction. Then, the fragment exon 1-8 was amplified from the PRO_{ASY1}*:*CDS_{ASY1}*:GFP* and recombined with the backbone above by SLiCE. The intron 1-8 sequence was synthesised by GENEWIZ Germany GmbH. All primers used for cloning in this study are shown in the Supplementary Table S1.

The destination constructs were transformed into *Agrobacterium tumefaciens* (MP90) by a 37°C heat shock for 5 minutes and then grown at 28°C for 2 days. *Arabidopsis thaliana* plants were transformed using the floral dip method (Clough and Bent 1998).

Confocal microscopy and intensity measurement

For protein localization analyses, young anthers or ovules during the meiotic stage were dissected and imaged directly by a Leica TCS SP8 inverted confocal microscope. Fluorescent signals were captured from two distinct channels. GFP was excited using a 488 nm laser, and emission was collected in the 498-550 nm range. Autofluorescence from chloroplasts was visualized using the same 488 nm excitation wavelength, but with signal collection shifted to the 680-750 nm range to isolate far-red emission.

Fluorescence intensity of ASY1-GFP was quantified using Fiji (ImageJ, version 2.16, https://imagej.net/software/fiji). ASY1 localization, which was broadly distributed across the chromosomes within the nucleus, was assessed by defining the nucleus as regions of interest (ROIs). The boundaries of ROIs were automatically segmented by intensity thresholding. Mean fluorescence intensities of ASY1-GFP were then measured after applying the thresholding.

amiRNA oligonucleotide design and cloning

Artificial microRNA (amiRNA) oligonucleotides were designed using P-SAMS (https://p-sams.carringtonlab.org) and assembled into a multimeric amiRNA expression cassette following the protocol described by Carbonell et al. and Zhang et al. (Carbonell et al. 2014; Zhang et al. 2018). The *amiRNA* sequences were introduced into level-1 modules using GoldenGate cloning with BsaI and T4 DNA ligase. Four different level-1 modules (AD, DE, EF, and FG) were used to accommodate the four amiRNAs. These modules were then assembled into a level-2 entry vector (pUCentry) via a second GoldenGate reaction using *BbsI*, resulting in a single expression cassette flanked by *attL1* and *attL2* recombination sites. To drive expression specifically in meiotic cells, the *DMC1* promoter was cloned into a pENTR entry vector containing *attL4* and *attR1* sites. The final construct was assembled by performing a MultiSite Gateway LR recombination to integrate both the *DMC1* promoter and the multi-*amiRNA* cassette into the binary vector R4pGWB601, yielding the PRO_{DMC1}*:amiREMs* construct. This vector was subsequently used for stable transformation of Arabidopsis.

Pollen viability assay

Pollen viability was analyzed using the Peterson staining solution, followed by heat treatment (Peterson, Slovin, and Chen 2010). Three mature flower buds containing dehiscent anthers were collected for pollen grain counting. Individual anthers were dipped in 16 µl of Peterson staining solution on a slide for 10 seconds and immediately covered with a cover slip. Then all slides were heated on a hotplate at 80°C for 10 minutes to stain viable and aborted pollen grains differentially. Stained samples were examined and imaged using brightfield light microscopy.

Cytological analysis

Chromosome spreads were performed as described previously (Wijnker et al. 2012). Fresh flower buds were fixed in an ethanol:acetic acid (3:1) solution at 4°C overnight. Following fixation, samples were washed twice with 75% ethanol and then stored in 75% ethanol at 4°C until further use. For chromosome spread, flower buds were digested in 10 mM citrate buffer containing 1.5% cellulase, 1.5% pectolyase, and 1.5% cytohelicase for 3 hours at 37°C. Then the digested flower buds were transferred onto

a glass slide and crushed, further spread with 10 µl of 45% acetic acid on a 46°C hotplate. Finally, the slides were rinsed with ice-cold ethanol:acetic acid (3:1) solution and mounted with DAPI-containing mounting medium overnight for later fluorescence microscopy. The number of chiasmata in metaphase I was counted referring to the features described in Sanchez Moran et al. (Sanchez Moran et al. 2001).

Supplementary Materials

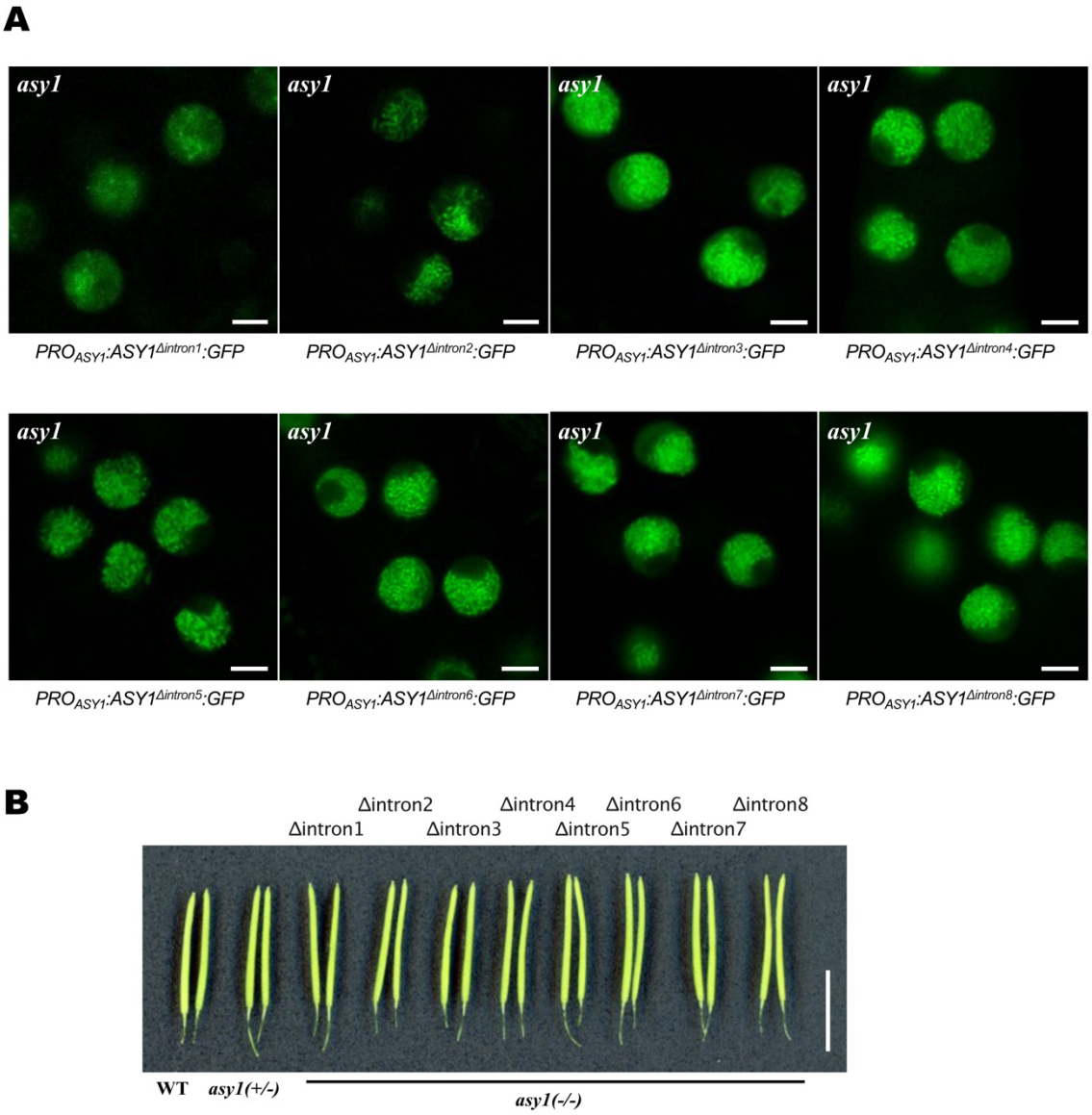

Figure S1. Single intron deletion leaves ASY1 expression unaffected in the male meiocyte. (A) Analysis of the localization of *ASY1-GFP* in male meiocytes of plants expressing *PRO$_{ASY1}$:ASY1$^{\Delta intron1}$:GFP*, *PRO$_{ASY1}$:ASY1$^{\Delta intron2}$:GFP*, *PRO$_{ASY1}$:ASY1$^{\Delta intron3}$:GFP*, *PRO$_{ASY1}$:ASY1$^{\Delta intron4}$:GFP*, *PRO$_{ASY1}$:ASY1$^{\Delta intron5}$:GFP*, *PRO$_{ASY1}$:ASY1$^{\Delta intron6}$:GFP*, *PRO$_{ASY1}$:ASY1$^{\Delta intron7}$:GFP*, and *PRO$_{ASY1}$:ASY1$^{\Delta intron8}$:GFP* in *asy1* background using confocal microscopy. Scale bar: 5 µm. **(B)** Siliques of WT, siliques of *asy1+/-* plants and siliques of *PRO$_{ASY1}$:ASY1$^{\Delta intron1}$:GFP*, *PRO$_{ASY1}$:ASY1$^{\Delta intron2}$:GFP*, *PRO$_{ASY1}$:ASY1$^{\Delta intron3}$:GFP*, *PRO$_{ASY1}$:ASY1$^{\Delta intron4}$:GFP*, *PRO$_{ASY1}$:ASY1$^{\Delta intron5}$:GFP*, *PRO$_{ASY1}$:ASY1$^{\Delta intron6}$:GFP*, *PRO$_{ASY1}$:ASY1$^{\Delta intron7}$:GFP*, and *PRO$_{ASY1}$:ASY1$^{\Delta intron8}$:GFP* expressing plants in *asy1-/-* background. Scale bar: 1 cm.

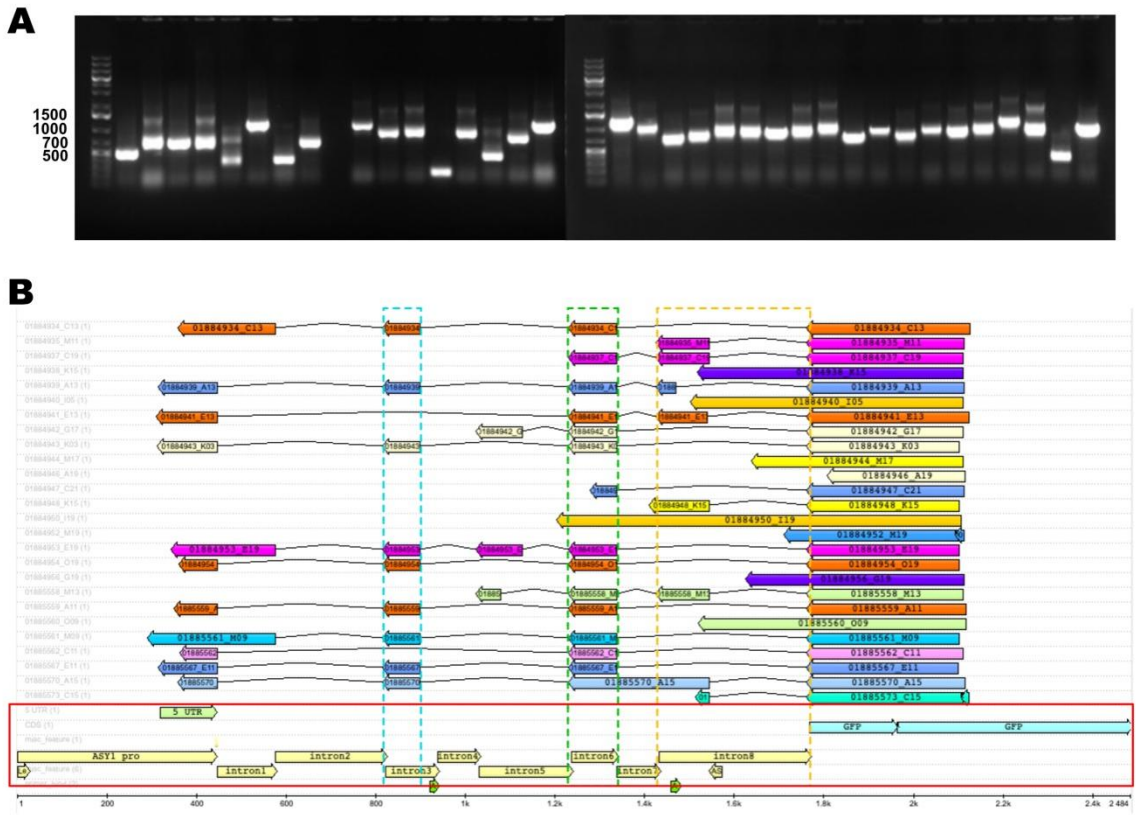

Figure S2. Analysis of the 5'region of the *GFP* transcripts generated from *PRO$_{ASY1}$:intron1-8:GFP* expressing plants by 5´RACE. (A) Agarose gel electrophoresis of cDNA products generated by 5´RACE. **(B)** Alignment of sequencing results of 5´RACE products to the *PRO$_{ASY1}$:intron1-8:GFP* template sequence. Red box: sequence of *PRO$_{ASY1}$:intron1-8:GFP* template. Blue dashed box: retained intron 3. Green dashed box: retained intron 6. Yellow dashed box: retained intron 8.

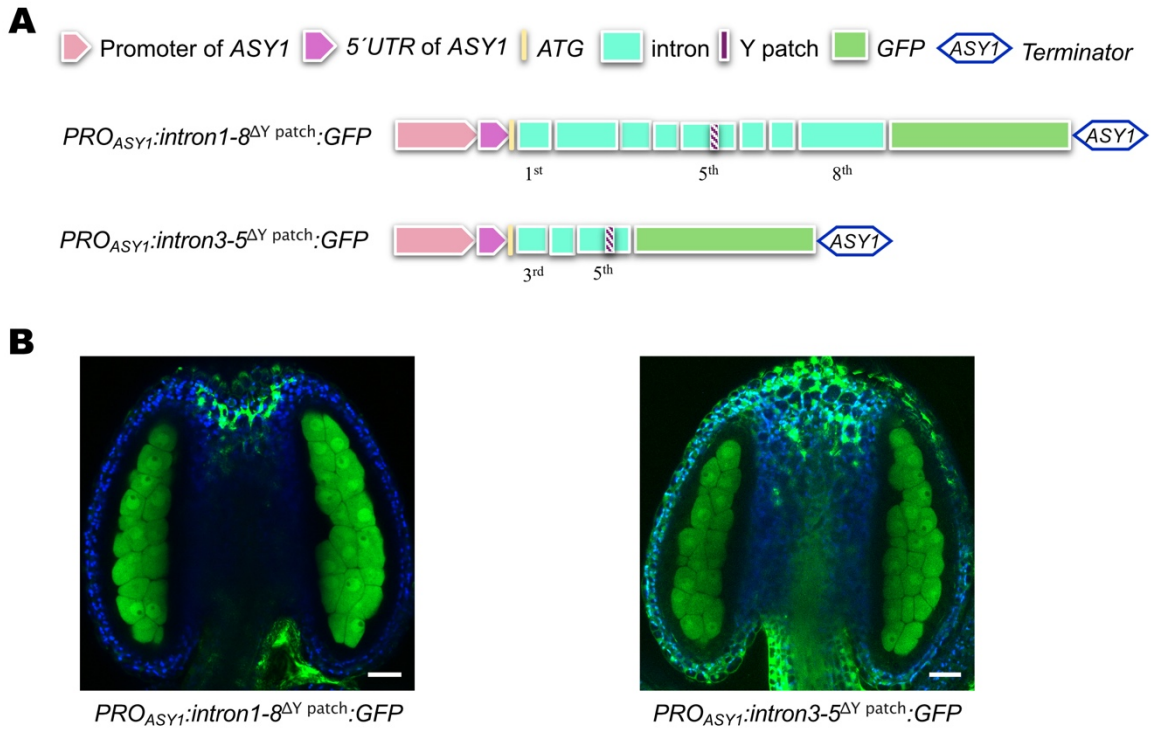

Figure S3. Deletion of the Y patch from intron 5 leaves meiocyte expression unaffected. (A) Schematic representation of the two Y patch deletion constructs used in this study: *PRO$_{ASY1}$:intron1-8$^{\Delta Y\ patch}$:GFP* and *PRO$_{ASY1}$:intron1-8$^{\Delta Y\ patch}$:GFP*. **(B)** Localization of GFP in anthers of WT background plants expressing *PRO$_{ASY1}$:intron1-8$^{\Delta Y\ patch}$:GFP* and *PRO$_{ASY1}$:intron1-8$^{\Delta Y\ patch}$:GFP*. Scale bar: 20 μm.

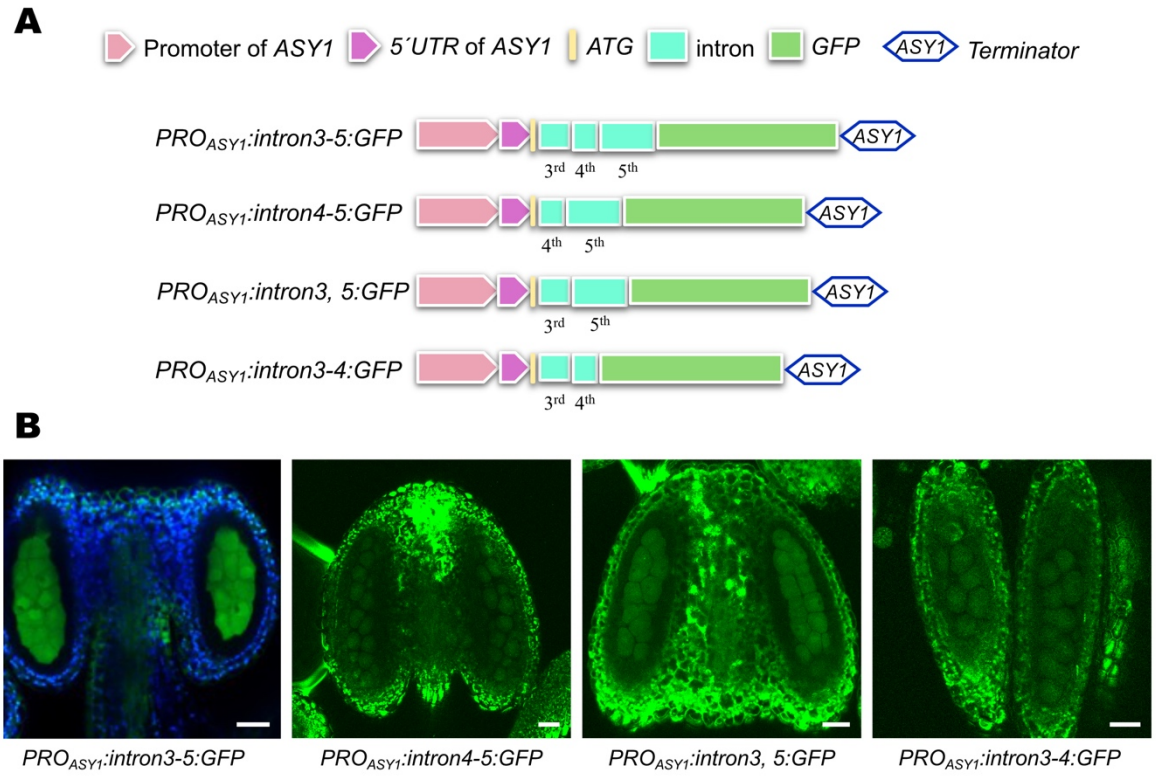

Figure S4. Intron 3, 4 and 5 are all needed for robust meiocyte expression in the anther. (A) Schematic representation of *PRO$_{ASY1}$:intron3-5:GFP, PRO$_{ASY1}$:intron4-5*:GFP, *PRO$_{ASY1}$:intron3,5:GFP, and PRO$_{ASY1}$:intron3-4:GFP*. **(B)** Localization of GFP in anthers of WT background plants expressing *PRO$_{ASY1}$:intron3-5:GFP*, *PRO$_{ASY1}$:intron4-5:GFP*, *PRO$_{ASY1}$:intron3,5:GFP, and PRO$_{ASY1}$:intron3-4:GFP*. Scale bar: 20 μm.

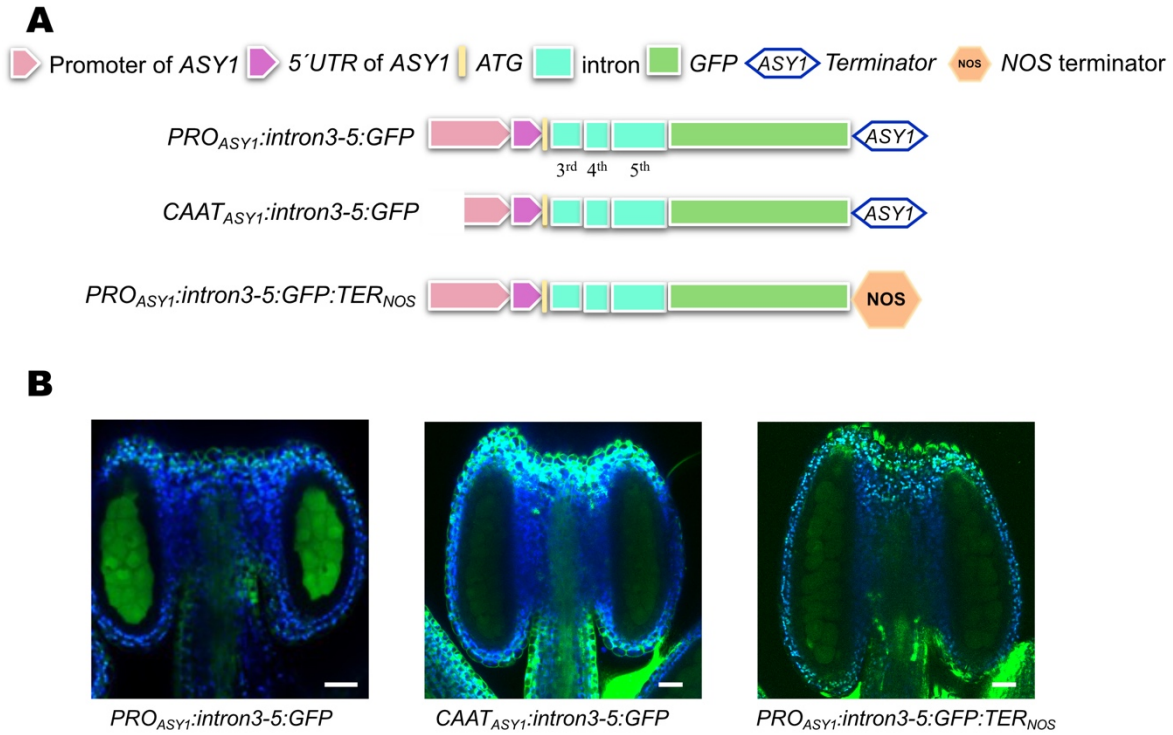

Figure S5. *ASY1* promoter and terminator are both needed for robust meiocyte expression in the anther. (A) Schematic representation of *PRO$_{ASY1}$:intron3-5:GFP, CAAT$_{ASY1}$:intron3-5*:GFP, and *PRO$_{ASY1}$:intron3-5:GFP:TER$_{NOS}$*. **(B)** Localization of GFP in anthers of WT background plants expressing *PRO$_{ASY1}$:intron3-5:GFP*, *CAAT$_{ASY1}$:intron3-5:GFP*, and *PRO$_{ASY1}$:intron3-5:GFP:TER$_{NOS}$*. Scale bar: 20 μm.

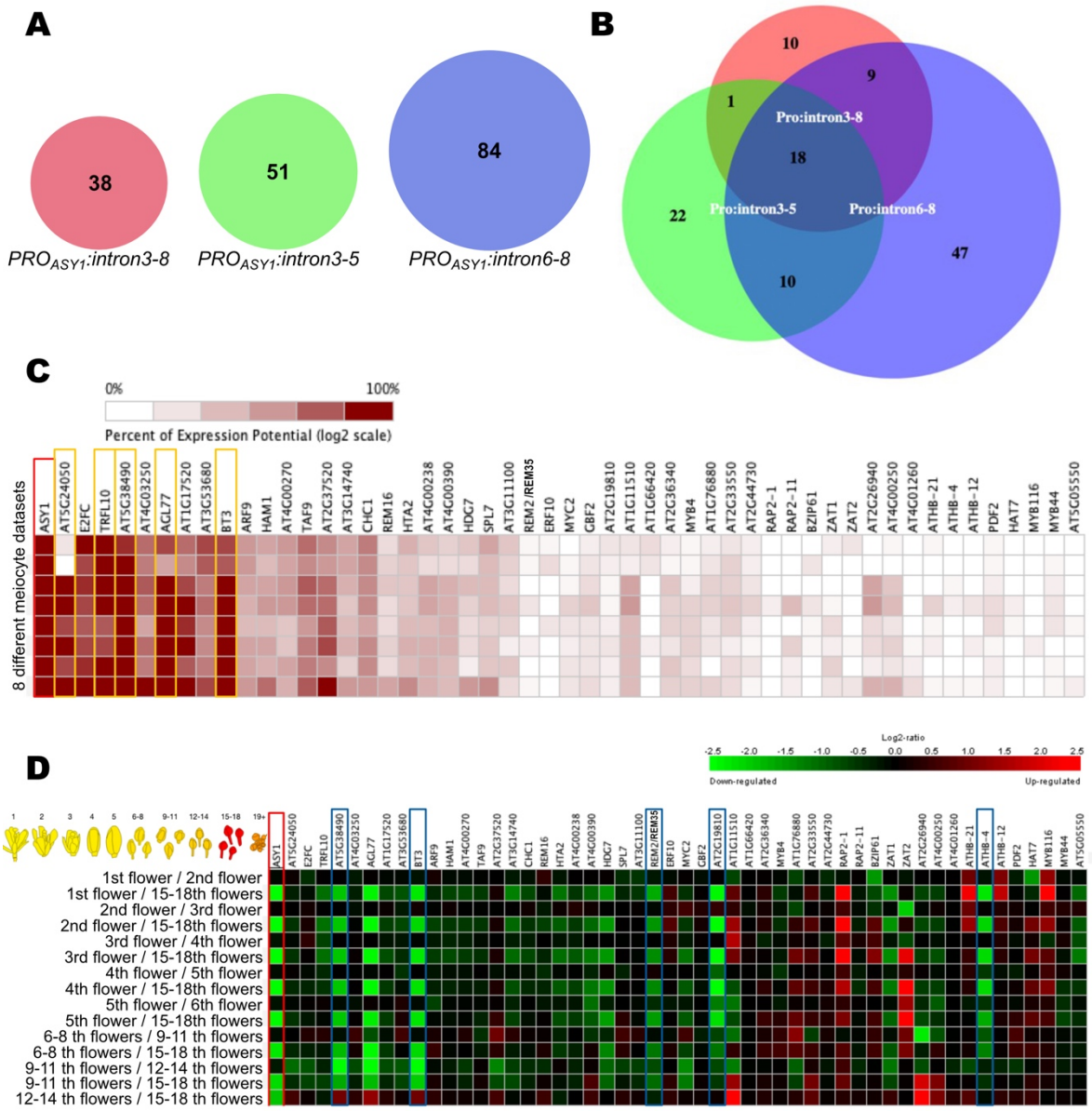

Figure S6. Transcription factors identified by yeast one-hybrid. (A) Numbers of transcription factors that interact with *PRO*$_{ASY1}$*:intron3-8*, *PRO*$_{ASY1}$*:intron3-5*, and *PRO*$_{ASY1}$*:intron6-8* as identified by yeast one-hybrid screens. **(B)** Venn diagram showing the overlap of transcription factors identified by the constructs detailed in (A). **(C)** mRNA sequencing data information based on different meiocyte datasets from Genevestigator showed the expression pattern of *ASY1* and 51 transcription factors that interacted with *PRO*$_{ASY1}$*: intron 3-5* in meiocytes. Red box: ASY1. Yellow box: candidates chosen by similar expression pattern in the meiocytes. **(D)** mRNA sequencing data for ASY1 and 51 transcription factors that interact with *PRO*$_{ASY1}$*:intron 3-5* during different flower development stages from Genevestigator. Red box: ASY1. Bule box: candidates chosen by similar expression pattern during flower development.

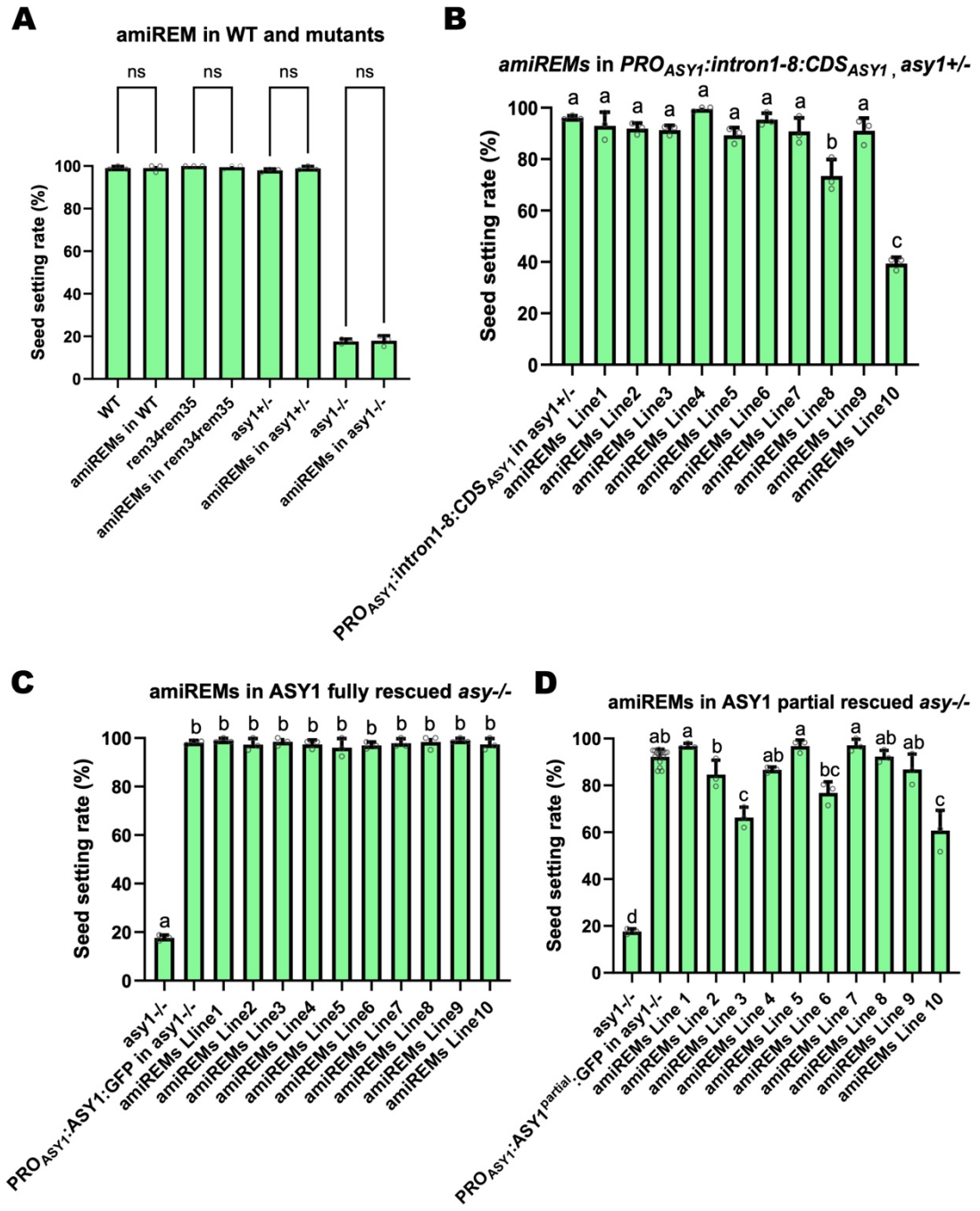

Figure S7. Knockdown of *REM34,REM35,REM36 and REM37* by amiREMs in different *asy1* backgrounds. (A) Seed setting rate in WT, *rem34rem35*, *asy1+/-*, *asy1-/-*, and *amiREMs* in the background mentioned on top of each chart. Seed setting rate of WT, *rem34rem35, asy1+/-, asy1-/-,* and *amiREMs* in the background mentioned on top of each chart. Data are presented as individual values (dots) and mean ± SD. Three individual siliques were counted per line. ns, not significant, determined by two-tailed Student's t-test. **(B)** Seed setting rate of *PRO$_{ASY1}$:intron1-8:CDS$_{ASY1}$* in *asy1+/-* background, and 10 lines of *amiREMs* in the same *PRO$_{ASY1}$:intron1-8:CDS$_{ASY1}$ asy1+/-* background. Data are presented as individual values (dots) and mean ± SD. Three individual siliques were counted per line. Groups labeled with different lowercase letters are significantly different (P < 0.05) by one-way ANOVA followed by Tukey's HSD test. **(C)** Seed setting rate of *asy1-/-*, *ASY1:GFP* fully resued *asy-/-,*

and 10 lines of *amiREMs* in *ASY1:GFP* fully rescued *asy1-/-* background. Data are presented as individual values (dots) and mean ± SD. Three individual siliques were counted per line. Groups labeled with different lowercase letters are significantly different ($P < 0.05$) by one-way ANOVA followed by Tukey's HSD test. **(D)** Seed setting rate of *asy1-/-, ASY1^{partial}:GFP* partially rescued *asy-/-,* and 10 lines of *amiREMs* in *ASY1^{partial}:GFP* partially rescued *asy1-/-* background. Data are presented as individual values (dots) and mean ± SD. Three individual siliques were counted per line. Groups labeled with different lowercase letters are significantly different ($P < 0.05$) by one-way ANOVA followed by Tukey's HSD test.

Table S1. Primers used in this study.

Purpose	Primer name	Sequence
PRO_{ASY1}:$ASY1^{\Delta intron1}$:GFP reporter	exon 2-F	GTGATGGCTCAGAAGCTGAAGGAAGCAG
	exon 1-R	CATTTTTGCAGAAGTGTGAAACGAATAACG
PRO_{ASY1}:$ASY1^{\Delta intron2}$:GFP reporter	exon 3-F	ACTAGAAATTTGCTTCGTATTGCTATCTTC
	exon 2-R	CAGAAGAAGCGAGTCCTGCTCAGTGATC
PRO_{ASY1}:$ASY1^{\Delta intron3}$:GFP reporter	exon 4-F	ATATGAAGATTAAGAAGCTAATGCCTATGG
	exon 3-R	CTAAAGCAGGAACCGATTTATCGTTGAAATAC
PRO_{ASY1}:$ASY1^{\Delta intron4}$:GFP reporter	exon 5-F	GAGTCTACGATGCGCTTCAGAGGAAATATTTG
	exon 4-R	CTTTCTCCATCCAATCAATTAATCGGCGAG
PRO_{ASY1}:$ASY1^{\Delta intron5}$:GFP reporter	exon 6-F	TTTCTTTCAGCTATTCAGATTCTGACAGCC
	exon 5-R	ATGAGTATTCCTCAATCATCGGACCATCAAC
PRO_{ASY1}:$ASY1^{\Delta intron6}$:GFP reporter	exon 7-F	GAGTTCAGCTTGCAAAATGGTTCGTACAC
	exon 6-R	CTCATTTGATTTGGGGTAATGTCAGCAGTGG
PRO_{ASY1}:$ASY1^{\Delta intron7}$:GFP reporter	exon 8-F	CGCACCATAGTGATGAAGCTTCTGTACTACG
	exon 7-R	CTCATCTGGCATTTTGTCAAGAGTCCTCATC
PRO_{ASY1}:$ASY1^{\Delta intron8}$:GFP reporter	exon 9-F	CCACCAGATTACGAGCCACCTTTCTTCAG
	exon 8-R	CGTCACATCATCGTAGTACAGAAGCTTC
PRO_{ASY1}:$ASY1^{\Delta intron1-2}$:GFP reporter	exon 3-F	ACTAGAAATTTGCTTCGTATTGCTATCTTC
	exon 2-R	CAGAAGAAGCGAGTCCTGCTCAGTGATC
PRO_{ASY1}:$ASY1^{\Delta intron1-8}$:GFP reporter	exon1-8_F	ATTCGTTTCACACTTCTGCAAAAATGGTGATGGCTCAGAAGCTGA
	exon1-8_R	CTCTGAAGAAAGGTGGCTCGTAATCTGGTGGAGAAAGGTGGCTCGTAATCTGGTGG
	exon9_F	CCACCAGATTACGAGCCACCTTTCTTCAGAG
	exon 1-R	CATTTTTGCAGAAGTGTGAAACGAATAACG
PRO_{ASY1}:GFP reporter	GFP-F	ATGGTGAGCAAGGGCGAGGAGCTGTTCA
	5'UTR-R	TTTTGCAGAAGTGTGAAACGAATAACGA
PRO_{ASY1}:intron1-8:GFP reporter	ATGintron1-F	TCGTTATTCGTTTCACACTTCTGCAAAAATGGTGAGAGCAGAAATCGCCGATCAT
	intron8-GFP-R	TGAACAGCTCCTCGCCCTTGCTCACCATCTGCAAAAAGGTTTAAACAACAGCTGTC
	GFP-F	ATGGTGAGCAAGGGCGAGGAGCTGTTCA
	Pro-R	TTTTGCAGAAGTGTGAAACGAATAACGA
$5'UTR_{ASY1}$:intron1-8:GFP reporter	BH45	ACTAGTCATAAACTGATAAACATTCTCTCC
	BH46	GGTGAAGGGGGCGGCCGGGAGCCTGCTTTTTT
PRO_{ASY1}:intron3-8:GFP reporter	intron3-F	GTGAGATGCTAATCTGGAAGTTTCTAG
	Pro-R	TTTTGCAGAAGTGTGAAACGAATAACGA
PRO_{ASY1}:intron3-5:GFP reporter	GFP-F	ATGGTGAGCAAGGGCGAGGAGCTGTTCA
	intron5-R	CTGCAATAACACAGACCCTTCATCA
PRO_{ASY1}:intron6-8:GFP reporter	intron6-F	GTGCAGTGTTGAGATAATTCTTTCC
	Pro-R	TTTTGCAGAAGTGTGAAACGAATAACGA
intron3-5:PRO_{ASY1}:GFP reporter	BH106	AAAAAAGCAGGCTCCGCGGCCGCCCCCTTCACCGTGAGATGCTAATCTGGAAGTTTCTAG
	BH107	TTGCTCTTCTTAACTGGACCCCACCCTGCTGCAATAACACAGACC

		CTTCATCAAT
	BH105	CAGGGTGGGGTCCAGTTAAGAAGAGCAA
	BH46	GGTGAAGGGGGCGGCCGCGGAGCCTGCTTTTTT
PRO_{ASY1}:intron4-5:GFP reporter	BH104	GTTTTCTATACTAATGATTTTGGC
	Pro-R	TTTTGCAGAAGTGTGAAACGAATAACGA
PRO_{ASY1}:intron3,5:GFP reporter	BH114	GTAAGTTCTGGCGAATGATTGATTAGC
	BH115	CTACAAAAGCGTCCGCCCAATATTAGT
PRO_{ASY1}:intron3-4:GFP reporter	BH116	ATGGTGAGCAAGGGCGAGGAGCTGTT
	BH117	CTAGATTCCATATTAAGAAACAAAATCATC
PRO_{ASY1}:intron1-8:CDS_{ASY1}:GFP reporter	Pro-intron1-F	TCGTTATTCGTTTCACACTCTGCAAAAGTGAGAGCAGAAATCGCCGATCAT
	intron8-CDS-R	CTTCCTTCAGCTTCTGAGCCATCACCATCTGCAAAAAGGTTTAAACAACAGCTG
	CDS-F	ATGGTGATGGCTCAGAAGCTGAAGGAAG
	Pro-R	TTTTGCAGAAGTGTGAAACGAATAACGA
PRO_{ASY1}:intron3-5:CDS_{ASY1}:GFP reporter	BH109	TCGTTATTCGTTTCACACTTCTGCAAAAGTGAGATGCTAATCTGGAAGTTTCTAG
	BH196	CTTCCTTCAGCTTCTGAGCCATCACCATCTGCAATAACACAGACCCTTCATCA
	BH195	ATGGTGATGGCTCAGAAGCTGAAGGAAG
	BH103	TTTTGCAGAAGTGTGAAACGAATAACGA
PRO_{ASY1}:intron1-$8^{\Delta Y}{}_{patch}$:GFP and PRO_{ASY1}:intron3-$5^{\Delta Y}{}_{patch}$:GFP reporter	BH197	GTTTAATTGGTGTATGCTTTGATGATTGTGC
	BH198	ATGAGGCATCAATTAATCAAATCACCCACC
$CAAT_{ASY1}$:intron3-5:GFP reporter	BH99	CGTTACCACTAAATATCTTTCGCGTCG
	BH46	GGTGAAGGGGGCGGCCGCGGAGCCTGCTTTTTT
PRO_{ASY1}:intron3-5:GFP:TER_{NOS} reporter	BH42	AAGGGTGGGCGCGCCGACCCAGCTTTCTTGTACAAA
	BH44	TCACCCGGGTCCACCTCCCTTGTACA

Table S2. Transcription factors interacted with PRO_{ASY1}:intron3-8 by yeast one-hybrid.

Number	#AGI	Gene name	Family	Positive
1	AT5G38490	AT5G38490	REM(B3)	His3
2	AT4G03250	AT4G03250	HB	LacZ
3	AT3G53680	AT3G53680	PHD	Both
4	AT4G23980	ARF9	ARF	LacZ
5	AT4G00270	AT4G00270	GeBP	LacZ
6	AT1G54140	TAF9/TAFII21	ND	His3
7	AT4G00238	AT4G00238	GeBP	LacZ
8	AT4G00390	AT4G00390	GeBP	LacZ
9	AT5G52170	HDG7	HB	LacZ
10	AT3G11100	AT3G11100	TRIHELIX	LacZ
11	AT4G31615	AT4G31615	ABI3-VP1	LacZ
12	AT1G03800	ATERF10	AP2-EREBP	Both
13	AT2G36340	AT2G36340	GeBP	LacZ
14	AT1G76880	AT1G76880	TRIHELIX	LacZ
15	AT2G44730	AT2G44730	TRIHELIX	LacZ
16	AT5G19790	RAP2.11	AP2-EREBP	LacZ
17	AT4G01260	AT4G01260	GeBP	LacZ
18	AT4G04890	PDF2	HB	LacZ
19	AT5G05550	AT5G05550	TRIHELIX	LacZ
20	AT5G15480	AT5G15480	C2H2	His3
21	AT3G56570	AT3G56570	SET/PG	His3
22	AT2G02090	CHA19/ETL1	SNF2	His3
23	AT2G25900	ATCTH/ATTZF1	C3H	His3
24	AT5G66770	AT5G66770	GRAS	His3
25	AT2G21240	ATBPC4/BBR	BBR-BPC	LacZ
26	AT2G35530	bZIP16	BZIP	LacZ
27	AT3G12680	HUA1	C3H	His3
28	AT1G51060	HTA10	CCAAT	His3
29	AT3G20670	HTA13	CCAAT	His3
30	AT5G23090	NF-YB13	CCAAT-DR1	His3
31	AT5G47790	AT5G47790	FHA	His3
32	AT1G19180	AtJAZ1/TIFY10A	ZIM	His3
33	AT5G58620	TZF9	C3H	His3
34	AT2G45480	AtGRF9	GRF	LacZ
35	AT4G34590	ATB2/AtbZIP11/GBF6	bZIP	LacZ
36	AT2G41900	OXS2/TZF7	C3H	His3
37	AT5G54640	ATHTA1/RAT5	CCAAT	His3
38	AT1G16530	LBD3	NA	His3

Table S3. Transcription factors interacted with PRO_{ASY1}:intron3-5 by yeast one-hybrid.

Number	#AGI	Gene name	Family	Positive
1	AT5G24050	AT5G24050	REM(B3)	His3
2	AT1G47870	ATE2F2	E2F/DP	LacZ
3	AT5G03780	TRFL10	MYB-related	His3
4	AT5G38490	AT5G38490	REM(B3)	His3
5	AT4G03250	AT4G03250	HB	LacZ
6	AT5G38740	AGL77	MADS	His3
7	AT1G17520	AT1G17520	MYB	His3
8	AT3G53680	AT3G53680	PHD	His3
9	AT1G05690	BT3	TRAF/TAZ	His3
10	AT4G23980	ARF9	ARF	LacZ
11	AT5G64610	HAM1	C2H2	His3
12	AT4G00270	AT4G00270	GeBP	LacZ
13	AT1G54140	TAF9/TAFII21	ND	His3
14	AT2G37520	AT2G37520	PHD	LacZ
15	AT3G14740	AT3G14740	PHD	His3
16	AT5G14170	BAF60/CHC1	SWI/SNF-BAF60	LacZ
17	AT4G33280	AT4G33280	ABI3-VP1	LacZ
18	AT4G27230	HTA2	CCAAT	His3
19	AT4G00238	AT4G00238	GeBP	LacZ
20	AT4G00390	AT4G00390	GeBP	LacZ
21	AT5G52170	HDG7	HB	LacZ
22	AT5G18830	SPL7	SBP	His3
23	AT3G11100	AT3G11100	TRIHELIX	LacZ
24	AT4G31615	AT4G31615	ABI3-VP1	LacZ
25	AT1G03800	ATERF10	AP2-EREBP	LacZ
26	AT1G32640	ATMYC2	BHLH	His3
27	AT4G01120	GBF2	BZIP	LacZ
28	AT2G19810	AtOZF1/AtTZF2	C3H	His3
29	AT1G11510	AT1G11510	GeBP	His3
30	AT1G66420	AT1G66420	GeBP	LacZ
31	AT2G36340	AT2G36340	GeBP	Both
32	AT4G38620	ATMYB4	MYB	His3
33	AT1G76880	AT1G76880	TRIHELIX	LacZ
34	AT2G33550	AT2G33550	TRIHELIX	His3
35	AT2G44730	AT2G44730	TRIHELIX	LacZ
36	AT1G46768	RAP2.1	AP2-EREBP	His3
37	AT5G19790	RAP2.11	AP2-EREBP	LacZ
38	AT3G58120	ATBZIP61	BZIP	His3
39	AT1G02030	AT1G02030	C2H2	His3
40	AT2G17180	DAZ1	C2H2	His3
41	AT2G26940	AT2G26940	C2H2	His3
42	AT4G00250	AT4G00250	GeBP	LacZ
43	AT4G01260	AT4G01260	GeBP	LacZ
44	AT2G18550	ATHB21/HB-2	HB	LacZ
45	AT2G44910	ATHB4	HB	LacZ
46	AT3G61890	ATHB-12	HB	LacZ
47	AT4G04890	PDF2	HB	LacZ
48	AT5G15150	ATHB3/HAT7	HB	LacZ
49	AT1G25340	AtMYB116	MYB	His3
50	AT5G67300	ATMYBR1	MYB	His3
51	AT5G05550	AT5G05550	TRIHELIX	LacZ

Table S4. Transcription factors interacted with PRO_{ASY1}:intron6-8 by yeast one-hybrid.

Number	#AGI	Gene name	Family	Positive
1	AT5G24050	AT5G24050	REM(B3)	His3
2	AT1G47870	ATE2F2	E2F/DP	LacZ
3	AT5G38490	AT5G38490	REM(B3)	His3
4	AT4G03250	AT4G03250	HB	LacZ
5	AT3G53680	AT3G53680	PHD	Both
6	AT4G23980	ARF9	ARF	LacZ
7	AT4G00270	AT4G00270	GeBP	LacZ
8	AT2G37520	AT2G37520	PHD	LacZ
9	AT3G14740	AT3G14740	PHD	His3
10	AT5G14170	BAF60/CHC1	SWI/SNF-BAF60	LacZ
11	AT4G33280	AT4G33280	ABI3-VP1	LacZ
12	AT4G27230	HTA2	CCAAT	His3
13	AT4G00238	AT4G00238	GeBP	LacZ
14	AT4G00390	AT4G00390	GeBP	LacZ
15	AT5G52170	HDG7	HB	LacZ
16	AT3G11100	AT3G11100	TRIHELIX	LacZ
17	AT4G31615	AT4G31615	ABI3-VP1	LacZ
18	AT1G03800	ATERF10	AP2-EREBP	LacZ
19	AT4G01120	GBF2	BZIP	LacZ
20	AT1G66420	AT1G66420	GeBP	LacZ
21	AT2G36340	AT2G36340	GeBP	Both
22	AT1G76880	AT1G76880	TRIHELIX	LacZ
23	AT2G44730	AT2G44730	TRIHELIX	LacZ
24	AT5G19790	RAP2.11	AP2-EREBP	LacZ
25	AT2G26940	AT2G26940	C2H2	His3
26	AT4G01260	AT4G01260	GeBP	LacZ
27	AT4G04890	PDF2	HB	LacZ
28	AT5G05550	AT5G05550	TRIHELIX	LacZ
29	AT5G15480	AT5G15480	C2H2	Both
30	AT2G23290	AtMYB70	MYB	LacZ
31	AT3G01890	AT3G01890	SWI/SNF-BAF60	LacZ
32	AT5G05410	DREB2A	AP2/EREBP	LacZ
33	AT1G06850	AtbZIP52	bZIP	Both
34	AT2G25900	ATCTH/ATTZF1	C3H	His3
35	AT1G71130	AT1G71130	AP2/EREBP	LacZ
36	AT3G61830	ARF18	ARF	LacZ
37	AT2G21240	ATBPC4/BBR	BBR-BPC	LacZ
38	AT2G35530	bZIP16	BZIP	LacZ
39	AT2G24790	COL3	C2C2-CO-LIKE	His3
40	AT1G51060	HTA10	CCAAT	His3
41	AT3G20670	HTA13	CCAAT	His3
42	AT1G45249	ABF2	NA	LacZ
43	AT3G03200	anac045	NAC	LacZ
44	AT4G38910	ATBPC5BBR/BPC5	BBR-BPC	LacZ
45	AT2G46270	GBF3	BZIP	LacZ
46	AT5G06960	OBF5	BZIP	LacZ
47	AT5G01860	AT5G01860	C2H2	LacZ
48	AT3G18640	AT3G18640	C3H	His3
49	AT2G45480	AtGRF9	GRF	LacZ
50	AT1G09060	AT1G09060	JUMONJI	LacZ

51	AT4G18960	AG	MADS	His3
52	AT1G62120	AT1G62120	mTERF	LacZ
53	AT3G10500	anac053	NAC	LacZ
54	AT4G27900	AT4G27900	Orphans/C2C2-CO-like	His3
55	AT5G67480	ATBT4	TAZ	LacZ
56	AT2G31070	TPC10	TCP	His3
57	AT5G60142	AT5G60142	ABI3-VP1/B3	LacZ
58	AT1G72570	AT1G72570	AP2-EREBP	LacZ
59	AT5G11190	SHN2	AP2-EREBP	LacZ
60	AT5G25190	ESE3	AP2-EREBP	LacZ
61	AT1G21910	DREB26	AP2/EREBP	LacZ
62	AT1G50640	ERF3	AP2/EREBP	LacZ
63	AT3G15210	ATERF-4	AP2/EREBP	LacZ
64	AT5G13330	Rap2.6L	AP2/EREBP	LacZ
65	AT1G55650	AT1G55650	ARID	LacZ
66	AT5G54680	ILR3	BHLH	LacZ
67	AT1G43700	VIP1	BZIP	LacZ
68	AT1G75390	AtbZIP44	bZIP	LacZ
69	AT2G18160	ATBZIP2/FTM3/GBF5	bZIP	LacZ
70	AT2G42380	ATBZIP34	bZIP	LacZ
71	AT4G34590	ATB2/AtbZIP11/GBF6	bZIP	LacZ
72	AT2G33500	BBX12	C2C2-CO-like	His3
73	AT1G07640	OBP2	C2C2-DOF	His3
74	AT1G03790	AtTZF4/SOM	C3H	His3
75	AT1G32360	AT1G32360	C3H	His3
76	AT5G44260	AtTZF5	C3H	His3
77	AT5G54640	ATHTA1/RAT5	CCAAT	His3
78	AT3G12730	AT3G12730	G2-like	LacZ
79	AT2G06200	AtGRF6	GRF	LacZ
80	AT2G45410	LBD19	LOB/AS2	His3
81	AT4G00210	LBD31	LOB/AS2	His3
82	AT2G47190	ATMYB2	MYB	His3
83	AT3G18400	NAC058	NAC	LacZ
84	AT3G12977	AT3G12977	NAC/NAM	LacZ

Table S5. Oligos used in this study for amiRNA synthesis.

Purpose	Primer name	Sequence
amiREMs#1	F1_oligos_amiREM34 and amiREM36	TGTATCATCATCATCATCATCTCTCATGATGATCACATT CGTTATCTATTTTTTGAGAGATGATTATGATGATGA
	R1_oligos_amiREM34 and amiREM36	AATGTCATCATCATAATCATCTCTCAAAAAATAGATAAC GAATGTGATCATCATGAGAGATGATGATGATGATGA
amiREMs#2	F2_oligos_amiREM34 and amiREM36	TGTATTGAAAACCAAAACGTCGCCCATGATGATCACATT CGTTATCTATTTTTTGGGCGACGTTGTGGTTTTCAA
	R2_oligos_amiREM34 and amiREM36	AATGTTGAAAACCACAACGTCGCCCAAAAAATAGATAAC GAATGTGATCATCATGGGCGACGTTTTGGTTTTCAA
amiREMs#3	F3_oligos_amiREM35 and amiREM37	TGTATTTGGACAAGCTTAAACCCGAATGATGATCACATT CGTTATCTATTTTTTTCGGGTTTAATCTTGTCCAAA
	R3_oligos_amiREM35 and amiREM37	AATGTTTGGACAAGATTAAACCCGAAAAAAATAGATAAC GAATGTGATCATCATTCGGGTTTAAGCTTGTCCAAA
amiREMs#4	F4_oligos_amiREM35 and amiREM37	TGTATTGGACAAGCTTAAACCTCTTATGATGATCACATT CGTTATCTATTTTTTAAGAGGTTTACGCTTGTCCAA
	R4_oligos_amiREM35 and amiREM37	AATGTTGGACAAGCGTAAACCTCTTAAAAAATAGATAAC GAATGTGATCATCATAAGAGGTTTAAGCTTGTCCAA

References

Al Husini, Nadra, Paul Kudla, and Athar Ansari. 2013. “A Role for CF1A 3’ End Processing Complex in Promoter-Associated Transcription.” *PLoS Genetics* 9 (8). Public Library of Science (PLoS): e1003722. doi:10.1371/journal.pgen.1003722.

Anderson, Ericka L., Andrew E. Baltus, Hermien L. Roepers-Gajadien, Terry J. Hassold, Dirk G. de Rooij, Ans M. M. van Pelt, and David C. Page. 2008. “Stra8 and Its Inducer, Retinoic Acid, Regulate Meiotic Initiation in Both Spermatogenesis and Oogenesis in Mice.” *Proceedings of the National Academy of Sciences of the United States of America* 105 (39). Proceedings of the National Academy of Sciences: 14976–80. doi:10.1073/pnas.0807297105.

Andersson, Robin, and Albin Sandelin. 2020. “Determinants of Enhancer and Promoter Activities of Regulatory Elements.” *Nature Reviews. Genetics* 21 (2). Springer Science and Business Media LLC: 71–87. doi:10.1038/s41576-019-0173-8.

Ansari, Athar, and Michael Hampsey. 2005. “A Role for the CPF 3’-End Processing Machinery in RNAP II-Dependent Gene Looping.” *Genes & Development* 19 (24). Cold Spring Harbor Laboratory: 2969–78. doi:10.1101/gad.1362305.

Banerji, J., S. Rusconi, and W. Schaffner. 1981. “Expression of a Beta-Globin Gene Is Enhanced by Remote SV40 DNA Sequences.” *Cell* 27 (2 Pt 1): 299–308. doi:10.1016/0092-8674(81)90413-x.

Bates, Michael D., Lynn C. Schatzman, Richard P. Harvey, and S. Steven Potter. 2001. “Two CCAAT Boxes in a Novel Inverted Repeat Motif Are Required for Hlx Homeobox Gene Expression.” *Biochimica et Biophysica Acta - Gene Structure and Expression* 1519 (1–2). Elsevier BV: 96–105. doi:10.1016/s0167-4781(01)00217-2.

Borsari, Beatrice, Pablo Villegas-Mirón, Sílvia Pérez-Lluch, Isabel Turpin, Hafid Laayouni, Alba Segarra-Casas, Jaume Bertranpetit, Roderic Guigó, and Sandra Acosta. 2021. “Enhancers with Tissue-Specific Activity Are Enriched in Intronic Regions.” *Genome Research* 31 (8). Cold Spring Harbor Laboratory: 1325–36. doi:10.1101/gr.270371.120.

Brès, Vanessa, Nathan Gomes, Loni Pickle, and Katherine A. Jones. 2005. “A Human Splicing Factor, SKIP, Associates with P-TEFb and Enhances Transcription Elongation by HIV-1 Tat.” *Genes & Development* 19 (10). Cold Spring Harbor Laboratory: 1211–26. doi:10.1101/gad.1291705.

Callis, J., M. Fromm, and V. Walbot. 1987. “Introns Increase Gene Expression in Cultured Maize Cells.” *Genes & Development* 1 (10). Cold Spring Harbor Laboratory: 1183–1200. doi:10.1101/gad.1.10.1183.

Carbonell, Alberto, Atsushi Takeda, Noah Fahlgren, Simon C. Johnson, Josh T. Cuperus, and James C. Carrington. 2014. “New Generation of Artificial MicroRNA and Synthetic Trans-Acting Small Interfering RNA Vectors for Efficient Gene Silencing in Arabidopsis.” *Plant Physiology* 165 (1). Oxford University Press (OUP): 15–29. doi:10.1104/pp.113.234989.

Caselli, Francesca, Veronica Maria Beretta, Otho Mantegazza, Rosanna Petrella, Giulia Leo, Andrea Guazzotti, Humberto Herrera-Ubaldo, et al. 2019. “REM34 and REM35 Control Female and Male Gametophyte Development in Arabidopsis Thaliana.” *Frontiers in Plant Science* 10 (October). Frontiers Media SA: 1351. doi:10.3389/fpls.2019.01351.

Clough, Steven J., and Andrew F. Bent. 1998. “Floral Dip: A Simplified Method for*Agrobacterium*-mediated Transformation of*Arabidopsis Thaliana*.” *The Plant Journal: For Cell and Molecular Biology* 16 (6). Wiley: 735–43. doi:10.1046/j.1365-313x.1998.00343.x.

Damgaard, Christian Kroun, Søren Kahns, Søren Lykke-Andersen, Anders Lade Nielsen, Torben Heick Jensen, and Jørgen Kjems. 2008. “A 5’ Splice Site Enhances the Recruitment of Basal Transcription Initiation Factors in Vivo.” *Molecular Cell* 29 (2). Elsevier BV: 271–78. doi:10.1016/j.molcel.2007.11.035.

Danino, Yehuda M., Dan Even, Diana Ideses, and Tamar Juven-Gershon. 2015. “The Core Promoter: At the Heart of Gene Expression.” *Biochimica et Biophysica Acta* 1849 (8). Elsevier BV: 1116–31. doi:10.1016/j.bbagrm.2015.04.003.

Das, Rita, Jiong Yu, Zuo Zhang, Melanie P. Gygi, Adrian R. Krainer, Steven P. Gygi, and Robin Reed. 2007. “SR Proteins Function in Coupling RNAP II Transcription to Pre-MRNA Splicing.” *Molecular Cell* 26 (6). Elsevier BV: 867–81. doi:10.1016/j.molcel.2007.05.036.

Desimio, Maria Giovanna, Eleonora Cesari, Maria Sorrenti, Massimo De Felici, and Donatella Farini. 2021. “Stimulated by Retinoic Acid Gene 8 (STRA8) Interacts with the Germ Cell Specific BHLH Factor SOHLH1 and Represses c-KIT Expression in Vitro.” *Journal of Cellular and Molecular Medicine* 25 (1). Wiley: 383–96. doi:10.1111/jcmm.16087.

Dwyer, Katherine, Neha Agarwal, Lori Pile, and Athar Ansari. 2021. “Gene Architecture Facilitates Intron-Mediated Enhancement of Transcription.” *Frontiers in Molecular Biosciences* 8 (April). Frontiers Media SA: 669004. doi:10.3389/fmolb.2021.669004.

Emami, Shahram, Dinah Arumainayagam, Ian Korf, and Alan B. Rose. 2013. “The Effects of a Stimulating Intron on the Expression of Heterologous Genes in Arabidopsis Thaliana.” *Plant Biotechnology Journal* 11 (5). Wiley: 555–63. doi:10.1111/pbi.12043.

Fauser, Friedrich, Simon Schiml, and Holger Puchta. 2014. “Both CRISPR/Cas-Based Nucleases and Nickases Can Be Used Efficiently for Genome Engineering in Arabidopsis Thaliana.” *The Plant Journal: For Cell and Molecular Biology* 79 (2). Wiley: 348–59. doi:10.1111/tpj.12554.

Fong, Y. W., and Q. Zhou. 2001. “Stimulatory Effect of Splicing Factors on Transcriptional Elongation.” *Nature* 414 (6866). Springer Science and Business Media LLC: 929–33. doi:10.1038/414929a.

Gallegos, Jenna E., and Alan B. Rose. 2017. “Intron DNA Sequences Can Be More Important than the Proximal Promoter in Determining the Site of Transcript Initiation.” *The Plant Cell* 29 (4): 843–53. doi:10.1105/tpc.17.00020.

Gallegos, Jenna E., and Alan B. Rose. 2019. “An Intron-Derived Motif Strongly Increases Gene Expression from Transcribed Sequences through a Splicing Independent Mechanism in Arabidopsis Thaliana.” *Scientific Reports* 9 (1). Springer Science and Business Media LLC: 13777. doi:10.1038/s41598-019-50389-5.

Gaudinier, Allison, Lifang Zhang, John S. Reece-Hoyes, Mallorie Taylor-Teeples, Li Pu, Zhijie Liu, Ghislain Breton, et al. 2011. “Enhanced Y1H Assays for Arabidopsis.” *Nature Methods* 8 (12). Springer Science and Business Media LLC: 1053–55. doi:10.1038/nmeth.1750.

Ishiguro, Kei-Ichiro, Kumi Matsuura, Naoki Tani, Naoki Takeda, Shingo Usuki, Mariko Yamane, Michihiko Sugimoto, et al. 2020. “MEIOSIN Directs the

Switch from Mitosis to Meiosis in Mammalian Germ Cells." *Developmental Cell* 52 (4). Elsevier BV: 429-445.e10. doi:10.1016/j.devcel.2020.01.010.

Jores, Tobias, Jackson Tonnies, Travis Wrightsman, Edward S. Buckler, Josh T. Cuperus, Stanley Fields, and Christine Queitsch. 2021. "Synthetic Promoter Designs Enabled by a Comprehensive Analysis of Plant Core Promoters." *Nature Plants* 7 (6). Springer Science and Business Media LLC: 842–55. doi:10.1038/s41477-021-00932-y.

Kassir, Y., D. Granot, and G. Simchen. 1988. "IME1, a Positive Regulator Gene of Meiosis in S. Cerevisiae." *Cell* 52 (6). Elsevier BV: 853–62. doi:10.1016/0092-8674(88)90427-8.

Knoll, Alexander, Susan Schröpfer, and Holger Puchta. 2014. "The RTR Complex as Caretaker of Genome Stability and Its Unique Meiotic Function in Plants." *Frontiers in Plant Science* 5 (February). Frontiers Media SA: 33. doi:10.3389/fpls.2014.00033.

Kyrchanova, Olga, and Pavel Georgiev. 2021. "Mechanisms of Enhancer-Promoter Interactions in Higher Eukaryotes." *International Journal of Molecular Sciences* 22 (2). MDPI AG: 671. doi:10.3390/ijms22020671.

Li, Shaofang, Yuan Wang, Yonghui Zhao, Xinjie Zhao, Xuemei Chen, and Zhizhong Gong. 2020. "Global Co-Transcriptional Splicing in Arabidopsis and the Correlation with Splicing Regulation in Mature RNAs." *Molecular Plant* 13 (2). Elsevier BV: 266–77. doi:10.1016/j.molp.2019.11.003.

Lin, Shengrong, Gabriela Coutinho-Mansfield, Dong Wang, Shatakshi Pandit, and Xiang-Dong Fu. 2008. "The Splicing Factor SC35 Has an Active Role in Transcriptional Elongation." *Nature Structural & Molecular Biology* 15 (8). Springer Science and Business Media LLC: 819–26. doi:10.1038/nsmb.1461.

Misteli, Tom. 2007. "Beyond the Sequence: Cellular Organization of Genome Function." *Cell* 128 (4). Elsevier BV: 787–800. doi:10.1016/j.cell.2007.01.028.

Moabbi, Aboudi M., Neha Agarwal, Belal El Kaderi, and Athar Ansari. 2012. "Role for Gene Looping in Intron-Mediated Enhancement of Transcription." *Proceedings of the National Academy of Sciences of the United States of America* 109 (22). Proceedings of the National Academy of Sciences: 8505–10. doi:10.1073/pnas.1112400109.

Nachman, Iftach, Aviv Regev, and Sharad Ramanathan. 2007. “Dissecting Timing Variability in Yeast Meiosis.” *Cell* 131 (3). Elsevier BV: 544–56. doi:10.1016/j.cell.2007.09.044.

Nojima, Takayuki, Kenny Rebelo, Tomás Gomes, Ana Rita Grosso, Nicholas J. Proudfoot, and Maria Carmo-Fonseca. 2018. “RNA Polymerase II Phosphorylated on CTD Serine 5 Interacts with the Spliceosome during Co-Transcriptional Splicing.” *Molecular Cell* 72 (2). Elsevier BV: 369-379.e4. doi:10.1016/j.molcel.2018.09.004.

Norris, S. R., S. E. Meyer, and J. Callis. 1993. “The Intron of Arabidopsis Thaliana Polyubiquitin Genes Is Conserved in Location and Is a Quantitative Determinant of Chimeric Gene Expression.” *Plant Molecular Biology* 21 (5). Springer Science and Business Media LLC: 895–906. doi:10.1007/bf00027120.

Oatley, Jon M., and Michael D. Griswold. 2020. “MEIOSIN: A New Watchman of Meiotic Initiation in Mammalian Germ Cells.” *Developmental Cell*. Elsevier BV. doi:10.1016/j.devcel.2020.02.002.

Palstra, Robert-Jan, and Frank Grosveld. 2012. “Transcription Factor Binding at Enhancers: Shaping a Genomic Regulatory Landscape in Flux.” *Frontiers in Genetics* 3 (September). Frontiers Media SA: 195. doi:10.3389/fgene.2012.00195.

Peterson, Ross, Janet P. Slovin, and Changbin Chen. 2010. “A Simplified Method for Differential Staining of Aborted and Non-Aborted Pollen Grains.” *International Journal of Plant Biology* 1 (2). MDPI AG: e13. doi:10.4081/pb.2010.e13.

Pochon, Gaetan, Isabelle M. Henry, Chao Yang, Niels Lory, Nadia Fernández-Jiménez, Franziska Böwer, Bingyan Hu, et al. 2023. “The Arabidopsis Hop1 Homolog ASY1 Mediates Cross-over Assurance and Interference.” *PNAS Nexus* 2 (3). Oxford University Press (OUP): gac302. doi:10.1093/pnasnexus/pgac302.

Pruneda-Paz, Jose L., Ghislain Breton, Dawn H. Nagel, S. Earl Kang, Katia Bonaldi, Colleen J. Doherty, Stephanie Ravelo, Mary Galli, Joseph R. Ecker, and Steve A. Kay. 2014. “A Genome-Scale Resource for the Functional Characterization of Arabidopsis Transcription Factors.” *Cell Reports* 8 (2). Elsevier BV: 622–32. doi:10.1016/j.celrep.2014.06.033.

Reddy, Anireddy S. N. 2007. “Alternative Splicing of Pre-Messenger RNAs in Plants in the Genomic Era.” *Annual Review of Plant Biology* 58 (1). Annual Reviews: 267–94. doi:10.1146/annurev.arplant.58.032806.103754.

Ricci, William A., Zefu Lu, Lexiang Ji, Alexandre P. Marand, Christina L. Ethridge, Nathalie G. Murphy, Jaclyn M. Noshay, et al. 2019. “Widespread Long-Range Cis-Regulatory Elements in the Maize Genome.” *Nature Plants* 5 (12). Springer Science and Business Media LLC: 1237–49. doi:10.1038/s41477-019-0547-0.

Rose, Alan B. 2004. “The Effect of Intron Location on Intron-Mediated Enhancement of Gene Expression in Arabidopsis.” *The Plant Journal: For Cell and Molecular Biology* 40 (5). Wiley: 744–51. doi:10.1111/j.1365-313X.2004.02247.x.

Sanchez Moran, E., S. J. Armstrong, J. L. Santos, F. C. Franklin, and G. H. Jones. 2001. “Chiasma Formation in Arabidopsis Thaliana Accession Wassileskija and in Two Meiotic Mutants.” *Chromosome Research: An International Journal on the Molecular, Supramolecular and Evolutionary Aspects of Chromosome Biology* 9 (2): 121–28. doi:10.1023/a:1009278902994.

Seemann, Silja Janina. 2022. “Transcriptional Control of ASYNAPTIC 1 (ASY1) from Arabidopsis Thaliana - Characterization of a Meiocyte-specific Promoter Construct and its Regulating Transcription Factors.” University of Hamburg. Bachelor's thesis.

Séguéla-Arnaud, Mathilde, Wayne Crismani, Cécile Larchevêque, Julien Mazel, Nicole Froger, Sandrine Choinard, Afef Lemhemdi, et al. 2015. “Multiple Mechanisms Limit Meiotic Crossovers: TOP3α and Two BLM Homologs Antagonize Crossovers in Parallel to FANCM.” *Proceedings of the National Academy of Sciences of the United States of America* 112 (15). Proceedings of the National Academy of Sciences: 4713–18. doi:10.1073/pnas.1423107112.

Shaul, Orit. 2017. “How Introns Enhance Gene Expression.” *The International Journal of Biochemistry & Cell Biology* 91 (Pt B): 145–55. doi:10.1016/j.biocel.2017.06.016.

Smale, Stephen T., and James T. Kadonaga. 2003. “The RNA Polymerase II Core Promoter.” *Annual Review of Biochemistry* 72 (1). Annual Reviews: 449–79. doi:10.1146/annurev.biochem.72.121801.161520.

Song, B., and C. S. Young. 1998. “Functional Analysis of the CAAT Box in the Major Late Promoter of the Subgroup C Human Adenoviruses.” *Journal of Virology* 72 (4). American Society for Microbiology: 3213–20. doi:10.1128/JVI.72.4.3213-3220.1998.

Tam, Janis, and Folkert J. van Werven. 2020. “Regulated Repression Governs the Cell Fate Promoter Controlling Yeast Meiosis.” *Nature Communications* 11 (1). Springer Science and Business Media LLC: 2271. doi:10.1038/s41467-020-16107-w.

Tan-Wong, Sue Mei, Judith B. Zaugg, Jurgi Camblong, Zhenyu Xu, David W. Zhang, Hannah E. Mischo, Aseem Z. Ansari, Nicholas M. Luscombe, Lars M. Steinmetz, and Nick J. Proudfoot. 2012. “Gene Loops Enhance Transcriptional Directionality.” *Science (New York, N.Y.)* 338 (6107). American Association for the Advancement of Science (AAAS): 671–75. doi:10.1126/science.1224350.

Thangavel, Gokilavani, Paulo G. Hofstatter, Raphaël Mercier, and André Marques. 2023. “Tracing the Evolution of the Plant Meiotic Molecular Machinery.” *Plant Reproduction* 36 (1). Springer Science and Business Media LLC: 73–95. doi:10.1007/s00497-022-00456-1.

Thomas, Mary C., and Cheng-Ming Chiang. 2006. “The General Transcription Machinery and General Cofactors.” *Critical Reviews in Biochemistry and Molecular Biology* 41 (3). Informa UK Limited: 105–78. doi:10.1080/10409230600648736.

Tian, H. 2001. “RNA Ligands Generated against Complex Nuclear Targets Indicate a Role for U1 SnRNP in Co-Ordinating Transcription and RNA Splicing.” *FEBS Letters* 509 (2). Wiley: 282–86. doi:10.1016/s0014-5793(01)03188-x.

Vernimmen, Douglas, and Wendy A. Bickmore. 2015. “The Hierarchy of Transcriptional Activation: From Enhancer to Promoter.” *Trends in Genetics: TIG* 31 (12). Elsevier BV: 696–708. doi:10.1016/j.tig.2015.10.004.

Westphal, Jonas. 2024. “Expression and Purification of the Arabidopsis thaliana KNO1-RTR Complex for Structural Analysis by Cryo Electron Microscopy.” University of Hamburg. Master's thesis.

Wijnker, Erik, Kees van Dun, C. Bastiaan de Snoo, Cilia L. C. Lelivelt, Joost J. B. Keurentjes, Nazatul Shima Naharudin, Maruthachalam Ravi, Simon W. L. Chan, Hans de Jong, and Rob Dirks. 2012. “Reverse Breeding in Arabidopsis

Thaliana Generates Homozygous Parental Lines from a Heterozygous Plant." *Nature Genetics* 44 (4). Springer Science and Business Media LLC: 467–70. doi:10.1038/ng.2203.

Xie, Kabin, Bastian Minkenberg, and Yinong Yang. 2015. "Boosting CRISPR/Cas9 Multiplex Editing Capability with the Endogenous TRNA-Processing System." *Proceedings of the National Academy of Sciences of the United States of America* 112 (11). Proceedings of the National Academy of Sciences: 3570–75. doi:10.1073/pnas.1420294112.

Xu, Penghui, Hang Su, Wanli Chen, and Pingli Lu. 2018. "The Application of a Meiocyte-Specific CRISPR/Cas9 (MSC) System and a Suicide-MSC System in Generating Inheritable and Stable Mutations in Arabidopsis." *Frontiers in Plant Science* 9 (July): 1007. doi:10.3389/fpls.2018.01007.

Yang, Chao, Yuki Hamamura, Kostika Sofroni, Franziska Böwer, Sara Christina Stolze, Hirofumi Nakagami, and Arp Schnittger. 2019. "SWITCH 1/DYAD Is a Novel WINGS APART-LIKE Antagonist That Maintains Sister Chromatid Cohesion in Meiosis." *BioRxiv*. bioRxiv. doi:10.1101/551317.

Yang, Chao, Bingyan Hu, Stephan Michael Portheine, Pichaporn Chuenban, and Arp Schnittger. 2020. "State Changes of the HORMA Protein ASY1 Are Mediated by an Interplay between Its Closure Motif and PCH2." *Nucleic Acids Research* 48 (20). Oxford University Press (OUP): 11521–35. doi:10.1093/nar/gkaa527.

Yang, Chao, Kostika Sofroni, Erik Wijnker, Yuki Hamamura, Lena Carstens, Hirofumi Harashima, Sara Christina Stolze, et al. 2020. "The Arabidopsis Cdk1/Cdk2 Homolog CDKA;1 Controls Chromosome Axis Assembly during Plant Meiosis." *The EMBO Journal* 39 (3). EMBO: e101625. doi:10.15252/embj.2019101625.

Zhang, Luoyan, Hongzhi Kong, Hong Ma, and Ji Yang. 2018. "Phylogenomic Detection and Functional Prediction of Genes Potentially Important for Plant Meiosis." *Gene* 643 (February). Elsevier BV: 83–97. doi:10.1016/j.gene.2017.12.005.

Zhang, Nannan, Dandan Zhang, Samuel L. Chen, Ben-Qiang Gong, Yanjun Guo, Lahong Xu, Xiao-Ning Zhang, and Jian-Feng Li. 2018. "Engineering Artificial MicroRNAs for Multiplex Gene Silencing and Simplified Transgenic Screen." *Plant Physiology* 178 (3). Oxford University Press (OUP): 989–1001. doi:10.1104/pp.18.00828.

Chapter II

A cytological framework of female meiosis in *Arabidopsis thaliana*

Bingyan Hu[#1], Maria Ada Prusicki[#1], Katharina Stahlmann[2], Linda Krause[2] and Arp Schnittger[1]*

[1]: Department of Developmental Biology, Institute of Plant Science and Microbiology, University of Hamburg, Hamburg, Germany
[2]: Institute of Medical Biometry and Epidemiology, University Medical Center Hamburg-Eppendorf, Hamburg, Germany

[#]: These authors contributed equally
*: Lead contact: arp.schnittger@uni-hamburg.de

Contributions of authors

All the analyses and results presented in this chapter were generated exclusively by me, Bingyan Hu, except for those indicated below. I am sincerely grateful to all collaborators for their invaluable contributions to this work.

Dr. Maria Ada Prusicki has performed half of the original acquisition of female meiosis movies used in this study, contributing to Figure 1G-H, Figure 2A, Figure 3A-B and Figure 5 A-B.

Katharina Stahlmann has performed the time course calculation using the imaging data I analyzed in this study, contributing to Figure 4C.

A cytological framework of female meiosis in *Arabidopsis thaliana*

Highlights

Establishment of a live-cell imaging system captures dynamic features of female meiosis.

Identification of cytological landmarks ensures robust assignment of meiotic stages.

Time-lapse imaging enables quantitative dissection of meiotic phases.

Application of the framework reveals great plasticity in the commitment to meiosis.

Summary

Female and male meiosis often differ in many aspects, such as their duration and the frequency as well as the positioning of crossovers. However, studying female meiosis is often very challenging and thus, much less is known about female versus male meiosis in many species including plants. To approach this gap, we have developed a live-cell imaging system for female meiocytes in Arabidopsis. This allowed us to obtain a temporally resolved cytological framework of female meiosis in the wildtype that serves as a guiding system for future studies. Here, we have applied this imaging system to study mutants in cyclin-dependent kinase inhibitors, in which a designated female meiocyte undergoes several mitotic divisions before entering meiosis. This enabled us to address when a meiocyte is committed to meiosis, a key question during reproductive development, particularly for the analysis of apomictic species.

Introduction

Meiosis is key for sexual reproduction and a major driving force for evolution. Meiosis ensures genetic stability across generations by reducing the genomic content by half so that the full genomic complement is restored after fertilization. Additionally, meiosis promotes genetic diversity through the reciprocal exchange of genetic material between homologous chromosomes. The molecular machinery of meiotic recombination and chromosome segregation is highly conserved among such diverse eukaryotes as mammals and flowering plants, suggesting that meiosis was probably invented more than one billion years ago in the last common ancestor of all eukaryotes. Given its fundamental characteristics and high degree of conservation, it is notable that there is a substantial level of dimorphism between the sexes in one species.

One of the most prominent examples of the specifics of female meiosis is seen in mammals, where oocytes start meiosis synchronously but get arrested twice during meiosis for years and even decades. In contrast, spermatocytes in males continuously undergo meiosis without interruption (Handel and Eppig 1998; Hua and Liu 2021). Not only do meiosis timing and duration differ, but the number of living meiotic products also differs between sexes, with typically one meiotic product from female meiosis versus four meiotic products from male meiosis surviving. Furthermore, crossover (CO) frequencies also differ with human oocytes exhibiting higher CO rates than spermatocytes (Rasmussen and Holm 1978; Charles Tease, Hartshorne, and Hultén 2002; Bhérer, Campbell, and Auton 2017).

Similarly, flowering plants show differences between female and male meiosis. For instance, CO frequency is lower in female meiocytes (megaspore mother cells, MMCs) than in male meiocytes (pollen mother cells, PMCs) in *Arabidopsis thaliana* (Arabidopsis) *(Drouaud et al. 2007; Giraut et al. 2011)*. The observation that many mutants in meiotic regulators, for instance in the A-type cyclin TARDY ASYNCHRONOUS MEIOSIS and the anaphase-promoting complex inhibitor OMISSION OF SECOND MEIOTIC DIVISION/GIGAS CELLS, affect female versus male meiosis to a different level indicates that the full extent and the molecular basis of these differences are far from being understood (d'Erfurth et al. 2010; Cromer et al. 2012). Over the past decades, more than 100 plant genes have been functionally studied in the regulation of meiosis (Zhang et al. 2018; Thangavel et al. 2023), mainly

in the model plant Arabidopsis, where the meiotic regulation is primarily studied in PMCs which can be found at a quantity of 100-120 per male floral organ (anther, with six anthers present per flower) and which are relatively easily accessible.

In contrast, female meiosis remains much less known. In Arabidopsis, female meiosis occurs within ovules, which are deeply embedded in maternal floral organs (carpels) and thus are not readily accessible. Moreover, the roughly 700 PMCs per flower bud are matched by only approximately 50 MMCs. This low proportion makes it, for instance, very laborious to find MMC in squash preparations typically used for immuno-cytochemistry experiments of plant meiosis. Moreover, very little is known about the dynamics of female meiosis and the few studies that have addressed this question have relied on time course experiments with fixed material, precluding the tracing of a single cell and an estimation of the biological variation (Armstrong and Jones 2001).

Recent advances in live-cell imaging of meiosis have opened new possibilities for observing cellular processes with great spatial and temporal resolution. This has provided important insights into male meiosis including the analysis of meiotic progression (Maria A. Prusicki et al. 2019; Valuchova et al. 2020; De Jaeger-Braet et al. 2022), chromosome movement (Cromer et al. 2024; Sheehan and Pawlowski 2009), meiotic spindle dynamics (Nannas and Dawe 2016; Higgins, Nannas, and Dawe 2016; Sofroni et al. 2020), positioning of crossovers (Morgan et al. 2021), repositioning of the division plane (Nannas, Higgins, and Dawe 2016), and chromosome axis organization (Yang et al. 2019, 2020).

In this study, we have established a live-cell imaging system to visualize female meiosis in Arabidopsis. Based on the difference between female and male meiosis, a new analysis system had to be adapted that relied on the formation of a contig of meiotic reporter lines revealing landmarks of female meiosis and allowing the quantification of meiotic stages with high temporal resolution.

With this, we have obtained a temporal and spatial framework of female meiosis that also provides criteria for evaluating meiotic mutants. Here, we have used this system to reanalyze quadruple mutants in cyclin-dependent kinase inhibitors which undergo several mitotic divisions before executing meiosis (Zhao et al. 2017). This work highlights that a meiotic division can be converted to a mitotic division with several meiotic structures already established. Understanding the commitment to meiosis is also relevant to get further insights into apomixis, a process in which meiosis

is skipped, offering a promising route for plant breeding to maintain high yields in hybrid crops (Koltunow and Grossniklaus 2003).

Results

Set up of a live-cell imaging system for female meiosis in Arabidopsis

To develop a live-cell imaging system of female meiosis in its developmental context, we established a procedure in which we harvested the inflorescences on an agar plate and cut off all flower buds, leaving one young flower bud at a meiotic/premeiotic stage with a part of the stem from the inflorescence (Figure 1A, B). Sepals, petals and stamens were further removed, giving access to the pistil in the middle. Next, one side of the valve of the ovary was cut off, and the ovule primordia revealing the MMCs were adjusted face up then embedded into half-strength MS medium with 0.8% agarose and stabilized with a drop of 1% agarose, filling up the petri dish with water in the end (Figure 1C-E). One primordium is then imaged with a water-dipping lens on an upright confocal laser scanning microscope (Figure 1E-G).

Since female and male meiosis are not initiated at the same time during Arabidopsis flower development (Armstrong and Jones 2001), previous estimates on the floral stage when male meiosis takes place could not be used as a proxy for the time point of female meiosis (Maria A. Prusicki et al. 2019). We therefore first established a rough developmental time course in which we correlated the length of the ovary with the time point when meiosis occurs, revealing that under our growth conditions, female meiosis takes place when the pistil is between 0.7 and 1.6 mm long harboring an ovary between 0.5 and 1 mm in a 5-week-old plant (Figure 1B).

Next, we determined that ovules containing MMCs can be kept alive for more than 60 hours with this setup. Since we observed that the same meiotic stages lasted for approximately the same duration, irrespective of whether a movie started immediately at this stage or earlier (Table S1), we conclude that our setup does not, at least not grossly, interfere with meiotic progression, paving the way for a detailed live-cell imaging approach.

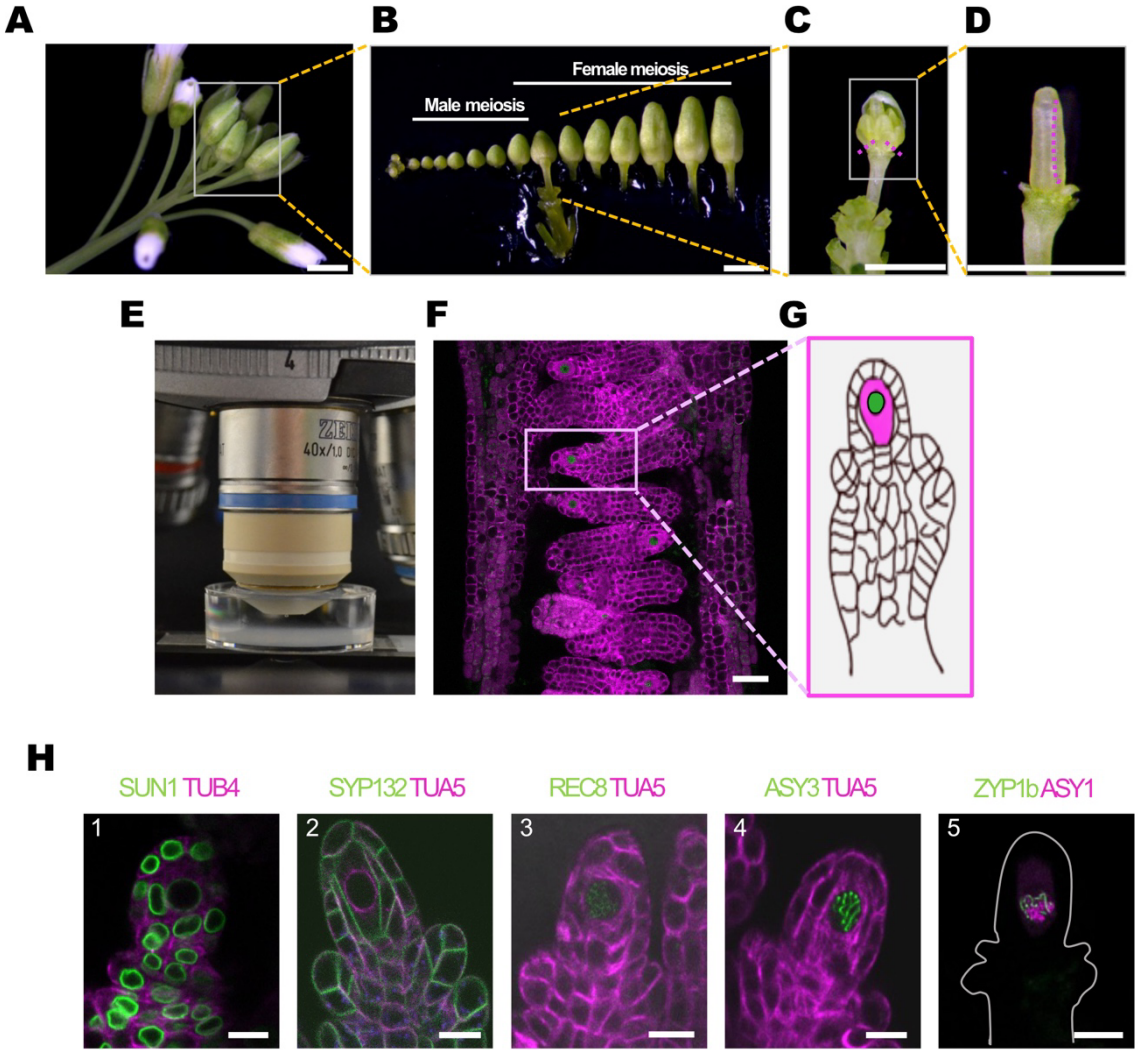

Figure 1. Live-cell imaging setup of female meiocytes. (A) Inflorescence of a 5-week-old plant. Scale bar: 1 mm. **(B)** Flower buds during meiosis. Scale bar: 1mm. **(C)** Removal of sepals, petals, and stamens from a flower bud gives access to the ovary. Scale bar: 1mm. **(D)** Removal of one valve of the ovary gives access to the ovule primordium containing the MMCs. **(E)** The specimen is embedded in agar on a plate and submerged in water to be imaged using a water-dipping lens. **(F)** Confocal laser scanning micrograph of several ovule primordia with MMCs highlighted by a meiosis-specific reporter line. Scale bar: 25 µm. **(G)** Sketch of one ovule primordium with the distally located MMC highlighted in magenta and its nucleus in green. **(H)** Snapshots of meiotic reporter lines used in this analysis: 1, SUN1 in green and TUB4 in magenta; 2, SYP132 in green and TUA in magenta; 3, REC8 in green and TUA5 in magenta; 4, ASY3 in green and TUA5 in magenta; 5, ZYP1b in green and ASY1 in magenta. Scale bar: 10 µm.

Microtubule dynamics during female meiosis

The cellular changes during meiosis are mostly a continuum. Thus, a challenge for the analysis of live-cell images is to either find a means to quantify these changes and/or convert these gradual, quantitative changes into qualitative ones to define cytological stages. In previous live-cell imaging experiments of male meiocytes in Arabidopsis,

we observed that the microtubule cytoskeleton is highly dynamic and adopts distinct cellular states, which can serve as landmarks to dissect meiosis (Maria A. Prusicki et al. 2019). In total, 11 different microtubule states could be observed, e.g., microtubules forming a crescent around the nucleus (leading to the definition of the “half moon”-stage) or microtubules fully embracing the nucleus (“full moon”-stage). Thus, just using a microtubule reporter line already allows a fine-grained dissection of male meiosis.

Therefore, we explored the microtubule cytoskeleton during female meiosis with a tubulin reporter in which TagRFP is fused to TUB4 or TUA5. However, the microtubule organization during prophase I provided only a few criteria to dissect meiosis. At the onset of meiosis, microtubules were homogeneously distributed in the cytoplasm (Figure S1A). In the early prophase I, distinct microtubule bundles extend from the spindle poles to anchor the nucleus, allowing it to rotate without translocating within the cell (Figure S1A). As meiosis progresses to late prophase I, microtubules accumulate around the nuclear membrane of female meiocytes, and form a perinuclear ring at diplotene (Figure S1A), resembling the “full-moon” structure previously described for pollen mother cell in Arabidopsis at pachytene by live cell imaging (Maria A. Prusicki et al. 2019), potato (Conicella et al. 2003), wheat and tomato by MT immunolocalization (Shamina 2005). This ring persisted until nuclear envelope breakdown in diplotene.

Upon nuclear envelope breakdown, the perinuclear ring collapses and microtubules straighten and invade the former nuclear area. The microtubule fibers then reorganize into bipolar spindle fibers, anchoring chromosomes at the metaphase plate (Figure S1A). The bipolar spindle fibers converge at the poles and stretch in parallel along the division axis. During anaphase I, kinetochore-attached microtubules shortened, pulling homologous chromosomes toward the opposite poles. As the chromosomes reach the poles at telophase I, the spindle disassembles and the nuclear envelopes begin to reform around the segregated chromosomes (Figure S1C). The phragmoplast between two daughter nuclei starts to form, with parallel microtubules aligned, guiding the deposition of the new cell wall. As the first division proceeds, the phragmoplast separates from the middle towards two sides along the cell plate at cytokinesis until it fuses with the parental plasma membrane (Figure S1A).

We conclude that a microtubule reporter line can be used to reveal stages at the end of meiosis I (from metaphase onwards, Figure S1A) and meiosis II (Figure S1B), primarily due to chromosome separation and cell division structures such as the

spindle and the phragmoplast. However, this reporter only provides limited temporal resolution during prophase I. On the one hand, this might be because the shape of the MMC does not change significantly during meiosis, unlike the PMC, which instead maintains a club-shaped appearance while growing (Figure S1A, see below). On the other hand, other microtubule structures, foremost a “half moon” arrangement of microtubules surrounding the nucleus, were absent. This also has interesting implications for the interpretation of this crescent arrangement of microtubules during male meiosis.

Analysis of meiotic reporter lines during prophase I

Recognizing the limited resolution of a microtubule reporter, we sought an alternative system to monitor meiotic progression through prophase I. In the past, we and others have generated several fluorescently tagged functional genomic reporter lines for many meiotic regulators (Maria Ada Prusicki et al. 2021), including REC8 (Maria A. Prusicki et al. 2019), ASY1 (Yang et al. 2020; Valuchova et al. 2020; Feng et al. 2023), ASY3 (Yang et al. 2020; Feng et al. 2023), and ZYP1 (Yang et al. 2020). In addition, we and others have also constructed many other reporter lines that allow monitoring of cell division events, such as SYP132 (Enami et al. 2009; Sofroni et al. 2020). Therefore, we explored the possibility of monitoring female meiosis with these reporters.

REC8 is a meiosis-specific subunit of cohesin, which extrudes chromatin loops and holds the loops of sister chromatids together (Mayerova, Cipak, and Gregan 2020). REC8 is also a crucial component of the chromosome axis and plays a key role in recruiting other axis proteins, such as ASY3 (Sakuno et al. 2022). Monitoring REC8 can therefore be used to track chromosomes and monitor their organization.

Similar to male meiosis (Maria A. Prusicki et al. 2019), we found that REC8 is among the earliest proteins that accumulate specifically in female meiocytes. REC8:GFP appears as a diffused dotty signal within the nucleoplasm in early prophase I (Figure 2A). As REC8 loading continues and chromosomes start to condense, the GFP signal intensifies, forming thin thread-like structures (Figure 2B, Movie S1). With the synapses of homologs during zygotene, REC8-marked threads can be seen rotating and spinning in the nucleus (Movie S2). These threads thickened from zygotene to pachytene, indicating the completion of synapsis and further

chromosome condensation. REC8 threads shorten as meiosis progresses and the REC:GFP signal becomes dim, likely due to the removal of REC8 by WAPL, marking the disassembly of the synaptonemal complex and homolog desynapsis (Yang et al. 2019). At diakinesis, chromatin condenses into compact, short rod-like structures, the nucleolus disintegrates, and the nuclear envelope begins to break down in preparation for metaphase I. After the nuclear envelope breakdown, we could detect REC8:GFP signals aligning in the middle of the spindle microtubules during metaphase I, representing highly condensed chromosomes. However, we could not visualize chromatin behavior after homolog segregation at metaphase I with the REC8 reporter presumably because only very few cohesion molecules reside after anaphase I at centromeres, providing not sufficient fluorescence to be imaged.

Following the chromatin dynamics with REC8:GFP also gives an approximation of where the nucleus is located in the cell. In contrast to male meiocytes, we found that the nucleus in the MMC resides in a central position, although some variation could be occasionally observed. At the same time, the nucleolus can also be visualized by the absence of REC8:GFP fluorescence (Figure 2A). At meiosis onset, the nucleolus was half the size of the nucleus and remained centrally positioned in the nucleus of female meiocytes. The nucleolus was centrally located within the nucleus at meiotic onset. At S-phase or late G2, when REC8:GFP gradually appeared with diffused dotty signals, the nucleolus migrated off-center. Furthermore, during leptotene, the nucleolus gradually migrated to the nuclear periphery, touching the inner nuclear envelope and rotating together with the nuclear envelope throughout prophase (Movie S3).

ASY1 is a chromosome axis-associated HORMA-domain protein, which plays a crucial role in Arabidopsis in CO positioning, interference and assurance (Sanchez-Moran et al. 2007; Lambing et al. 2020; Pochon et al. 2023). To precisely track ASY1 and use its loading as a landmark in our analysis system, we combined a PRO_{ASY1}:ASY1:TagRFP reporter with the PRO_{REC8}:REC8:GFP (Figure 2C,D). This revealed that ASY1:RFP accumulated in early prophase before the nucleolus moves to the nuclear periphery, and on average 1500 min after REC8:GFP appeared on chromosomes.

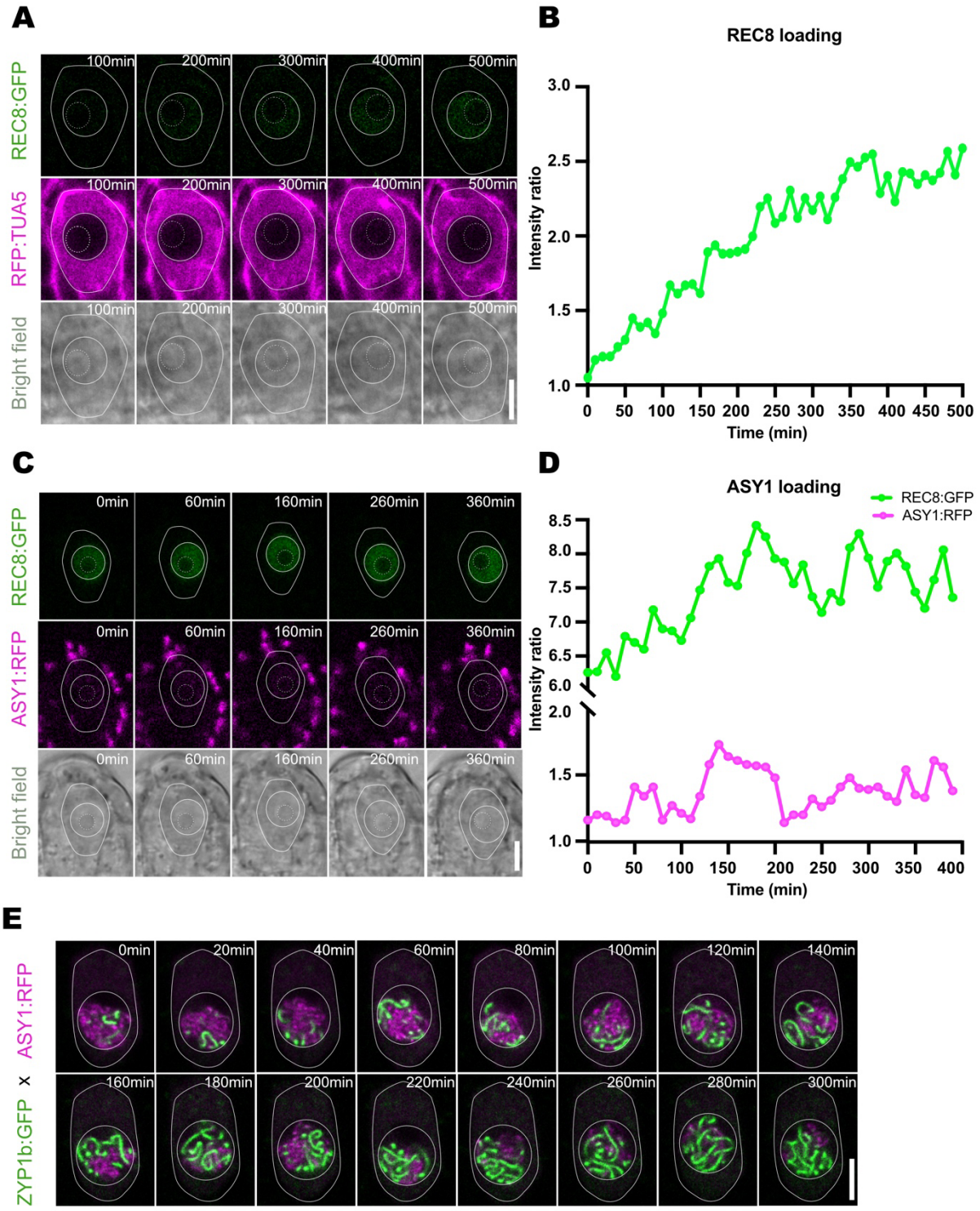

Figure 2. Visualization of chromatin dynamics by a set of reporter lines. (A) Loading of REC8:GFP onto the chromatin in female meiocytes. Meiocytes and nucleus marked with white circles, the nucleolus marked in white dashed circles. Scale bar: 5 µm. **(B)** Fluorescence intensity ratio of nuclear versus cytoplasmic REC8:GFP during REC8 loading. **(C)** Concomitant analysis of the loading of ASY1:RFP and REC8:RFP in female meiocytes. Scale bar: 5 µm. **(D)** Fluorescence intensity ratio of nuclear versus cytoplasmic REC8:GFP and ASY1:RFP during ASY1 loading. **(E)** Synaptonemal complex assembly visualized by the loading of ZYP1b:GFP and removal of ASY1:RFP during synapsis. Scale bar: 5 µm.

ASY1 presence on chromosomes is temporally restricted and with the installation of the synaptonemal complex, which establishes a proteinaceous connection between the homologous chromosomes, it is removed from the axis (Balboni et al. 2020; Yang et al. 2022). The formation of the synaptonemal complex can be visualized by accumulation of the transverse filament protein ZYP1, which polymerizes between the paired chromosome axes. Therefore, we also combined the ASY1 reporter (PRO_{ASY1}:ASY1:TagRFP) with a ZYP1 reporter (PRO_{ZYP1b}:ZYP1b:GFP). This allowed us to visualize the beginning of synaptonemal complex formation (accumulation of ZYP1b:GFP in short stretches, which grow into long filaments) and its full installment (absence of ASY1:RFP).

Chromosome pairing, recombination and synapsis have been found to be associated with fast chromosome movements (Cromer et al. 2024; Sheehan and Pawlowski 2009; Maria A. Prusicki et al. 2019). Chromosome movements are driven by external forces, such as microtubules, actin filaments, and myosin, which interact with nuclear envelope proteins to generate force. With the help of the LINKER OF THE NUCLEOSKELETON AND CYTOSKELETON (LINC) complex, the external force is transmitted through the nuclear envelope to drive chromosome movements within the nucleus. SUN1 is one of the Sad1/UNC-84 (SUN) domain proteins, which is localized to the inner nuclear membrane. SUN1 is a central component of the LINC complex, tethering telomeres to the nuclear envelope during meiosis (Varas et al. 2015). Thus, the SUN1 distribution pattern is a proxy for the attachment of telomeres to the nuclear envelope driving chromosome movement and bouquet formation.

To examine chromosome movement behavior, we generated the reporter of PRO_{SUN1}:SUN1:GFP and combined it with PRO_{RPS5A}:TagRFP:TUA5. SUN1:GFP localized uniformly in the nuclear envelope, forming a wrinkled ring when nucleolus was centrally located, then gradually tensed as meiosis progressed to leptotene, where the nucleolus was off center (Figure 3A). From late leptotene, SUN1:GFP displayed a heterogeneous distribution, with several intensely labeled domains interspersed within an otherwise uniform SUN1:GFP signal. Notably, approximately one-third of the envelope lacked SUN1:GFP signal entirely (Figure 3B).

By late pachytene, SUN1 distribution became uniform again and remained unchanged until nuclear envelope breakdown, after which SUN1:GFP signals were undetectable (Figure 3B). The nuclear envelope was absent during metaphase I and anaphase I, but reformed around decondensed chromosomes at telophase I, with

SUN1:GFP uniformly reappearing at the nuclear periphery of each daughter cell (Figure 3B).

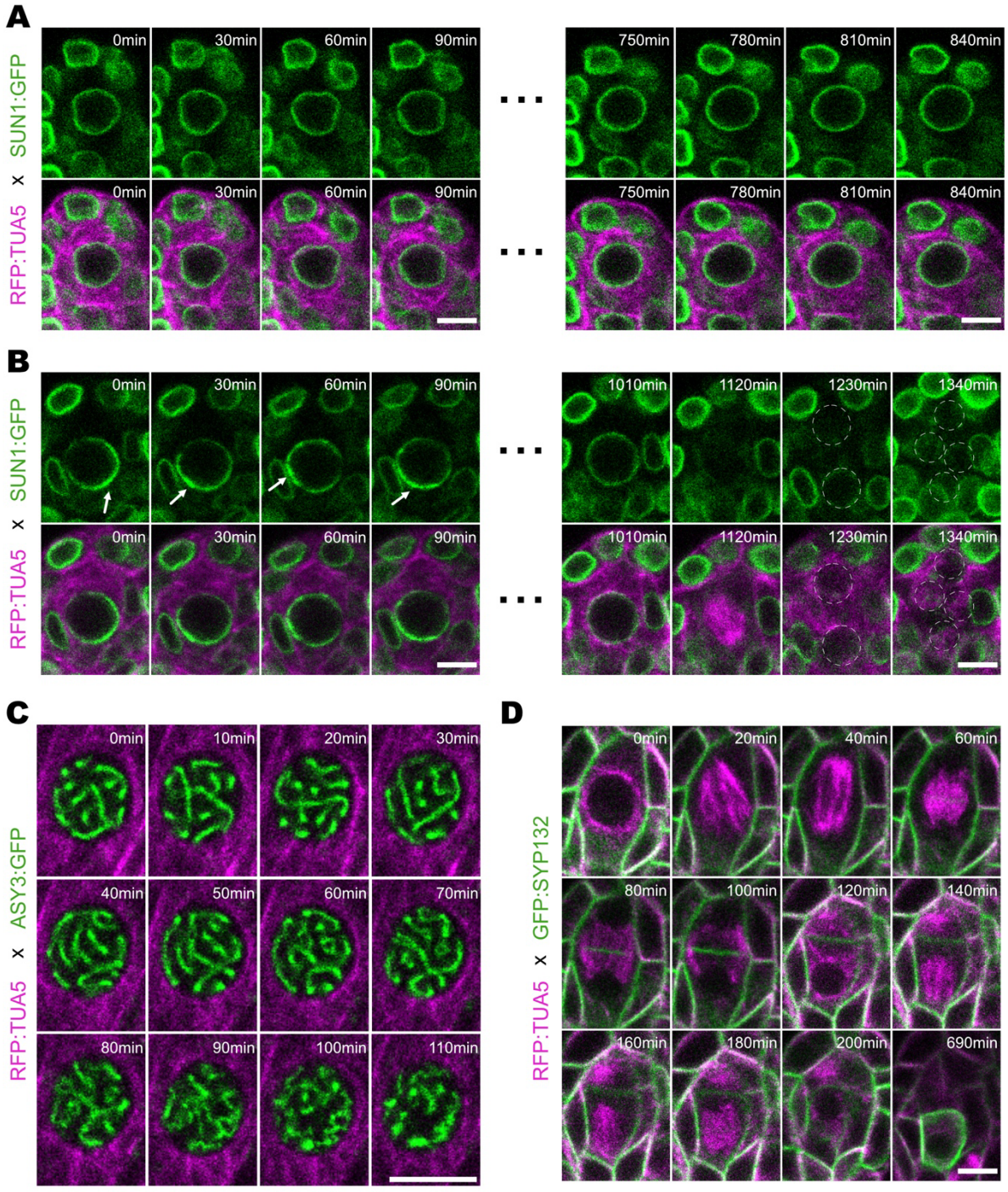

Figure 3. Visualization of nuclear envelope organization, chromosome dynamics, and cell wall formation. (A) Live cell imaging of PRO_{SUN1}:SUN1:GFPxPRO_{RPS5A}TagRFP:TUA5 in a female meiocyte during early prophase. The nuclear envelope was wrinkled at the late G2 stages, then gradually intensified as meiosis progressed into early leptotene. Scale bar: 5 μm. **(B)** Live cell imaging of PRO_{SUN1}:SUN1:GFPxPRO_{RPS5A}TagRFP:TUA5 in a female meiocyte during late prophase. SUN1:GFP signal was depleted from ⅓ of the nuclear envelope, aggregated together (white arrow) during zygotene and pachytene. As diplotene, SUN1 was uniformly distributed on the nuclear envelope again. Scale bar: 5 μm. **(C)** Live cell imaging of PRO_{ASY3}:ASY3:GFPxPRO_{RPS5A}TagRFP:TUA5 in a female meiocyte at diplotene. There is a quiescence period during which rapid chromosome movement is lost;

chromosomes freeze when the synaptonemal complex disassembles. Scale bar: 5 μm. **(D)** Live cell imaging of PRO_{SYP132}GFP:SYP132xPRO_{RPS5A}TagRFP:TUA5 in a female meiocyte during division. Phragmoplast formation and inside-to-outside deposition of cell wall during successive cytokinesis in female meiosis. The signal of SYP132 intensifies in only one meiotic product after tetrad formation. Scale bar: 5 μm.

Since REC8:GFP signal becomes diffuse in late prophase (see above), we also followed the axis protein ASY3 with a PRO_{ASY3}:ASY3:TagRFP reporter to monitor chromatin movement. This reporter also allowed the visualization of the rapid movements of chromosomes prior to and during synapsis (Movie S4). Remarkably, when the synaptonemal complex starts to break down but before nuclear envelope breakdown, the rapid chromosome movement abruptly transitions into a relatively static configuration that persists for nearly two hours. During this interval, ASY3 remains associated with chromosome axes. The thick thread marked by ASY3:GFP split into two thin threads as the synaptonemal complex disassembled. As chromosomes underwent further condensation after the disassembly of the synaptonemal complex, the ASY3:GFP-marked thread-like morphology progressively resolved into discrete, short, rod-like structures in diakinesis (Figure 3C, Movie S5).

Analysis of cytological reporter lines during female meiotic division

SYP132, a SNARE (SOLUBLE N-ETHYLMALEIMIDE-SENSITIVE FACTOR ATTACHMENT PROTEIN RECEPTOR), which is involved in membrane trafficking to the plasma membrane protein and localized at the plasma membrane in all plant tissues (Enami et al. 2009; Sofroni et al. 2020). Using the SYP132 reporter line enables the precise observation of cytokinesis in meiosis I, where the phragmoplast is deposited starting from the center of the cell, progressing successively to produce a temporary dyad after the first meiotic division (Figure 3D). With SUN1 reporter, we could also see the newly formed nuclear membranes of the dyad (Figure 3B). Using GFP-tagged SYP132 in combination with RFP-tagged TUA5, we clearly visualize the formation of two daughter cells after cytokinesis, oriented along the nucellus-chalaza direction (Figure 3D).

During interkinesis, curved microtubules accumulate around the two nuclear membranes, forming two perinuclear rings (Figure 3D). Upon nuclear envelope breakdown, these perinuclear rings collapse simultaneously, and microtubules straighten to invade the former nucleus space, assembling two spindle apparatuses

oriented in the same direction as in metaphase I (Figure 3D). During the second meiosis division, microtubules in each cell behave identically to meiosis I, as visualized from metaphase to telophase. At anaphase II, sister chromatids separate towards opposite poles, and spindle structures subsequently disassemble. Nuclear envelopes reform around the four sets of segregated chromosomes, while two phragmoplasts are deposited from the center simultaneously between each newly reformed nucleus (Figure 3B, 3D). As cytokinesis progresses, these two phragmoplasts expand laterally along the division plane until they fuse with the parental plasma membrane, like the cytokinetic pattern of meiosis I (Figure 3D).

Ultimately, four haploid daughter cells are generated in a linear tetrad within the ovule. Approximately three to four hours post-division, three of these meiotic products undergo programmed cell death, while the one positioned at the chalaza end survives, marked by an enrichment of SYP132 fluorescence (Figure 3D). The surviving megaspore subsequently enlarges, occupying the space of the degenerated cells.

Defining landmarks of female meiosis by a reporter contig system

Analyzing the above-described reporters allowed us to identify distinct events during female meiosis. We refer to these events as landmarks. In total, we were able to define 15 landmarks (**L1** to **L15**, Figure 4). Importantly, a defined order of these landmarks could be established in a contig-based manner due to the cross-anchoring of the observed features by three aspects: First, different reporters can sometimes mark the same feature, at least during some meiotic stages, e.g., REC8 and ASY1 can both be used to highlight chromosomes until synapsis. Second, most of our reporter lines expressed two fluorescently labelled proteins (Figure 1H), e.g., *PRO_{REC8}:REC8:GFP x PRO_{RPS5A}TagRFP:TUA5.* Finally, since the bright field channel can always be detected, the nucleolus position and the presence/absence of the nuclear envelope can usually be determined. This resulted in the order depicted in Figure 4A for prophase I and Figure 4B for meiosis division.

Prior to meiosis, a destined female meiocyte in Arabidopsis and also other plant species expands, making it usually the largest cell at the distal (chalazal) end of an ovule primordium. Associated with cell growth, the meiocyte exhibits gradually thickening cortical microtubules (Figure S1). At this stage, the nucleus is positioned centrally and the nucleolus is present in the center of the nucleus (Figure S1). The first

landmark (**L1**) is the loading of REC8 onto chromosomes and the beginning of chromosome condensation so that the chromosomes become visible as thin, thread-like structures. Based on work in yeast and animals, the loading of REC8 likely takes place in the *premeiotic S-phase* or *early G2-phase* (Watanabe and Nurse 1999; Eijpe et al. 2003). The second landmark (**L2**) is the migration of the nucleolus from the center of the nucleus to the periphery. This is made possible through the release of chromosomes from the nuclear envelope, allowing them to pair (Cromer et al. 2024); this defines *late leptotene*. *Zygotene* is defined as the beginning of the installation of the synaptonemal complex leading to synapsis, which can be visualized by the loading of ZYP1 along the chromosome axes (**L3**). As synapsis progresses, the chromosome axis-associated protein ASY1 is widely removed from the chromosome axes, and the chromosomes further condense (**L4**), marking the transition to *pachytene* (Figure 4B). Chromosomes exhibit fast movement from late leptotene onwards, possibly facilitating homolog recognition, pairing, and recombination (Movie S3). Interestingly, this movement becomes more rapid in *zygotene* and *pachytene*. However, chromosome movement suddenly slows down to an almost complete arrest likely through the re-anchoring of chromosomes to the inner nuclear membrane (Cromer et al. 2024; Yuan et al. 2025); at the same time, homologous chromosomes begin to desynapse defining **L5** and *diplotene*. Chromosomes condense further in diakinesis, and the linear threads of chromosome axis protein ASY3 compacted into short rods (**L6**), appearing as highly condensed bivalents. Then, the nuclear envelope breaks down, marking the end of prophase I.

At *metaphase I*, the microtubule spindle apparatus appears in the middle of the cell (**L7**), aligning the highly condensed chromosomes along the metaphase plate. The transition to *anaphase I* is marked by the shortening of spindle fibers separating the homologous chromosomes toward opposite poles (**L8**). As the chromosomes reach the poles, the spindle disassembles, and the nuclear envelopes begin to reform around the segregated chromosomes. The phragmoplast between the two daughter nuclei starts to form in *telophase I* highlighted by microtubules aligning in the middle of the cell (**L9**). As the first division proceeds, the phragmoplast dissolves from the middle towards the two sides along the cell plate revealed by the newly formed plasma membrane that separates the first two meiotic products representing the end of the first meiotic division. In the following *interkinesis*, two perinuclear ring structures formed by microtubules appear (**L10**). Shortly after, the nuclear envelope of the two

daughter nuclei breaks down, and meiosis II commences. The two spindles of the second meiotic divisions are formed by microtubules (**L11**) marking *metaphase II*. **L12** represents *anaphase II* and is visualized by the shortening of microtubules, which pull the homologous chromosomes to the opposite poles within each daughter cell simultaneously. Two phragmoplasts form in the middle of each daughter cell (**L13**) indicating *telophase II*. At *telophase II*, four nuclear envelopes form around the segregated chromatids. Then *cytokinesis II* results in the formation of a linear tetrad (**L14**) of four haploid daughter cells highlighted by GFP:SYP132 marking the end of the second meiotic division. Finally, only the meiotic product that is closest to the basal (micropylar) end of the ovule primordium survives and starts to strongly accumulate SYP132 at the plasma membrane, gradually filling the space of the former meiocyte and representing the differentiation of the functional female megaspore (**L15**), which will then undergo three mitotic divisions in Arabidopsis to form the embryo sac.

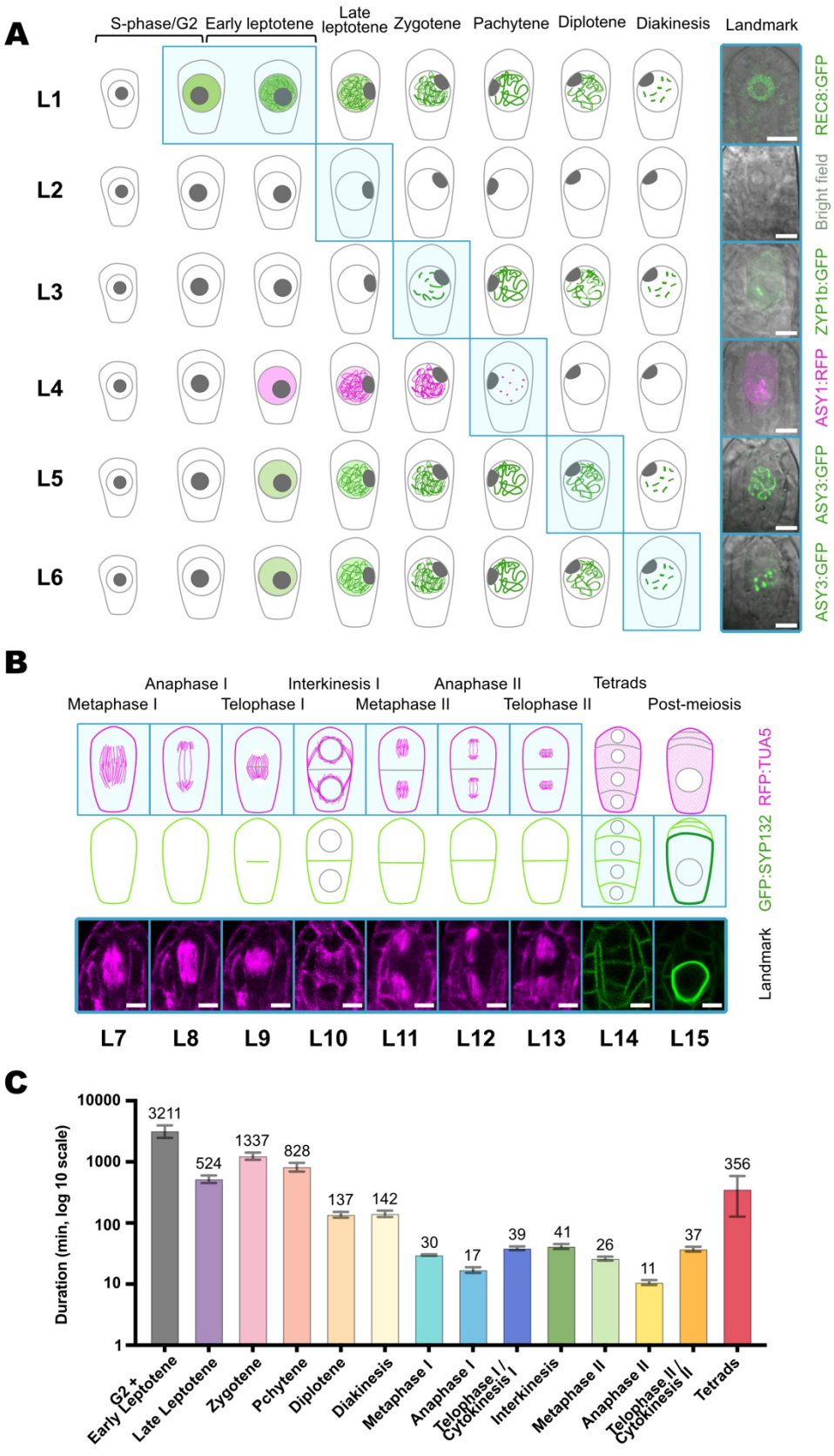

Figure 4. Landmark scheme illustration of the 15 meiotic landmarks (L1-L15). (A) Six landmarks (L1-L6) are shown in blue boxes identified by chromosome behaviors and cytological features. The last column provides a microscopy picture of the meiocyte at each stage. L1 is defined by the loading of REC8, making the late G2 and early leptotene stage. L2 marks the beginning of late leptotene defined

by the nucleolus moving aside. L3 represents the beginning of zygotene with ZYP1b loaded onto the chromosomes. L4 marks the complete removal of ASY1 at the beginning of pachytene. L5 represents the beginning of diplotene where chromosomes freeze and the synaptonemal complex disassembles. L6 marks the beginning of diakinesis, where the chromosomes compact into dotty signals. Scale bar: 5 μm. **(B)** Nine landmarks (L7-L15) are shown in blue boxes identified by the microtubule behaviors and cell wall formation. The last row displays microscopy images corresponding to each landmark. Scale bar: 5 μm. **(C)** Duration of each stage in minutes between every two landmarks as observed in WT plants. Median as shown on each column in minutes; the error bar represents the 95% confidence interval of the stage duration.

Time course of female meiosis progression

With the landmark-based classification of different meiosis stages, we could then estimate the time frame of female meiosis progression in Arabidopsis (Figure 4C). To this end, at least 109 movies were recorded that captured the transition from one landmark to the next.

However, the statistical analysis of the timing was not trivial. First, MMCs from one carpel cannot be regarded as statistically independent measurements but represent clustered data. In addition, the above-mentioned nature of defined meiotic stages gives rise to a multi-state nature of our dataset. Moreover, our measurements occasionally did not capture the exact start and/or end point (left, right, and/or interval-censored data), as the observed MMCs sometimes moved out of the focal plane (but also occasionally moved back into focus). Including the combination of the three characteristics of our data, that is, clustered data, left/right, and/or interval censoring, as well as having a multistate nature, was not possible in one statistical model. Therefore, we reduced the multistate complexity of the analysis and built a separate model for each meiotic phase, as defined by our reporter contigs (see above) which also allowed us to simplify the mixture of left/right and/or interval-censored data with respect to the duration of each state to interval and right censoring. For detailed description of the models, please see the subsection “Statistical methods” in the section “Materials and methods”.

The minimal duration of the phase between the premeiotic G1 and S-phase and the first landmark (L1) was at least 590 minutes, nearly 10 hours (Table S2). As meiosis progresses, the phase between L1 and L2 (early leptotene) was 3211 minutes (n = 31 MMCs). L2 to L3 (late leptotene) lasted approximately 524 minutes (n = 35). Zygotene duration (L3 to L4) was estimated to be 1337 minutes (n = 33). The pachytene stage (L4 to L5) lasted 828 minutes (n = 40). Diplotene (L5 to L6) lasted

around 137 minutes (n = 37). The duration of diakinesis (L6 to L7) was about 142 minutes (n = 36). With the nuclear envelope breaking down, metaphase I (L7 to L8) lasted for 30 minutes (n = 34). The phase between L8 and L9 (anaphase I) was 17 minutes (n = 34). L9 to L10 (telophase I) lasted about 39 minutes (n = 34). The phase between L10 and L11 (interkinesis I) lasted around 41 minutes (n = 34). Then meiosis II starts. The duration of meiosis II division is shorter than that of meiosis I. The metaphase II duration (L11 to L12) was estimated around 26 minutes (n = 34). The anaphase II (L12 to L13) lasted about 11 minutes (n = 34). The telophase II (L13 to L14) was observed to last approximately 37 minutes (n = 34). Then, cytokinesis occurs simultaneously for both daughter cells. The linear tetrads (L14 to L15) lasted 356 minutes (n = 34), almost 6 hours, during which the survival female microspore was enriched with brighter SYP132 signaling (Figure 4B-C).

Adding these durations, we estimated that the total duration of female meiosis, from early leptotene to the appearance of the functional megaspore, is approximately 112 hours, or more than four and a half days. Prophase I was found to be exceptionally long, almost 103 hours, i.e., representing more than 90% of the total duration. Division stages of meiosis I and meiosis II are much shorter compared to prophase I. The duration of metaphase is nearly the same between meiosis I and meiosis II.

Determination of meiotic commitment

The establishment of a temporally resolved cytological framework for female meiosis enables the investigation of previously not (easily) accessible biological questions, such as conducting detailed analyses of meiotic mutants during female meiosis and examining the effects of various environmental conditions, including heat stress, on female meiotic progression. Here, we have focused on the question when an MMC is committed to undergo meiosis. To address this question, we have analyzed the quadruple mutant *krp3 krp4 krp6 krp7* in which a family of CDK inhibitors (KIP27-RELATED PROTEINS, KRPs) is defective. In these mutants, the designated MMC undergoes several mitotic divisions prior to meiosis, resulting in the formation of supernumerary meiocytes and, consequently, multiple gametophytes within a single ovule (Zhao et al. 2017).

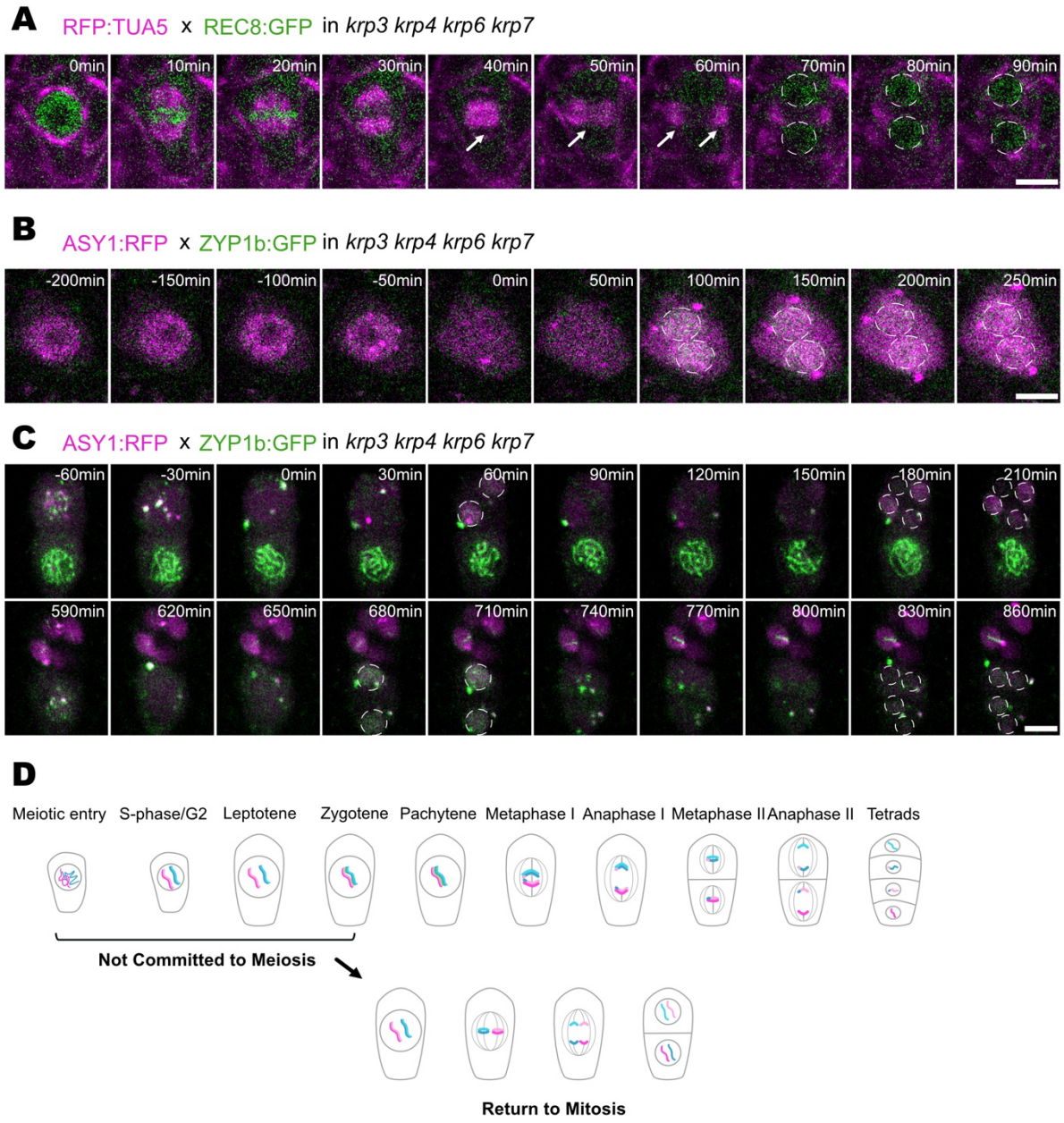

Figure 5. Analysis of meiotic commitment using a set of reporters in *krp3 krp4 krp6 krp7* by live-cell imaging. (A) An MMC of a *krp3 krp4 krp6 krp7* mutant plant with REC8 loaded undergoes one complete division resulting in two separated cells as visualized by the formation of a phragmoplast (white arrow). Notably, REC8 re-accumulated onto chromosomes in both daughter nuclei (highlighted in white dashed circles). Tubulin marked by TUA5 in magenta. Nuclear envelope breakdown marked as 0 min. Scale bar: 5 µm. **(B)** Meiocyte with ASY1:RFP loaded onto chromosomes undergoes one division resulting in two products (highlighted in white dashed circles) expressing both ASY1:RFP (magenta) and ZYP1:GFP (green, at 100min background) in *krp3 krp4 krp6 krp7*. Nuclear envelope breakdown marked as 0 min. Scale bar: 5 µm. **(C)** Two MMCs of a *krp3 krp4 krp6 krp7* mutant plant expressing ASY1:RFP (magenta) and ZYP1:GFP (green) go through two rounds of division in resulting in four products from each meiocyte. Upper meiocyte started first division at 0 min, two products (white dashed circles) expressing ASY1:RFP (magenta), and the second NEB at 90 min leading to four products (white dashed circles) with ASY:RFP (magenta). The lower meiocyte followed the meiotic division, with first NEB at 620 min and second NEB at 740 min. Division products highlighted with white dashed circles. Scale bar: 5 µm. **(D)** Model of meiosis and return to mitosis in *krp3 krp4 krp6 krp7*. Even after meiotic entry, cells were not committed to meiosis until zygotene.

Given the key role of REC8 for the regulation of cohesion in meiosis and with that for chromosome segregation, a simple hypothesis was that the replacement of RAD21 by the meiosis-specific REC8 kleisin variant could be decisive for meiotic progression. Therefore, we concomitantly introduced PRO_{REC8}:REC8:GFP with PRO_{RPS5A}:TagRFP:TUA5 into the *krp3 krp4 krp6 krp7* background and subjected the resulting plants to live-cell imaging. A total of 68 ovules from 61 independent plants were filmed and eleven movies from ten different plants captured the initiation of meiosis allowing the analysis of REC8:GFP dynamics. Of these eleven movies, five showed meiocytes undergoing a single mitotic division prior to REC8 loading, resulting in multiple meiocytes within the same ovule as judged by the subsequent accumulation of REC8:GFP in both daughter cells. We conclude that supernumerary meiocytes can arise before REC8 associates with chromatin indicating that meiotic fate is already inheritably established in or before the pre-meiotic S-phase. In 30 out of 68 movies, REC8 was already expressed in at least two meiocytes within the same ovule when the imaging started. In 17 movies, one or more MMC already expressed REC8:GFP and underwent a mitotic division (Figure 5A, S3). The resulting cells all expressed REC8:GFP again indicating that they still have MMC fate. These observations indicate that while meiotic fate is apparently fixed very early (see above), a meiotic division can be replaced with a mitotic division after REC8 loading and conversely, that a mitotic division can be executed with this kleisin subunit being loaded instead of RAD21.

Therefore, we assessed next whether MMCs can still mitotically divide when later meiotic structures are established, i.e., the chromosome axis and the synaptonemal complex. To analyze this, we introduced PRO_{ASY1}:ASY1:TagRFP along with PRO_{ZYP1b}:ZYP1b:GFP into the *krp* quadrupel mutants.

A total of 28 movies were analyzed. In 24, dynamic ASY1 or ZYP1 loading was detected. In one ovule, a single early leptotene meiocyte divided prior to ASY1 loading, yielding two MMCs as judged by the later accumulation of ASY1. In eight movies, ASY1 signal diminished in some or all meiocytes during imaging, including one case with three ASY1-expressing meiocytes, two of which lost ASY1 while the third loaded ZYP1 and completed meiotic division. Strikingly, ASY1-positive meiocytes underwent mitosis-like division followed by progression to late leptotene in two movies (Figure 5B). These findings show that even ASY1 loading and with this an at least partially established chromosome axis is still compatible with mitosis and that a meiotic division is not fixed even after approximately 50 hours into meiosis.

In contrast, in all 16 movies where ZYP1 loading was observed in one or more MMCs in one ovule primordium ZYP1-positive cells did not undergo a mitotic division and invariably progressed through meiosis until tetrad formation (Figure 5C). Thus, we conclude that a meiotic division is not fixed till at least zygotene. Since we currently cannot judge whether the mitosis promoting force diminishes over time in *krp3 krp4 krp6 krp7*, we cannot exclude that it might be even possible to induce a mitosis after zygotene, possibly with a reduced probability that would require a much larger sample size than ours to be detected. For the same reason, it is currently difficult to determine whether the synaptonemal complex itself represents a determinant of a meiotic division or whether its establishment reflects just the time until when division can be reprogrammed.

Taken together, meiotic fate is heritably established prior to REC8 loading but surprisingly, mitotic divisions can overwrite a meiotic program at least until the synaptonemal complex is established demonstrating a great level of developmental flexibility of an MMC.

Discussion

Female and male meiosis differ in many aspects in most if not all eukaryotic species. However, the insight into female meiosis largely lags behind the knowledge gained on the male side. Understanding female meiosis and comparing it with male meiosis is not only important to get crucial insight into female reproductive development but also to extract general principles of meiotic regulation in one species and between different species. To approach the knowledge gap between female and male meiosis, we have established a live-cell imaging system for MMCs in the flowering plant Arabidopsis. This system is based on confocal laser scanning microscopy and a reporter contig-based approach allowing the dissection of female meiosis with great temporal resolution. With our set-up, we could keep ovule primorida alive for more than 60 hours with an image taken every ten minutes. In total, we could distinguish 15 distinct meiotic stages, referred to as landmarks. Assigning these landmarks to the classical stages of meiosis allowed us to obtain statistically relevant time intervals for these stages, which led to an estimated total length of at least 112 hours for female meiosis. Our work establishes a cytological framework of female meiosis, spanning from the meiotic

G2 phase to the formation of a functional megaspore after telophase II.

The cytological framework of female meiosis enabled us to compare the difference in meiosis between the sexes in Arabidopsis. To this end, we mainly considered cytological data from our previous analysis of male meiosis due to similar growth conditions and the overall comparable setup of our imaging approaches (Maria A. Prusicki et al. 2019).

A first striking difference is the much longer duration of female versus male meiosis (minimum of 112 hours versus 34.5 hours) (Figure 6A). One reason for this is that the premeiotic S-phase, G2-phase, and early leptotene appear to be much longer in females than in males (approximately 55 versus 9 hours). It is currently difficult to shed light on these phases due to still lacking reporters. Interestingly, the difference in these early stages closely reflects the difference in the onset of female versus male meiosis in young flower buds (Armstrong and Jones 2001), i.e., approximately 40-50 hours, suggesting that the developmental trigger to initiate meiosis in both species could be synchronous, and possibly be even the same. One reason for the longer time to start meiosis in the female versus male could be that MMC specification relies on the selection of one cell from a group of germline-competent cells (Böwer and Schnittger 2021; Dresselhaus et al. 2025) and that this selection/fixation of cell fate takes additional time.

Furthermore, late leptotene, zygotene, pachytene, diplotene, and diakinesis are also substantially longer in female versus male meiosis (approximately 50h versus 20h). With this, leptotene in female meiosis is four times longer than in male meiosis, zygotene three times longer, and pachytene, diplotene and diakinesis are each one and a half times longer (Figure 6A). Interestingly, the relative timings are also different and zygotene is much longer than pachytene in female meiosis while in male meiosis, pachytene is longer than zygotene. This suggests that chromosome pairing and synapsis occur more slowly in female meiosis than in male meiosis.

Notably, female meiosis appears to have lower levels of CYCLIN-DEPENDENT KINASE A;1 (CDKA;1) activity, one of the major drivers of meiotic progression (Sofroni et al. 2020; Yang et al. 2019, 2020; Dissmeyer et al. 2007), as seen by observation that a reduction of CDKA;1 activity leads to more severe effects on female versus male meiosis (Sofroni et al. 2020; Wijnker et al. 2019). Given that many meiotic regulators contain CDKA;1 consensus phosphorylation sites and might be targets of CDK regulation, the slower progression on the female side may be associated with lower

levels of CDKA;1 activity. In this context, it is interesting to note that a modest reduction of CDKA;1 activity on the male side triggers cytokinesis followed by a second meiotic division (Sofroni et al. 2020). Cytokinesis is also observed on the female side, as visualized here by the SYP132 reporter, which highlights complete cytokinesis after the first division of the MMC, further arguing for overall lower levels of CDKA;1 activity during female meiosis.

Another difference between female and male is the shape of the meiocyte and the positioning of the nucleus within the meiocyte (Figure 6B). While on the male side, the shape of the meiocyte changes during progression through meiosis in the order of rectangular, trapezoidal, oval and circular (Maria A. Prusicki et al. 2019), the MMC keeps the same club-shape appearance from the beginning to the end of meiosis. The positioning of the nucleus is also different. In male meiosis, the nucleus starts at the middle of the meiocytes, moves to one side of the cell at zygotene, and then moves back to the center of the meiocyte at the late pachytene (Maria A. Prusicki et al. 2019). In female meiosis, the nucleus, with the exception of small fluctuations, remains in the middle of the meiocyte during prophase I. In fact, we found several microtubule cables emergating from the side of the cell that apparently anchored the position of the nucleus in the MMC (Figure 6B,S1). It is an interesting speculation whether this anchoring might interfere with or slow down the machinery that moves chromosomes (see below).

In contrast, the nucleolus within the nucleus behaves the same way during both female and male meiosis progression, where it only moves from the center to the side during the leptotene stage where it stays until it dissolves in late pachytene. The nucleolus movement is very likely associated with the release of chromosomes from the nuclear envelope through the degradation of the nuclear lamina-like CROWN proteins (Yuan et al. 2025). In fact, if the lamina is not degraded and chromosomes are not released from the nuclear envelope, also maintaining the centrally positioned nucleus.

Remarkably, a very prominent microtubule structure, phrased the “half-moon”, is absent in female meiosis. The half-moon assembles in male meiosis at the side of the nucleus, which faces the cytoplasm with the nucleolus being already at the side of the nucleus but located outside of half-moon domain, i.e., closer to the cell wall of the male meiocyte (Figure 6B). Notably, the migration of the nucleus and the nucleolus within are strongly associated with rapid movements of chromosomes that are thought to

promote pairing, synapsis, and recombination (Cromer et al. 2024; Maria A. Prusicki et al. 2019). The rapid movement of chromosomes is driven by the external forces transmitted by the LINC complex, where SUN1 is one of the components of LINC complexes. It´s worth noting that after telomeres are detached from the nucleolus, they cluster in a restricted region of the nuclear envelope, forming the chromosome bouquet. In zygotene of male meiosis, SUN1 is assembled at one side of the inner nuclear envelope to anchor the telomeres while the microtubules form the half-moon (arc-shaped) structure at the opposite side of the nucleus (Sofroni et al. 2020) to generate the pulling force for the chromosomes to move around for pairing and synapsis. Telomere attachment is a relatively conserved meiotic process, and the patterns of telomere attachment to the nuclear envelope and chromosome movement known as the bouquet are largely similar in males and females among most if not all organisms studied so far (Zickler and Kleckner 2016). Thus, the half moon arrangement of microtubules might be linked to nucleus movement within the meiocyte.

The rapid chromosome movement in zygotene and pachytene is very much slowed down, almost to a complete halt in diplotene of both female and male meiosis (Movie S5). Similarly, both male and female meiosis have a microtubule full-moon-like structure around the nucleus, here described as the perinuclear ring. However, the duration of this perinuclear ring in female meiosis is much shorter than in males, only visible in diplotene and diakinesis until the nuclear envelope breaks down. In male meiosis, it clearly covers almost half of the pachytene duration until the nuclear envelope breaks down, coinciding with the repositioning of the nucleus to the center of the meiocyte (Figure 5B). This migration of nucleus appears to be driven by the assembly of the second half of the microtubule array, which exerts force to restore the nucleus to a central position. Therefore, without migration of nucleus in female meiosis, the microtubule full moon structure only forms during diplotene (Figure 5B), preparing for the nuclear envelope breakdown and subsequent spindle assembly.

A further difference in the microtubule organization between female and male meiosis is the direction of the spindles in meiosis II. In male meiosis II, the two spindles in the daughter cells are usually perpendicular to each other within the same meiocyte, and the direction of each pair of spindles is different within the same anther (Figure 5B). In contrast, the spindles are positioned in the same direction within the ovule and are always aligned perpendicular to the nucellus to chalaza direction (Figure 5B, Movie S6), thus forming a linear tetrad in contrast to the tetrahedral arrangement on the male

side.

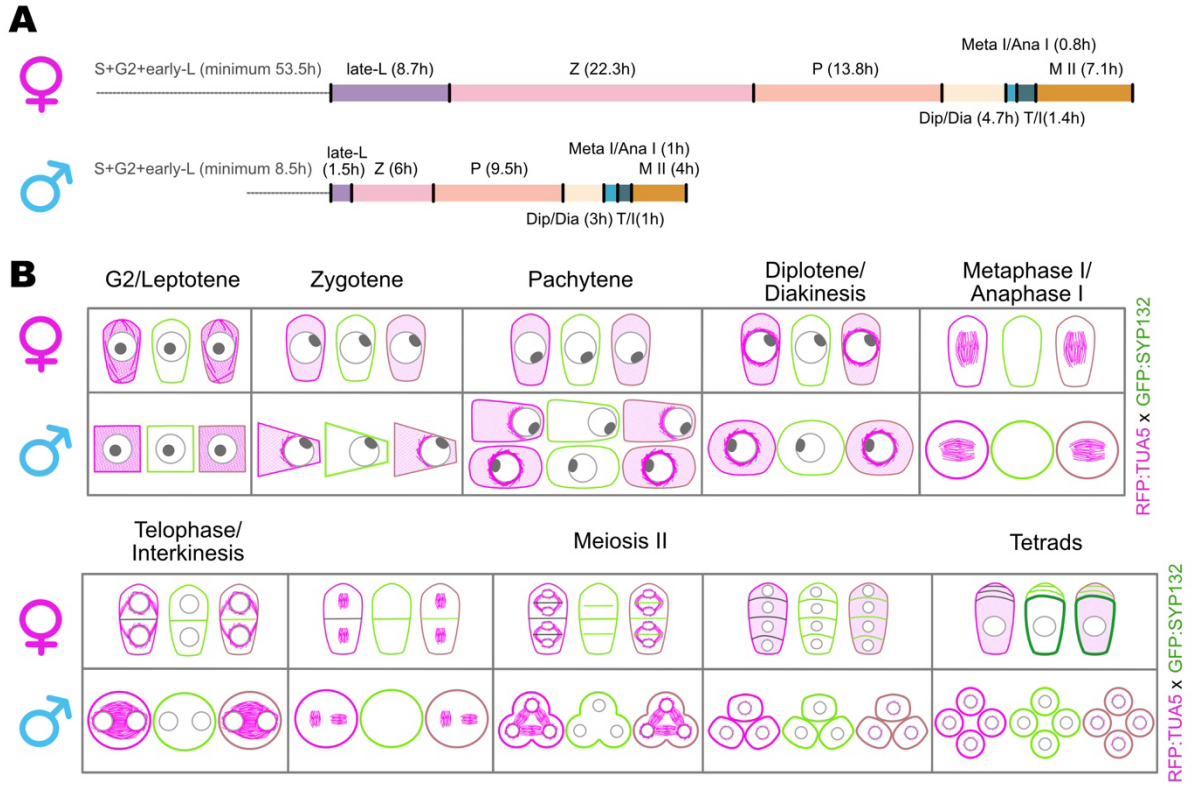

Figure 6. Comparison of female and male meiosis. (A) Comparison of meiotic timelines of female and male meiosis. The time displayed for female meiosis is based on the time course calculation of the average duration between different landmarks, as indicated in Figure 4C. The duration of male meiosis is from (Prusicki et al. 2019). S stands for S-phase; L for Leptotene; Z for Zygotene; P for Pachytene; Dip/Dia for Diplotene and Diakinesis; Meta I/Ana I for Metaphase I and Anaphase I; T/I for Telophase and Interkinesis; M II for Meiosis II. The duration of each stage is shown in hours. **(B)** Comparison of meiotic features of female and male meiosis. Tubulin in magenta (RFP:TUA5) and the plasma membrane in green (GFP:SYP132) showed the differences between female and male meiosis in cell shape, nucleus and nucleolus movement, microtubule organization, and the living meiotic products.

Materials and Methods

Plant material and growth conditions

The Arabidopsis Thaliana plants used in this study were all Columbia (Col-0) background. All the seeds were first surface-sterilized with chlorine gas, then stored in a 4°C fridge overnight. Afterwards, seeds were sown on a 0.7% plant agar plate containing half-strength Murashige and Skoog (MS) medium and 1% sucrose. Antibiotics were added to the plate for selection when required. Then leave plates with seeds in growth chambers at 21°C for 16h of light and 18°C for 8h of dark cycle for

germination. Ten days later, the seedlings were transferred to soil and grown in the growth chamber under the same long-day conditions as above, with 70% humidity.

KRP T-DNA insertion lines *krp3* (At5g48820, WsDSLox49707H), *krp4* (At2g32710, Sail_248_B06), *krp6* (At3g19150, Sail_548_B03), *krp7* (At1g49620, GK_841D12), and the triple mutant *krp4krp6krp7* have been described previously (Zhao et al. 2012, 2017). The reporter lines KINGBIRD2 (*PRO_{REC8}:REC8:GFPxPRO_{RPS5A}TagRFP:TUA5*), *PRO_{RPS5A}:TagRFP:TUA5*, *PRO_{ASY1}:ASY1:TagRFP*, *PRO_{ZYP1b}:ZYP1b:GFP*, *PRO_{ASY3}:ASY3:GFP*, *PRO_{SYP132}GFP:SYP132*, *PRO_{RPS5A}:TagRFP:TUB4*, and *PRO_{SUN1}:SUN1:GFP* were described previously(Maria A. Prusicki et al. 2019; Yang et al. 2019, 2020; Sofroni et al. 2020; Oda and Fukuda 2011). The classical floral dip method was employed for *Arabidopsis thaliana* transformation. All genotypes were confirmed by polymerase chain reaction (PCR) and/or antibiotic selection. All crosses were generated by emasculating the female parent 1 day before anthesis and hand-pollinating 1 to 2 days later.

Live imaging of meiotic division

Flowers of 0.7-1.7 mm were isolated and prepared as shown in the results section “Live-cell imaging set up of female meiosis in Arabidopsis”. Within the same ovary, more than one ovule can be imaged. Up to 8 opened ovaries were positioned in the same petri dish and cultured in an agar plate with half-strength Murashige and Skoog (MS) and 1% sucrose. Time-lapse image acquisition was performed using a Zeiss LSM 880 confocal laser scanning microscope, with each time point comprising a Z-stack of 5 or 7 optical sections, spaced 2 to 3 µm apart. The interval time was adjusted from 3 minutes to 10 minutes, depending on the developmental stage and physiological condition of the specimen, in order to balance temporal resolution and phototoxicity. The W-plan Apochromat 40X/1.0 DIC objective was used for image acquisition, which enabled the acquisition of clear, brightfield images for cell shape determination and nucleolus position. Fluorescent signals were captured from three distinct channels. GFP was excited using a 488 nm laser, and emission was collected in the 498-550 nm range. TagRFP was excited at 561 nm, with emission detected between 578-650 nm. Additionally, autofluorescence from chloroplasts was visualized using the same 488 nm excitation wavelength, but with signal collection shifted to the

680-750 nm range to isolate far-red emission. The sample chamber was stabilized at 21°C during imaging to maintain optimal conditions for long-term observation.

Image processing

The time-lapse datasets were initially transformed into sequential image stacks representing temporal progression. For each time point, the optimal focal plane was selected using aMPkit (unpublished). This software can review multidimensional data and then export different combinations of xyzt dimension image sequences, saving them as Tagged Image File Format (TIFF) to preserve uncompressed pixel data. Image drift was corrected by the Stack Reg plugin from Fiji (ImageJ, version 2.16, https://imagej.net/software/fiji).

Fluorescence intensity measurement

Fluorescence intensity was measured using Fiji. For each time point and Z-stack, regions of interest (ROIs) corresponding to the nucleus and cytoplasm were manually defined based on the brightfield channel. The cytoplasmic ROI was generated by applying the XOR function to subtract the nuclear region from the boundary. Similarly, the nucleolus was excluded from nuclear measurements by defining a smaller inner ROI representing the nucleolus and using the XOR function to isolate the nucleoplasm. Fluorescence intensities were measured across all time points in the relevant fluorescence channel, and the mean gray values were used for quantification.

Calculation of meiotic time course

This calculation of meiotic duration was performed as described in (De Jaeger-Braet et al. 2022). Stage-specific parametric models for censored time-to-event data were used as the duration of the stages is independent of each other. STATA SE version 17.0 was used for the statistical analysis. All models include only the intercept and a clustered sandwich estimator of variance to account for the clustered structure of meiocytes within different plants. They differ regarding their underlying distribution, which is chosen based on the Akaike Information Criterion (AIC). Potential distributions are exponential, Gompertz, log-logistic, Weibull, and log-normal. Thus, Gompertz was chosen as underlying distribution for the parametric model for late G2 and early leptotene, zygotene, anaphase I and metaphase II, Weibull for late leptotene,

telophase I and telophase II, Log-normal was chosen for pachytene, diplotene, interkinesis and tetrad, and loglogistic was chosen for stages diakinesis, metaphase I and anaphase II.

Supplementary Materials

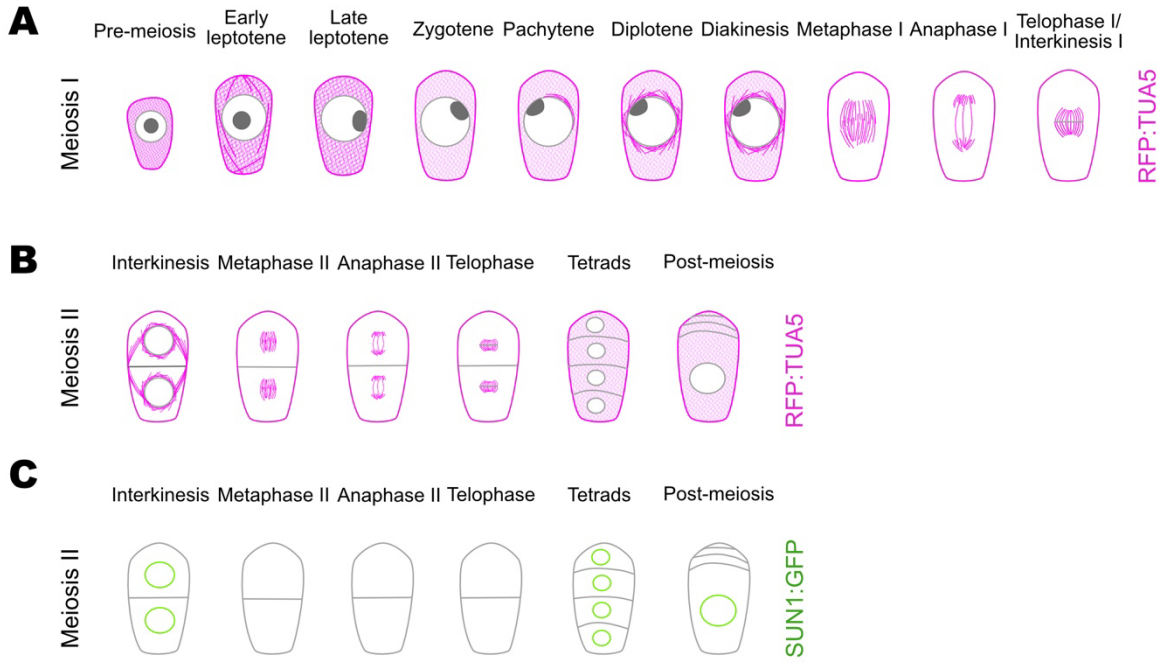

Figure S1. Microtubule and nuclear envelope organization during female meiosis. (A) Schematic illustration of microtubule array at different stages in meiosis I. TUA:RFP marked tubulin in magenta, nucleus in grey circle, and nucleolus in solid dark grey circle. **(B)** Schematic illustration of microtubule array at different stages in meiosis II. TUA:RFP marked tubulin in magenta, nucleus in grey circle, and nucleolus in solid dark grey circle. **(C)** Schematic illustration of nuclear envelope formation at different stages in meiosis II. SUN1:GFP marked the nuclear envelope in green, and the cell wall is shown in grey lines.

Table S1. Duration of the diplotene was not affect by the imaging starting time.

Reporter	Acquisition time (min)	Diplotene duration (min)
ZYP1b:GFP x ASY1:RFP	1480	80
ZYP1b:GFP x ASY1:RFP	1260	90
ZYP1b:GFP x ASY1:RFP	1330	70
ZYP1b:GFP x ASY1:RFP	1450	210
ZYP1b:GFP x ASY1:RFP	1720	110
ZYP1b:GFP x ASY1:RFP	1390	130
ZYP1b:GFP x ASY3:RFP	410	120
ZYP1b:GFP x ASY3:RFP	450	80
ZYP1b:GFP x ASY3:RFP	690	140
ZYP1b:GFP x ASY3:RFP	480	140
ZYP1b:GFP x ASY3:RFP	500	130
ZYP1b:GFP x ASY3:RFP	410	100
ZYP1b:GFP x ASY3:RFP	510	150
ZYP1b:GFP x ASY3:RFP	450	140
ZYP1b:GFP x ASY3:RFP	700	100
ZYP1b:GFP x ASY1:RFP	2420	100
ZYP1b:GFP x ASY1:RFP	2310	100
ZYP1b:GFP x ASY1:RFP	1950	110
ZYP1b:GFP x ASY1:RFP	2580	140
ZYP1b:GFP x ASY1:RFP	0	100
ASY3:GFP x RFP:TUA5	300	110

Table S2. Overview of the duration of the female meiotic phases

Meiotic stage	Median	95% CI	
G2+Early leptotene	3211	3956	2466
Late leptotene	524	599	450
Zygotene	1337	1541	1134
Pachytene	828	964	692
Diplotene	137	152	122
Diakinesis	142	164	130
Metaphase I	30	31	29
Anaphase I	17	19	15
Telophase I/ cytokinesis I	39	41	36
Interkinesis	41	45	37
Metaphase II	26	28	24
Anaphase II	11	12	10
Telophase II/cytokinesis II	37	41	34
Tetrads	356	585	127

Moive S1. REC8:GFP forms thin thread at the late leptotene. Live cell imaging of REC8:GFP x RFP:TUA5 was performed in female meiocyte. Video starts at the late leptotene stage and runs for 3 hours with scanning intervals of 10 minutes.

Moive S2. REC8:GFP signal weaken over pachytene progression. Live cell imaging of REC8:GFP x RFP:TUA5 was performed in female meiocyte. Video starts at the early pachytene stage and runs for 10 hours with scanning intervals of 10 minutes.

Moive S3. Nucleolus migrates to the side of the nucleus at the late leptotene. Live cell imaging was performed in female meiocyte with brightfield. Nucleolus highlighted in white circle. Video starts at the early leptotene, nucleolus moves to aside at 100 min reaches the late leptotene with scanning intervals of 10 minutes.

Moive S4. Rapid chromosome movements during zygotene and pachytene. Live cell imaging of ZYP1b:GFP x ASY1:RFP was performed in female meiocyte. Video starts at the late zygotene and runs 3 hours reaches pachytene with ASY1:RFP removed, and continues running for 5 hours with scanning intervals of 10 minutes.

Moive S5. Rapid chromosome movements disappear during diplotene. Live cell imaging of ASY3:GFP x RFP:TUA5 was performed in female meiocyte. Video starts at late pachytene with rapid chromosome movements and runs 2 hours reaches diplotene with chromosome stay static and microtubule full moon formation at 120 minutes, and continues running for 3 hours with scanning intervals of 10 minutes.

Moive S6. Microtubule and nuclear envelop organization during meiotic division. Live cell imaging of SUN1:GFP x RFP:TUA5 was performed in female meiocyte. Video starts at diplotene with full moon structure (magenta) and reaches the first NEB at 200 minutes, and the second NEB at 350 mintues continues running for 2 hours with scanning intervals of 10 minutes.

References

Armstrong, S. J., and G. H. Jones. 2001. “Female Meiosis in Wild-Type Arabidopsis Thaliana and in Two Meiotic Mutants.” *Sexual Plant Reproduction* 13 (4): 177–83.

Balboni, Martina, Chao Yang, Shinichiro Komaki, Jordan Brun, and Arp Schnittger. 2020. “COMET Functions as a PCH2 Cofactor in Regulating the HORMA Domain Protein ASY1.” *Current Biology : CB* 30 (21): 4113–27.e6.

Bhérer, Claude, Christopher L. Campbell, and Adam Auton. 2017. “Refined Genetic Maps Reveal Sexual Dimorphism in Human Meiotic Recombination at Multiple Scales.” *Nature Communications* 8 (April):14994.

Böwer, Franziska, and Arp Schnittger. 2021. “How to Switch from Mitosis to Meiosis: Regulation of Germline Entry in Plants.” *Annual Review of Genetics* 55 (November):427–52.

Capilla-Pérez, Laia, Stéphanie Durand, Aurélie Hurel, Qichao Lian, Aurélie Chambon, Christelle Taochy, Victor Solier, Mathilde Grelon, and Raphael Mercier. 2021. “The Synaptonemal Complex Imposes Crossover Interference and Heterochiasmy in.” *Proceedings of the National Academy of Sciences of the United States of America* 118 (12). https://doi.org/10.1073/pnas.2023613118.

Conicella, Clara, Antonella Capo, Maria Cammareri, Angela Errico, Natalia Shamina, and Luigi M. Monti. 2003. *Euphytica; Netherlands Journal of Plant Breeding* 133 (1): 107–15.

Cromer, Laurence, Jefri Heyman, Sandra Touati, Hirofumi Harashima, Emilie Araou, Chloe Girard, Christine Horlow, et al. 2012. “OSD1 Promotes Meiotic Progression via APC/C Inhibition and Forms a Regulatory Network with TDM and CYCA1;2/TAM.” *PLoS Genetics* 8 (7): e1002865.

Cromer, Laurence, Mariana Tiscareno-Andrade, Sandrine Lefranc, Aurélie Chambon, Aurélie Hurel, Manon Brogniez, Julie Guérin, et al. 2024. “Rapid Meiotic Prophase Chromosome Movements in Arabidopsis Thaliana Are Linked to Essential Reorganization at the Nuclear Envelope.” *Nature Communications* 15 (1): 5964.

De Jaeger-Braet, Joke, Linda Krause, Anika Buchholz, and Arp Schnittger. 2022. “Heat Stress Reveals a Specialized Variant of the Pachytene Checkpoint in

Meiosis of Arabidopsis Thaliana." *The Plant Cell* 34 (1): 433–54.

Dissmeyer, Nico, Moritz K. Nowack, Stefan Pusch, Hilde Stals, Dirk Inzé, Paul E. Grini, and Arp Schnittger. 2007. "T-Loop Phosphorylation of Arabidopsis CDKA;1 Is Required for Its Function and Can Be Partially Substituted by an Aspartate Residue." *The Plant Cell* 19 (3): 972–85.

Dresselhaus, Thomas, Martina Balboni, Lea Berg, Anika Dolata, Frank Hochholdinger, Yongyu Huang, Guojing Jiang, et al. 2025. "How Meristems Shape Plant Architecture in Cereals." *The Plant Cell*, June. https://doi.org/10.1093/plcell/koaf150.

Drouaud, Jan, Raphaël Mercier, Liudmila Chelysheva, Aurélie Bérard, Matthieu Falque, Olivier Martin, Vanessa Zanni, Dominique Brunel, and Christine Mézard. 2007. "Sex-Specific Crossover Distributions and Variations in Interference Level along Arabidopsis Thaliana Chromosome 4." *PLoS Genetics* 3 (6): e106.

Durand, Stéphanie, Qichao Lian, Juli Jing, Marcel Ernst, Mathilde Grelon, David Zwicker, and Raphael Mercier. 2022. "Joint Control of Meiotic Crossover Patterning by the Synaptonemal Complex and HEI10 Dosage." *Nature Communications* 13 (1): 5999.

Durand, Stéphanie, Qichao Lian, Victor Solier, Joiselle Blanche Fernandes, and Raphael Mercier. 2025. "MutLγ Enforces Meiotic Crossovers in Arabidopsis Thaliana." *Nucleic Acids Research* 53 (5). https://doi.org/10.1093/nar/gkaf157.

Eijpe, Maureen, Hildo Offenberg, Rolf Jessberger, Ekaterina Revenkova, and Christa Heyting. 2003. "Meiotic Cohesin REC8 Marks the Axial Elements of Rat Synaptonemal Complexes before Cohesins SMC1beta and SMC3." *The Journal of Cell Biology* 160 (5): 657–70.

Enami, Kazuhiko, Mie Ichikawa, Tomohiro Uemura, Natsumaro Kutsuna, Seiichiro Hasezawa, Tsuyoshi Nakagawa, Akihiko Nakano, and Masa H. Sato. 2009. "Differential Expression Control and Polarized Distribution of Plasma Membrane-Resident SYP1 SNAREs in Arabidopsis Thaliana." *Plant & Cell Physiology* 50 (2): 280–89.

Erfurth, Isabelle d', Laurence Cromer, Sylvie Jolivet, Chloé Girard, Christine Horlow, Yujin Sun, Jennifer P. C. To, Luke E. Berchowitz, Gregory P. Copenhaver, and Raphael Mercier. 2010. "The Cyclin-A CYCA1;2/TAM Is Required for the Meiosis I to Meiosis II Transition and Cooperates with OSD1 for the Prophase to First Meiotic Division Transition." *PLoS Genetics* 6 (6): e1000989.

Esposito, R. E., and M. S. Esposito. 1974. “Genetic Recombination and Commitment to Meiosis in Saccharomyces.” *Proceedings of the National Academy of Sciences of the United States of America* 71 (8): 3172–76.

Feng, Chao, Elisabeth Roitinger, Otto Hudecz, Maria Cuacos, Jana Lorenz, Veit Schubert, Baicui Wang, Rui Wang, Karl Mechtler, and Stefan Heckmann. 2023. “TurboID-Based Proteomic Profiling of Meiotic Chromosome Axes in Arabidopsis Thaliana.” *Nature Plants* 9 (4): 616–30.

Fozard, John A., Chris Morgan, and Martin Howard. 2023. “Coarsening Dynamics Can Explain Meiotic Crossover Patterning in Both the Presence and Absence of the Synaptonemal Complex.” *eLife* 12 (February). https://doi.org/10.7554/eLife.79408.

Friedlander, Gilgi, Daphna Joseph-Strauss, Miri Carmi, Drora Zenvirth, Giora Simchen, and Naama Barkai. 2006. “Modulation of the Transcription Regulatory Program in Yeast Cells Committed to Sporulation.” *Genome Biology* 7 (3): R20.

Giraut, Laurène, Matthieu Falque, Jan Drouaud, Lucie Pereira, Olivier C. Martin, and Christine Mézard. 2011. “Genome-Wide Crossover Distribution in Arabidopsis Thaliana Meiosis Reveals Sex-Specific Patterns along Chromosomes.” *PLoS Genetics* 7 (11): e1002354.

Handel, M. A., and J. J. Eppig. 1998. “Sexual Dimorphism in the Regulation of Mammalian Meiosis.” *Current Topics in Developmental Biology* 37:333–58.

Higgins, David M., Natalie J. Nannas, and R. Kelly Dawe. 2016. “The Maize Divergent Spindle-1 (dv1) Gene Encodes a Kinesin-14A Motor Protein Required for Meiotic Spindle Pole Organization.” *Frontiers in Plant Science* 7 (August):1277.

Honigberg, S. M., and R. E. Esposito. 1994. “Reversal of Cell Determination in Yeast Meiosis: Postcommitment Arrest Allows Return to Mitotic Growth.” *Proceedings of the National Academy of Sciences of the United States of America* 91 (14): 6559–63.

Hua, Rong, and Mingxi Liu. 2021. “Sexual Dimorphism in Mouse Meiosis.” *Frontiers in Cell and Developmental Biology* 9 (May):670599.

Kleckner, Nancy, Aurora Storlazzi, and Denise Zickler. 2003. “Coordinate Variation in Meiotic Pachytene SC Length and Total Crossover/chiasma Frequency under Conditions of Constant DNA Length.” *Trends in Genetics : TIG* 19 (11): 623–28.

Koltunow, Anna M., and Ueli Grossniklaus. 2003. “Apomixis: A Developmental

Perspective.” *Annual Review of Plant Biology* 54:547–74.

Lambing, Christophe, Pallas C. Kuo, Andrew J. Tock, Stephanie D. Topp, and Ian R. Henderson. 2020. “ASY1 Acts as a Dosage-Dependent Antagonist of Telomere-Led Recombination and Mediates Crossover Interference in.” *Proceedings of the National Academy of Sciences of the United States of America* 117 (24): 13647–58.

Lian, Qichao, Victor Solier, Birgit Walkemeier, Stéphanie Durand, Bruno Huettel, Korbinian Schneeberger, and Raphael Mercier. 2022. “The Megabase-Scale Crossover Landscape Is Largely Independent of Sequence Divergence.” *Nature Communications* 13 (1): 3828.

Mayerova, Nina, Lubos Cipak, and Juraj Gregan. 2020. “Cohesin Biology: From Passive Rings to Molecular Motors.” *Trends in Genetics : TIG* 36 (6): 387–89.

Morgan, Chris, John A. Fozard, Matthew Hartley, Ian R. Henderson, Kirsten Bomblies, and Martin Howard. 2021. “Diffusion-Mediated HEI10 Coarsening Can Explain Meiotic Crossover Positioning in Arabidopsis.” *Nature Communications* 12 (1): 4674.

Nannas, Natalie J., and R. Kelly Dawe. 2016. “Live-Cell Imaging of Meiotic Spindle and Chromosome Dynamics in Maize (Zea Mays).” *Current Protocols in Plant Biology* 1 (4): 546–65.

Nannas, Natalie J., David M. Higgins, and R. Kelly Dawe. 2016. “Anaphase Asymmetry and Dynamic Repositioning of the Division Plane during Maize Meiosis.” *Journal of Cell Science* 129 (21): 4014–24.

Oda, Yoshihisa, and Hiroo Fukuda. 2011. “Dynamics of Arabidopsis SUN Proteins during Mitosis and Their Involvement in Nuclear Shaping.” *The Plant Journal : For Cell and Molecular Biology* 66 (4): 629–41.

Pochon, Gaetan, Isabelle M. Henry, Chao Yang, Niels Lory, Nadia Fernández-Jiménez, Franziska Böwer, Bingyan Hu, et al. 2023. “The Arabidopsis Hop1 Homolog ASY1 Mediates Cross-over Assurance and Interference.” *PNAS Nexus* 2 (3): gac302.

Prusicki, Maria Ada, Martina Balboni, Kostika Sofroni, Yuki Hamamura, and Arp Schnittger. 2021. “Caught in the Act: Live-Cell Imaging of Plant Meiosis.” *Frontiers in Plant Science* 12 (December):718346.

Prusicki, Maria A., Emma M. Keizer, Rik P. van Rosmalen, Shinichiro Komaki, Felix Seifert, Katja Müller, Erik Wijnker, Christian Fleck, and Arp Schnittger. 2019.

"Live Cell Imaging of Meiosis in." *eLife* 8 (May). https://doi.org/10.7554/eLife.42834.

Rasmussen, Søren W., and Preben B. Holm. 1978. "Human Meiosis II. Chromosome Pairing and Recombination Nodules in Human Spermatocytes." *Carlsberg Research Communications* 43 (5): 275–327.

Sakuno, Takeshi, Sanki Tashiro, Hideki Tanizawa, Osamu Iwasaki, Da-Qiao Ding, Tokuko Haraguchi, Ken-Ichi Noma, and Yasushi Hiraoka. 2022. "Rec8 Cohesin-Mediated Axis-Loop Chromatin Architecture Is Required for Meiotic Recombination." *Nucleic Acids Research* 50 (7): 3799–3816.

Sanchez-Moran, Eugenio, Juan-Luis Santos, Gareth H. Jones, and F. Christopher H. Franklin. 2007. "ASY1 Mediates AtDMC1-Dependent Interhomolog Recombination during Meiosis in Arabidopsis." *Genes & Development* 21 (17): 2220–33.

Shamina, N. V. 2005. "Formation of Division Spindles in Higher Plant Meiosis." *Cell Biology International* 29 (4): 307–18.

Sheehan, Moira J., and Wojciech P. Pawlowski. 2009. "Live Imaging of Rapid Chromosome Movements in Meiotic Prophase I in Maize." *Proceedings of the National Academy of Sciences of the United States of America* 106 (49): 20989–94.

Sofroni, Kostika, Hirotomo Takatsuka, Chao Yang, Nico Dissmeyer, Shinichiro Komaki, Yuki Hamamura, Lev Böttger, Masaaki Umeda, and Arp Schnittger. 2020. "CDKD-Dependent Activation of CDKA;1 Controls Microtubule Dynamics and Cytokinesis during Meiosis." *The Journal of Cell Biology* 219 (8). https://doi.org/10.1083/jcb.201907016.

Tease, Charles, Geraldine M. Hartshorne, and Maj A. Hultén. 2002. "Patterns of Meiotic Recombination in Human Fetal Oocytes." *American Journal of Human Genetics* 70 (6): 1469–79.

Tease, C., and M. A. Hultén. 2004. "Inter-Sex Variation in Synaptonemal Complex Lengths Largely Determine the Different Recombination Rates in Male and Female Germ Cells." *Cytogenetic and Genome Research* 107 (3-4): 208–15.

Thangavel, Gokilavani, Paulo G. Hofstatter, Raphaël Mercier, and André Marques. 2023. "Tracing the Evolution of the Plant Meiotic Molecular Machinery." *Plant Reproduction* 36 (1): 73–95.

Valuchova, Sona, Pavlina Mikulkova, Jana Pecinkova, Jana Klimova, Michal

Krumnikl, Petr Bainar, Stefan Heckmann, Pavel Tomancak, and Karel Riha. 2020. “Imaging Plant Germline Differentiation within Arabidopsis Flowers by Light Sheet Microscopy.” *eLife* 9 (February). https://doi.org/10.7554/eLife.52546.

Varas, Javier, Katja Graumann, Kim Osman, Mónica Pradillo, David E. Evans, Juan L. Santos, and Susan J. Armstrong. 2015. “Absence of SUN1 and SUN2 Proteins in Arabidopsis Thaliana Leads to a Delay in Meiotic Progression and Defects in Synapsis and Recombination.” *The Plant Journal: For Cell and Molecular Biology* 81 (2): 329–46.

Watanabe, Y., and P. Nurse. 1999. “Cohesin Rec8 Is Required for Reductional Chromosome Segregation at Meiosis.” *Nature* 400 (6743): 461–64.

Wijnker, Erik, Hirofumi Harashima, Katja Müller, Pablo Parra-Nuñez, C. Bastiaan de Snoo, Jose van de Belt, Nico Dissmeyer, Martin Bayer, Monica Pradillo, and Arp Schnittger. 2019. “The Cdk1/Cdk2 Homolog CDKA;1 Controls the Recombination Landscape in.” *Proceedings of the National Academy of Sciences of the United States of America* 116 (25): 12534–39.

Yang, Chao, Yuki Hamamura, Kostika Sofroni, Franziska Böwer, Sara Christina Stolze, Hirofumi Nakagami, and Arp Schnittger. 2019. “SWITCH 1/DYAD Is a WINGS APART-LIKE Antagonist That Maintains Sister Chromatid Cohesion in Meiosis.” *Nature Communications* 10 (1): 1755.

Yang, Chao, Kostika Sofroni, Yuki Hamamura, Bingyan Hu, Hasibe Tunçay Elbasi, Martina Balboni, Lei Chu, Dagmar Stang, Maren Heese, and Arp Schnittger. 2022. “ZYP1-Mediated Recruitment of PCH2 to the Synaptonemal Complex Remodels the Chromosome Axis Leading to Crossover Restriction.” *Nucleic Acids Research* 50 (22): 12924–37.

Yang, Chao, Kostika Sofroni, Erik Wijnker, Yuki Hamamura, Lena Carstens, Hirofumi Harashima, Sara Christina Stolze, et al. 2020. “The Arabidopsis Cdk1/Cdk2 Homolog CDKA;1 Controls Chromosome Axis Assembly during Plant Meiosis.” *The EMBO Journal* 39 (3): e101625.

Yuan, Xinjie, Bowei Cai, Yuki Hamamura, Arp Schnittger, and Chao Yang. 2025. “SCF-Dependent Degradation of the Nuclear Lamina Releases the Somatic Chromatin Mobility Restriction for Meiotic Recombination.” *Science Advances* 11 (8): eadr4567.

Zenvirth, D., J. Loidl, S. Klein, A. Arbel, R. Shemesh, and G. Simchen. 1997. “Switching Yeast from Meiosis to Mitosis: Double-Strand Break Repair,

Recombination and Synaptonemal Complex." *Genes to Cells : Devoted to Molecular & Cellular Mechanisms* 2 (8): 487–98.

Zhang, Luoyan, Hongzhi Kong, Hong Ma, and Ji Yang. 2018. "Phylogenomic Detection and Functional Prediction of Genes Potentially Important for Plant Meiosis." *Gene* 643 (February):83–97.

Zhao, Xin 'ai, Jonathan Bramsiepe, Matthias Van Durme, Shinichiro Komaki, Maria Ada Prusicki, Daisuke Maruyama, Joachim Forner, et al. 2017. "RETINOBLASTOMA RELATED1 Mediates Germline Entry in." *Science (New York, N.Y.)* 356 (6336). https://doi.org/10.1126/science.aaf6532.

Zhao, Xin 'ai, Hirofumi Harashima, Nico Dissmeyer, Stefan Pusch, Annika K. Weimer, Jonathan Bramsiepe, Daniel Bouyer, et al. 2012. "A General G1/S-Phase Cell-Cycle Control Module in the Flowering Plant Arabidopsis Thaliana." *PLoS Genetics* 8 (8): e1002847.

Zickler, Denise, and Nancy Kleckner. 2016. "A Few of Our Favorite Things: Pairing, the Bouquet, Crossover Interference and Evolution of Meiosis." *Seminars in Cell & Developmental Biology* 54 (June):135–48.

Eidesstattliche Versicherung

Eidesstattliche Versicherung:

Hiermit versichere ich an Eides statt, die vorliegende Dissertationsschrift selbst verfasst und keine anderen als die angegebenen Hilfsmittel und Quellen benutzt zu haben.

Sofern im Zuge der Erstellung der vorliegenden Dissertationsschrift generative Künstliche Intelligenz (gKI) basierte elektronische Hilfsmittel verwendet wurden, versichere ich, dass meine eigene Leistung im Vordergrund stand und dass eine vollständige Dokumentation aller verwendeten Hilfsmittel gemäß der Guten wissenschaftlichen Praxis vorliegt. Ich trage die Verantwortung für eventuell durch die gKI generierte fehlerhafte oder verzerrte Inhalte, fehlerhafte Referenzen, Verstöße gegen das Datenschutz- und Urheberrecht oder Plagiate.

Affidavit:

I hereby declare and affirm that this doctoral dissertation is my own work and that I have not used any aids and sources other than those indicated.

If electronic resources based on generative artificial intelligence (gAI) were used in the course of writing this dissertation, I confirm that my own work was the main and value-adding contribution and that complete documentation of all resources used is available in accordance with good scientific practice. I am responsible for any erroneous or distorted content, incorrect references, violations of data protection and copyright law or plagiarism that may have been generated by the gAI.

Hamburg, den **21/07/2025** Unterschrift 

Acknowledgement

As I put all the chapters together for the dissertation, I realize that these pages capture only a small part of the work, experiences, and challenges I have lived through over the past six years. Now I am sitting alone in the office waiting for the sunrise again, reminds me of hundreds of late-night imaging days. It has been a long and winding journey, filled with moments of doubt and discovery, emotional ups and downs. But with all of your support, encouragement, and kindness, it somehow feels quite short at this moment. None of this would have been possible without you.

First and foremost, I would like to express my deepest gratitude to my supervisor Prof. Dr. Arp Schnittger, who offered me this great opportunity to pursue my PhD in his group and engaged me in several challenging projects. Your dedication, intelligence and passion for science have truly inspired me, and I have learned so much from you throughout these years. I would have never accomplished this without your guidance and support.

I would also like to sincerely thank Dr. Maren Hesse for always being open to any scientific discussions. Your sharp thinking and critical insights have pushed me to think more deeply, and your encouragement has always given me motivation when I got lost. Thank you and Lev for proofreading several chapters of this dissertation. Without your passionate input, this dissertation could not have been conducted successfully. I am very grateful to Dr. Magdalena Weingartner for kindly agreeing to be my second examiner. Your time, effort, and thoughtful feedback mean a lot to me.

I would like to thank Dr. Julia Kehr and the Dr. Elisabeth Appuhn Foundation for their generous financial support during the final and most critical phase of my Ph.D. journey. Receiving this fellowship made an enormous differences, allowing me to fully dedicate myself to bringing my two major research projects to completion.

I also want to thank Dr. Chao Yang for helping me settle down in Hamburg and in the lab. Your passion for science was contagious, and I learned many experimental techniques from you that made a real difference in my work.

A very special thanks goes to Dr. Maria Ada Prusicki and Dr. Yuki Hamamura, who taught me the art and beauty of live-cell imaging. Yuki, you were always there for me at late night in the lab, patiently troubleshooting with me. Your companionship

during those long nights made the lab feel like home. When I was overwhelmed during the pandemic, struggling with delayed experiments and thoughts of giving up, you were my mental support. You reminded me of how far I had come and helped me see the value of what I had achieved. I honestly cannot imagine how I would have made it through without you.

Many thanks to Dr. Seijiro Ono, my cloning sensei, who taught me many valuable techniques that made cloning faster and easier. Whenever I met the cloning problems, I knew I could always go to you. Thanks to Dr. Joke de Jaeger-Braet for always bringing the positive energy and the heartwarming Ferry to comfort me during the exhausting days. Many thanks to the former and current lab members for their help and the pleasant working environment we created together. I would like to specifically thank Katja, Yingqi, Franzi, Lucas, Ankit, Hasibe, Marti, Kostas, Misato, Jiayi, Mengmeng, Max, Oscar, and Zhijian for all the wonderful moments in and out of the lab.

Last but not least, a big thanks goes to my grandparents, my mother, and Tiantong, who always provided me with immense emotional support and were always at my side. Your presence, encouragement, and love have played an essential role in helping me reach this final milestone. I truly believe that without your support, I would not have been able to make it this far.

Thank you to everyone again from the bottom of my heart!